N73 27049

NASA CR-121215
SRI SCU-1377

INORGANIC SEPARATOR TECHNOLOGY PROGRAM

by J. S. Smatko, R. D. Weaver and F. R. Kalhammer

STANFORD RESEARCH INSTITUTE
333 Ravenswood Avenue
Menlo Park, California 94025

prepared for

NATIONAL AERONAUTICS AND SPACE ADMINISTRATION

NASA Lewis Research Center
Cleveland, Ohio
John M. Bozek, Project Manager
Direct Energy Conversion Division

1. Report No.
NASA CR-121215

2. Government Accession No.

3. Recipient's Catalog No.

4. Title and Subtitle
Inorganic Separator Technology Program

5. Report Date
January 1973

6. Performing Organization Code

7. Author(s)
Joseph S. Smatko, Robert D. Weaver, Fritz R. Kalhammer

8. Performing Organization Report No.

9. Performing Organization Name and Address
Stanford Research Institute
333 Ravenswood Avenue
Menlo Park, California 94025

10. Work Unit No.

11. Contract or Grant No.
NAS 3-15686

12. Sponsoring Agency Name and Address
National Aeronautics and Space Administration,
Lewis Research Laboratories, Cleveland, Ohio

13. Type of Report and Period Covered
Final Dec 1970-Nov 1972

14. Sponsoring Agency Code

15. Supplementary Notes
Project Manager, John M. Bozek, Direct Energy Conversion Division
NASA Lewis Research Center, Cleveland, Ohio

16. Abstract

Work on this contract was performed under three major technical tasks. In Task I, extensive testing and failure analysis of Astropower Laboratory 40 Ahr silver-zinc cells with largely inorganic separators was performed. The results showed that the wet stand and cycle life objectives of the silver-zinc cell development program under Contract NAS 3-10928 were essentially accomplished and led to recommendations for cell composition, design, and operation that should yield further improvements in wet and cycle life.

In Task II, a series of advanced inorganic materials was successfully developed and formulated into rigid and semiflexible separator samples. In Task III, suitable screening tests for evaluation of largely inorganic separators were selected and modified for application to the separator materials developed in Task II. The results showed that many of these formulations are potentially superior to previously used materials and permitted selection of three promising materials for further evaluation in silver-zinc cells.

17. Key Words (Suggested by Author(s))
Sealed silver-zinc cells
Inorganic battery separators
Cell failure analysis
Sterilized batteries-Separator Screening tests

18. Distribution Statement
Unclassified - Limited

19. Security Classif. (of this report)	20. Security Classif. (of this page)	21. No. of Pages	22. Price*
Unclassified	Unclassified	180	

* For sale by the National Technical Information Service, Springfield, Virginia 22151

NASA-C-168 (Rev. 6-71)

SUMMARY

Work under this Contract was performed under three major technical tasks.

Task I was concerned with testing and failure analysis of 40 Ahr silver-zinc cells with semiflexible, inorganic separators developed at Astropower Laboratories under Contract NAS 3-10928. After novation of this contract on 8 December 1970, cell testing was re-established at SRI. Substantially improved testing equipment and procedures were developed and used to accumulate a considerable body of cell testing and failure analysis data over a two-year period under Contracts NAS 3-10928 and NAS 3-15686. These data indicate that the major objective of the program--development of a heat-sterilizable, sealed silver zinc cell capable of extended stand and subsequent cycling--was accomplished. Specifically, the survival rate of cells in the reconditioning step after standing and their subsequent cycle life were both particularly high if cells were standing in the discharged condition. Although charged-stand and float charged-stand are detrimental standing conditions, a high survival rate nevertheless appears achievable by storing cells at subambient temperature.

Cell failure analysis showed shorting by zinc nodules or dendritic zinc filaments to be the almost exclusive failure modes; shorting by silver (found deposited in the separators of most cells) was not evident. Zinc nodule shorting appears to be associated with conditions--such as extended charged stand or a high average state of charge between cycles--that tend to result in degradation of separators by dissolved silver oxide. Zinc filament shorting is the dominant failure mode of cells that had undergone extended cycling; this type of shorting was frequently

(but not necessarily) associated with the observation of zinc extruding through splits in the negative electrode bags. The low incidence of zinc electrode slumping found in the analysis of failed cells points to the potential of Astropower-type electrode-separator composites for achieving extended cycle life with zinc electrodes in alkaline batteries.

Cell testing and failure analysis yielded useful information also on the influence of the other variables examined in the test program including cell design, cycling temperature, and cycling of individual cells versus batteries of cells.

The conclusions of the cell test program were used to formulate a series of recommendations for achieving improved silver-zinc cell standing and cycling capabilities. Recommendations include preferred environmental and electrical conditions for standing, reconditioning and operating cells, exploration and correction of factors responsible for separator degradation, and suggestions for improved construction of separators and seals.

Task II was concerned with the development of improved rigid and semiflexible separator formulations for use in alkaline cells, especially silver-zinc secondaries. The starting point was a number of inorganic materials (and their chemical modifications) that had shown promise as separators in preliminary work at Astropower Laboratories. Additional inorganic materials were selected on the basis of their anticipated chemical and electrochemical compatibility with the environment in silver-zinc cells. Relatively straightforward techniques of preparation were demonstrated for most of the materials that were not commercially available.

From these inorganic stock materials, rigid ceramic disks of high quality were prepared in good yields by firing suitably prepared ceramic powders at temperatures between $1368^{o}K$ and $1623^{o}K$. Semiflexible wafers were readily made from inorganic stock materials and organic binder systems using the procedure disclosed in U.S. Patent 3,625,770 (licensed to SRI by the McDonnell Douglas Corporation); these wafers had good uniformity and high surface quality.

Task III was concerned with the characterization of the rigid and semiflexible separator materials (developed under Task II) by suitable screening methods. Separator screening tests commonly used (most of which are described in an Air Force Aero Propulsion Laboratory booklet, Battery Separator Screening Methods, edited by J. E. Cooper and A. Fleischer) were reviewed with respect to their probable utility where applied to largely inorganic separators. A list of recommended tests was established and procedures were developed for this systematic application of selected tests to rigid and semiflexible separator materials.

Combining tests for zinc dendrite penetration, zinc gassing, and accelerated degradation in KOH with the determination of resistivity, porosity, water permeation, pore size distribution, and mechanical strength, permitted a rather complete and consistent characterization of rigid formulations in terms of key electrochemical, chemical and physical separator characteristics. Characterization of semiflexible separator formulations by the same tests (using appropriately modified measurements of mechanical properties) was somewhat less complete because of the inherently inhomogeneous structures of semiflexible separators and the resulting uncertainties regarding pore tortuosity and size distribution in these materials. However, together with the results for rigid formulations the screening test data permitted a relative ranking of all separator formulations developed under Task II in terms of their probable utility for silver-zinc cells.

On this basis, more than half of the inorganic materials developed and tested in this program appear to be superior to the baseline material

(Astropower Laboratory designation 3420-25) that has been showing promise in cell testing (see Task I). The three most promising of these--including a proprietary formulation that, independent of the somewhat arbitrary quantitative evaluation scheme, scored consistently higher than the remaining ones--were proposed for further testing and evaluation in actual cells.

Finally, analysis of the experimental data permitted formulation of several recommendations for tests, test equipment and procedures that should result in improved characterization and evaluation of separators in future development programs.

INTRODUCTION

Silver-zinc batteries, having higher energy densities than other alkaline batteries, are attractive energy sources for compact power applications, and especially for space applications. However, limited cycle and wet-stand life, and problems with achieving sealability, have been deterrents for some applications.

As demonstrated in a series of silver-zinc battery development programs supported by NASA (References Nos. 1-5), the development of inorganic battery separators represents a major advance toward the goal of long-life, hermetically sealed batteries. The usefulness of these separators continues to be confirmed by the results of the current program (NAS 3-15686). Under this program, many sealed silver-zinc cells (nominally 40 Ahr) are still cycling, more than three years after their construction and initial testing under a previous contract (NAS 3-10928). The results obtained in cell cycling and analysis of cells that have failed are given under Task I of this report.

Preliminary results of internal development programs at the former Astropower Laboratory of the McDonnell Douglas Corporation suggested that further improvements in inorganic separators and silver-zinc battery characteristics were likely to occur through modifications of the existent technology. Achievement of such improvements was the overall objective of the current program. The specific objective was to develop separator formulations with improved characteristics (such as better chemical compatibility and a negligible rate of gassing when in contact with zinc) that will permit further increases of stand and cycle life of alkaline cells, especially silver-zinc cells. Twenty different materials (including the 3420-09 and 3420-25 reference materials) were prepared and tested as rigid separators; sixteen of these materials were processed into semiflexible separators. The materials development and separator-fabrication efforts are reported below under Task II.

Although real-time testing in cells will always be required as the ultimate proof of separator suitability, screening techniques are widely used in separator development programs to keep time and costs of evaluation within practical limits. Application of screening tests to the separators developed was therefore an important aspect of the current program. Accepted methods of characterizing and screening battery separators are not sufficiently specific and refined to permit prediction of suitable separator materials--especially if these are substantially different from standard materials. Accordingly, a significant effort was expended to review and, where necessary, modify existing screening techniques for application to inorganic separators. This review, the systematic application of suitable tests, and the results obtained in these screening tests, are reported under Task III.

Finally, the report summarizes our conclusions and recommendations from the three major technical tasks performed under this program. The most promising separator formulations are identified and recommended for incorporation into simplified silver-zinc cells.

TASK I - CYCLING AND FAILURE ANALYSIS OF SILVER-ZINC CELLS

The Work Statement for NASA Contract NAS 3-15686 specified that SRI was to continue the testing of silver-zinc cells fabricated and placed on various long-term tests under Contract NAS 3-10928. The tests were to be performed in accordance with the previously established schedule and continued to cell failure or to the end of the contract. Failed cells were to be subjected to analysis, and complete failure analysis data were to be transmitted to the NASA project monitor.

Cycling Regimes, Equipment, and Procedures

The cycling regimes employed in this program are shown in Table 1.* The VK-1 regime was applied to cells by the individual test stations† that had been transferred from Astropower Laboratory and repaired, refurbished and reassembled at SRI. Similar test stations were used to apply the VK-3 regime either to individual cells or to batteries.‡ Regarding the 100% DOD regime, the large manpower effort required for manually testing the 20 cells that are standing in the charged condition for one month between 100% discharges had led to the building of a 5-station automatic test panel under Contract NAS 3-10928. This panel, after some modifications of its components to increase reliability, is still used to provide the once-a-month, 100% discharge for the cells remaining on test under this regime.

---

*The codes VK-1,-2, and -3 for the three continuous cycling regimes used in this program were established at NASA-Lewis to simulate load profiles anticipated for batteries used in Viking-type missions.

†Individual test stations consisted of a DC power supply, electric control panel, voltage limit switches, and a recorder; each individually tested cell required one station.

‡The term "battery" as used in this test program refers to a varying number of individual cells that are electrically in series and have the voltage limits for charge and discharge cutoff applied to the entire battery instead of to individual cells; when a cell in such a battery fails, it is removed from the circuit and the remaining battery is cycled with proportionately reduced voltage limits for charge and discharge.

Table 1

CYCLING REGIMES

Conditions / Regime Code (% DOD)	Cycling Period	Frequency	Discharge	Charge	Charging Voltage Limit (per cell)
VK-1 (10)	24 hr	one cycle per day	2A for 2 hr	0.32A for 22 hr	2.02
VK-2 (7.5 & 15)	24 hr	2 different cycles per day, (a) & (b)	(a) 3A for 1 hr (b) 3A for 2 hr	(a) 0.45A for 7 hr (b) 0.45A for 14 hr	2.00
VK-3 (35)	8 hr	3 cycles per day	7A for 2 hr	2.5A for 6 hr	2.00
100% DOD (NHS-114 Series)	1 mo	1 cycle followed by charged stand for 1 month	10A to 1.00V, followed by 2A to 1.00V	1.5A to 2.00V limit	2.00
100% DOD (HS-54-5,6, & HS-123-GX	defined by charge-disch. conditions	as frequently as convenient, with charged stand between cycles	6A to 1.00V, followed by 2A to 1.00V	1.5A to 2.00V limit	2.00
Modified (21.5) VK-1(a) (HS-15 Series)	24 hr	one cycle per day	0.7A for 2 hr	0.07A for 22 hr	2.02
Modified (10.5) VK-1(b) (HS-16 Series)	24 hr	one cycle per day	0.5A for 2 hr	0.06A for 22 hr	2.02

The VK-2 regime is applied to cells by an automatic cell cycling system developed at our laboratories. Encouraged by the success of the SRI-built 5-station system for the once-a-month, 100% DOD regime, an 18-station section of this system had been designed and built under Contract NAS 3-10928. A second, 17-station section was completed under the current contract in September 1971. The completed system provides the 35-station cycling capacity that was required to handle the maximum number of cells to be tested under the VK-2 regime. A set of electrical schematics for the system was transmitted to the NASA project manager early in this program.

Some features of this system include constant-current charging of cells to a settable voltage limit (2.000 ± 0.003 V for VK-2), followed by automatic switching of individual cells to a tapered-current charge at constant voltage also set at 2.000 ± 0.003 V for VK-2. Discharge is through a fixed (but adjustable) load, with automatic switching of individual cells from discharge to open circuit as soon as a settable lower voltage limit (1.00 V for all cycling regimes) is reached. During charge and discharge, individual cell voltages are sampled sequentially by two independent circuits. Each cell is sampled once every 70 seconds* for limit switching, every 210 seconds* for voltage recording. Individual cell currents can also be measured rapidly and conveniently whenever desired. To date, this system has performed very reliably and has provided improved cell testing at greatly reduced requirements for manpower and capital investment per cell while generating more accurate and accessible data for all cycling VK-2 cells. The only periodic maintenance required is replacement of the mechanical stepping switches in the sampling circuits.

Representative Cycling Behavior and Procedure

Live cells are cycled according to the regimes described in Table 1. During cycling, continuous or quasi-continuous voltage recordings are taken for each cell on test. These graphic displays of cell behavior are examined at least once a day, more frequently if the electric behavior of a cell suggests impending failure. In addition, entries of

---

*More often if less than the full 35-cell capacity of the system is used.

cell voltage and current are made at prescribed intervals into a tabular log kept for each cell.

Apparent failure of a cell usually becomes manifest electrically in one of two ways. The cell voltage during discharge may drop to 1.00V, suggesting that a cell has lost capacity. A typical course of cell capacity loss with age is shown in Figure 1. Although this figure refers specifically to one of the cells on the once-a-month, 100% DOD regime (where cell capacity is determined routinely for each cycle), the phenomenon is a general one; it will result in ultimate cell failure if no other type of failure occurs first. The other major failure mode, responsible for earlier failure, is a cell's inability to accept and deliver charge due to presence of an internal short.

Both failure modes show up electrically in the voltage recordings. To assist in the correct diagnosis of a true cell failure, the recordings of an apparently failed cell are examined in detail for several cycles prior to the first failure. We have found that a very useful indicator of the "health" of a cell is the height (and sharpness) of the voltage spike signaling onset of the silver (II) voltage pleateau: with increasing age many cells develop an increasingly sharp spike.* Other indicators of impending cell failure are: continuously declining average discharge voltages over a number (say, 2 to 12) of cycles, rapid voltage fluctuations during charge, rapid decline of open circuit voltage after charge, irregularities in the voltage-time trace during charge and open circuit stand, and significant cell heating on charge, discharge, or open circuit stand. The increasingly rapid voltage rise and several other indicators of cell aging and impending failure show up in the cycling curves presented in a group of figures later under Task I (subsection <u>Cycling Curves</u>), which update the information given in Reference No. 6 for the same set of cells. Features of these cycling curves and their relation to cell behavior will be examined in the Discussion section below.

*Although we have not investigated in detail how this phenomenon correlates with the state of health of silver-zinc cells, our observations suggest that it may offer the basis for development of a diagnostic test.

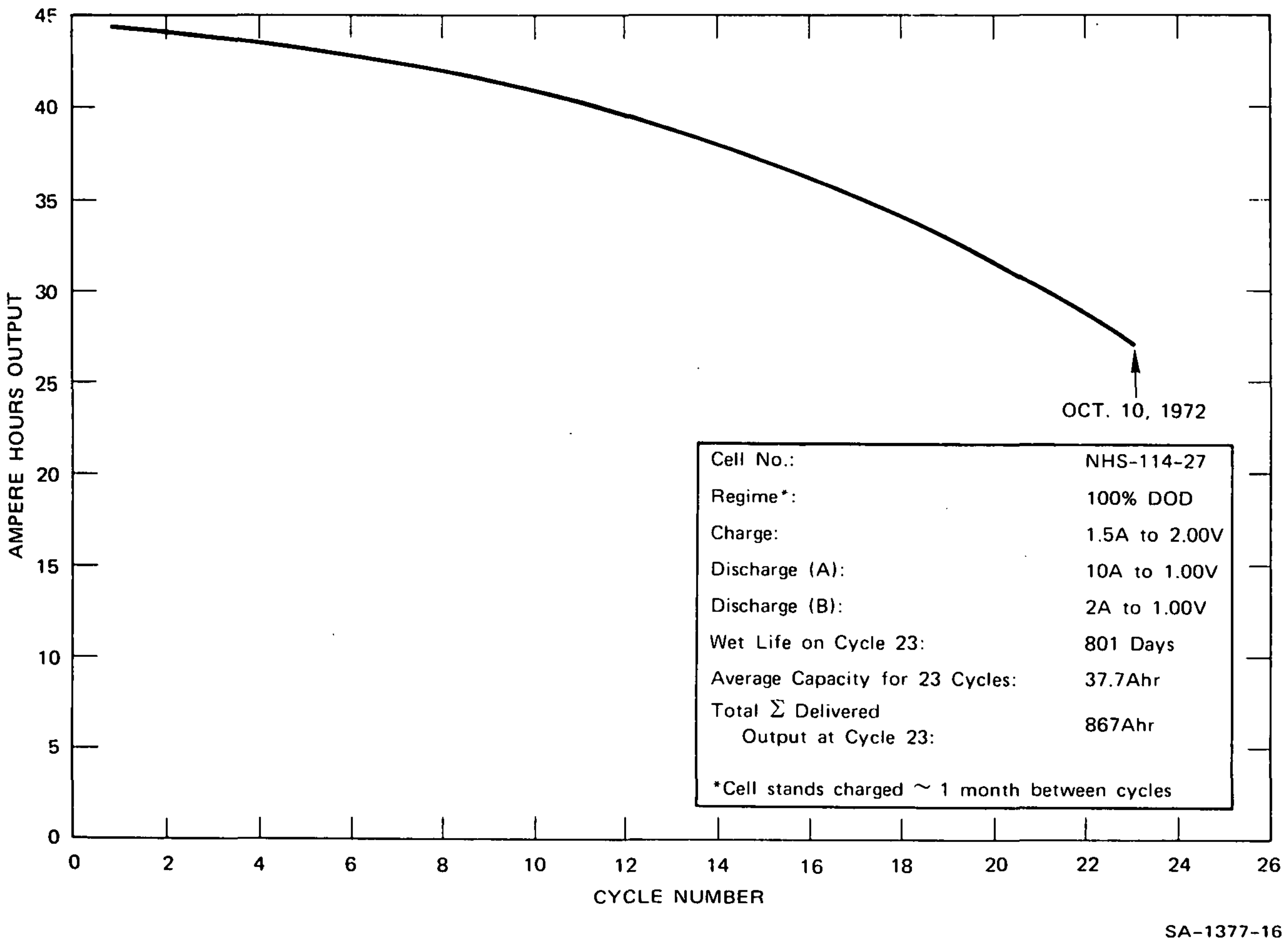

FIGURE 1 OUTPUT CAPACITY DECLINE WITH CYCLING (PLATE LOCK, 100% DOD CATEGORY)

To establish that a cell failure is indeed real and not caused by improperly adjusted cycling equipment (which might cause a progressive charge/discharge imbalance), the following procedure is followed. The cell is electrically disconnected from the cycling panel. At the next scheduled charge period, the cell is reconnected and allowed to charge, and the subsequent discharge period is skipped. The cell is then reconnected for charge and thereafter subjected to normal cycling. Experience has shown that within relatively few cycles the cell will tend to fail again. The procedure cited above is again applied; following the third failure, a reformation charge is applied. If the cell is capable of accepting the reformation charge, it is placed on automatic cycling again. Experience has shown that such cells fail again within a relatively short time, usually after a few days. This procedure has proved successful in screening out several artificial failures and returning such cells to normal cycling. Irreversibly failed cells are taken off cycling tests for subsequent dissection and analysis.

Cell Inventory

Table 2 is a summary, by cycling regimes, of the status of all cells originally transferred to SRI under the novated Contract NAS 3-10928 and continued on test under this program. The breakdown of the total cell population into test groups sharing a common experimental factor and the distribution of these groups into subgroups tested on various cycling regimes are shown in Table 3. This table also includes remarks pertaining to the experimental parameters varied within test groups. The objectives pursued with these test groups, the definition and composition of the cell subgroups employed, and the major findings from the cycling tests are discussed in the following sections.

Cell Testing Results: Cycling

Group of 3-Plate Pilot Cells* (Cycling Regime: Modified VK-1)

These cells were fabricated to provide design information on electrode capacities and separator structures that would permit the

*The alternate designation "Longest Test Cell" was also used in this program.

Table 2

INVENTORY AND STATUS OF CELLS ON TEST

Cycling Regime	Number of Cells							
	12/31/70		12/31/71		4/30/72		10/31/72	
	Cycling	Failed	Cycling	Failed	Cycling	Failed	Cycling	Failed
VK-1	43	3	30	16	27	19	21	25
VK-2	4	0	25	24	23*	28	17	34
VK-3	16	0	0	16	0	16	0	16
100% DOD (once/month; charged stand)	20	0	18	2	16	4	11	9
100% DOD (at irregular intervals; charged stand)	3	0	2	1	2	1	2	1
Total, cycling cells	86		75		68		51	
Total, failed cells		3		59		68		85
Total, cells on wet stand	52*		7		5†		5	
Total, all cells	141		141		141		141	

*Includes 17 cells on charged stand, 15 cells on float charged stand, and 15 cells on discharged stand, to be placed on the VK-2 regime early in 1971 after a 21+ month stand time.

†Two cells were transferred from wet stand to cycling on the VK-2 regime in January 1972.

Table 3

SUMMARY OF CELL TEST GROUPS AND CONDITIONS

Experimental Factor	No. of Cells	No. of Failed Cells*	Regime	Comments
3-Plate Pilot Cells	6	6	VK-1	3-plate cells; all negatives bagged; some positives bagged.
Viking	4	0	VK-2	Standard Design 7; 45 Ahr original capacity.
	17	15		Charged stand, 10°-42°C for 21+ months prior to cycling.
	15	14		Float stand at 10°-32°C for 21+ months prior to cycling.
	15	5		Discharged stand at 24°C for 21+ months prior to cycling.
	4	-	Stand	Discharged stand
Design Variation	5	3	VK-1	Design 7 ($6b^+/5b^-$); 24°C
	5	1		Design 6 ($4b^+/\ell/5b^-$); 24°C; extra separator layer between the 4 positive bags and 5 negative bags
	5	1		Design 8 ($6b^+/\ell/5b^-$); 24°C; extra separator layer between the 6 positive bags and 5 negative bags
Temperature-Battery/Cell	4	4	VK-1	Tested as a battery at 24°C (All cells of Design 7)
	2	1		Tested as single cells at 24°C
	4	2		Tested as a battery at 10°C
	2	0		Tested as single cells at 10°C
	3	2		Tested as a battery at 32°C
Plate Lock	4	4	VK-3	Design 7, no plate lock, environmentally tested
	4	4		Design 7, epoxy plate lock, normal cure; no environmental test
	3	3		Design 7, epoxy plate lock, normal cure; environmental test
	4	4		Design 7, epoxy plate lock, normal cure plus 24 hrs at 100°C; environmentally tested
	1	1		Design 7, GX film separator, plate lock, normal cure; environmentally tested
	20	9	100% DOD	Charged stand, discharged about once per month
	1	0	Stand	Continuous charged stand since original 3 cycles
Extra	2	1	100% DOD	Design 5 ($4b^+/L/5b^-$); extra supported separator layer between bags.
	1	0		Design 7; 8 wraps of GX film plus double plate lock
	3	0		Design 5; on 7 to 9-month stand before cycling.
	5	3		Design 3 ($5b^+/6b^-$); on 7 to 8.5-month stand before cycling.
	2	2		Design 2 ($5b^+/6b^-$); only negatives were bagged.

*Status as of October 31, 1972.

†The designs used for the cells tested under this program are described in Reference No. 6. As an example of the design notation, $6b^+/5b^-$ indicates that a cell comprises six bagged positive and five bagged negative electrodes. The letter (ℓ) indicates presence of an additional layer (usually an asbestos-free composite of binder and the inorganic material) between each pair of adjacent positive and negative electrodes. Capital letter (L) indicates that the extra layer consists of the semiflexible separator material used to fabricate separator bags.

design of cells with a full complement of negatives and positives.

Two cells (subgroup HS-15-1) were built with 20 g of silver in the positive sandwiched between two zinc negatives. All three electrodes were bagged*, and the cells were cycled on a modified† VK-1 regime to 21.5% DOD. Two other cells (subgroup HS-16-1) were of similar construction‡ but had 30 g of silver in the positive; these were cycled on a modified VK-1 regime to ~10.5% DOD. The remaining two cells (subgroup HS-16-2) were built with 30 g of silver in the positive, which was covered by a U-wrap layer of 3420-09 separator material on each face and sandwiched between two bagged zinc negatives; these cells were cycled on a modified VK-1 regime to 10.5% DOD.

Cycling results for the pilot cell group are shown in Table 4 . These data indicate that cycle and wet life were noticeably higher for the two cells incorporating a bagged silver positive of increased capacity. Cells with a lower-capacity, bagged positive and those with a higher-capacity positive covered only by separator sheets had comparable life.

Viking Cell Group (Cycling Regime: VK-2)

The primary objective for this test group was to explore the influence of cell charge status and storage temperature on wet life and cycle life of cells that (like the cells for a prospective Viking-type Mars probe) would experience an extended stand period prior to their use. The standing period originally selected for this test group was 21 months, but several subgroups were standing somewhat longer (up to 25 months).

---

*The negatives were enclosed in standard 3420-25 bags; the positive was in a bag of similar construction but of the 3420-09 composition.

†By prorating the current down for the lower capacity of 3-plate cells.

‡Cell HS-16-1-1 had the same separator arrangement as the HS-15-1 subgroup; cell HS-16-1-2 used the standard separator for all three electrodes.

Table 4

CYCLING RESULTS: 3-PLATE PILOT CELLS*

(Status as of October 31, 1972)

Cell subgroup HS-15-1†: total cells		2
No. of cells failed in cycling		2
Range and average‡ of wet life	(days)	984 - 1058 [1021]
Range and average‡ of cycle life	(cycles)	555 - 630 [592]
Cell subgroup HS-16-1: total cells		2
No. of cells failed in cycling		2
Range and average of wet life	(days)	1230 - 1288 [1259]
Range and average of cycle life	(cycles)	777 - 835 [806]
Cell subgroup HS-16-2: total cells		2
No. of cells failed in cycling		2
Range and average of wet life	(days)	937 - 1085 [1011]
Range and average of cycle life	(cycles)	480 - 633 [556]

*Cycling was on the VK-1 regime, with current prorated down to the capacity of 3-plate cells; temperature was nominally 24°C.

†See text for cell design specifications in subgroups.

‡Average values are in brackets.

The Viking cell test group contained five categories of cells; two of these were broken down further into subgroups. All Viking cells were of standard design (No. 7) and cycled on the VK-2 regime. The first test category comprised four cells that were placed on cycling without a standing period, that is, immediately after receiving the three initial forming and conditioning cycles.

The second category comprised 17 cells that were placed on a 21+ month charged stand (subgroups at 10°C, 22°C, 32°C, and 42°C) prior to cycling. The third category involved 15 cells that were on a 21+ month float charge stand at 1.88 (±0.02) V (subgroups at 10°C, 22°C, 32°C) prior to cycling. The fourth category comprised 15 cells* on a 21+ month discharged stand at room temperature prior to cycling. The fifth category has four cells that are being held on discharged stand (at room temperature) for 3 to 4 years prior to cycling.

Results from cycling the Viking cells are given in Table 5. Although the uncertainties and variations associated with the small numbers of cells per subgroup are considerable, several major trends are apparent. These may be summarized as follows:

(1) The percentage of cells capable of cycling after extended stand periods (21 to 25 months) is much higher for cells that were standing in the discharged condition (73%) than for cells standing in the charged or float-charged conditions (53% each). If the discharged-stand cells with a previous charged-stand history* are eliminated from comparison, the survival rate of discharged-stand cells is increased to 93%.

(2) Charged-stand and float charged-stand of cells are detrimental conditions not only for cell survival rates in the reconditioning step after standing but also for the wet life and cycle life expectancy of successfully reconditioned cells.

---

*Four of these cells were not virgin cells but had previously been kept on charged stand at elevated temperatures until their open circuit voltage had dropped to 1.65 V. This resulted in the following charged-stand history:

Cell No.	AH-39-3	AH-39-4	AH-39-5	AH-39-6
Standing Temperature (°C)	52	52	62	62
Standing Time (Average)	225	105	70	82

Table 5

CYCLING RESULTS: VIKING CELL GROUP*
(Status as of October 31, 1972)

Early-Cycling Category: 4 Total Cells

No. of cells still cycling	4
Wet life, all cycling cells (days)	982
Cycle life, all cycling cells (cycles)	1683

Float Charged-Stand Category: 15 Total Cells

Subgroup standing at 10°C: total cells	5
No. of cells failing reconditioning	1
No. of cells still cycling	0
No. of cells failed in cycling	4
Range and average of wet life (days)	869-1035 [929]
Range and average of cycle life (cycles)	152-480 [268]
Subgroup standing at 24°C	5
No. of cells failing reconditioning	2
No. of cells still cycling	1
Wet life (days)	1198
Cycle life (cycles)	801
No. of cells failed in cycling	2
Range and average of wet life (days)	903-1076 [989]
Range and average of cycle life (cycles)	218-560 [389]
Subgroup standing at 32°C	5
No. of cells failing reconditioning	4
No. of cells still cycling	0
No. of cells failed in cycling	1
Wet life (days)	974
Cycle life (cycles)	379

Charged-Stand Category: 17 Total Cells

Subgroup standing at 10°C: total cells	5
No. of cells failing reconditioning	0
No. of cells still cycling	2
Wet life (days)	1209
Cycle life (cycles)	898-899 [899]
No. of cells failed in cycling	3
Range and average of wet life (days)	795-861 [823]
Range and average of cycle life (cycles)	99-209 [150]
Subgroup standing at 24°C: total cells	5
No. of cells failing reconditioning	1
No. of cells still cycling	0
No. of cells failed in cycling	4
Range and average of wet life (days)	994-1107 [1039]
Range and average of cycle life (cycles)	474-699 [565]
Subgroup standing at 32°C: total cells	5
No. of cells failing reconditioning	5
Subgroup standing at 42°C: total cells	2
No. of cells failing reconditioning	2

Discharged-Stand Category:† 15 Total Cells

Subgroup of virgin‡ standing cells	
No. of cells failing reconditioning	2
No. of cells still cycling	8
Range and average of wet life (days)	922-1224 [1094]
Range and average of cycle life (cycles)	551-903 [754]
No. of cells failed in cycling	1
Wet life (days)	1168
Cycle life (cycles)	786
Subgroup of cells with charged-stand history	
No. of cells failing reconditioning	2
No. of cells still cycling	2
Range and average of wet life (days)	1144-1144 [1144]
Range and average of cycle life (cycles)	796-797 [796]

*Viking group cells were cycled on the VK-2 regime, with cells at laboratory temperature (nominally 24°C).

†Discharged stand was at 24°C

‡That is, cells not cycled (except in forming step) prior to stand; this was the standard condition for all Viking cells with exception of the subgroup of discharged-stand cells with charged-stand history.

(3) Increasing standing temperature decreases the survival rate (in the reconditioning step) of charged-stand and float charged-stand cells[*]. The effect of standing temperature is marked: while only one of the 10 cells standing at $32^{\circ}C$ or $42^{\circ}C$ survived, 9 out of 10 cells survived standing at $10^{\circ}C$. Cells standing at $24^{\circ}C$ were intermediate, with 7 out of 10 cells surviving the reconditioning step.

(4) An unexpected finding was that cells surviving charged or float-charged stand at $10^{\circ}C$ had markedly inferior cycle life compared to the subgroups standing at $24^{\circ}C$.

Cell Design Variation Group (Cycling Regime: VK-1)

In the performance of work under Contract NAS 3-10928 at the Astropower Laboratory, a considerable effort was devoted to cell design. The early designs emphasized potential use over a limited number of deep cycles, and high rate (pulse) capability of cells. Later designs were directed more toward achievement of long wet-stand and cycle life for cells capable of moderate rates of discharge.

The three latest designs[†] (Astropower Laboratory designation: Designs 6, 7, and 8) were chosen for comparison in long-term cycling that continued into this program. As mentioned previously, Design 7 of separator[‡] between each pair of bagged positives and negatives to provide increased resistance to silver and zinc penetration. Design 6 cells have two fewer positives but the same number of negatives as Design 7, giving a somewhat lower nominal cell capacity; Design 8 cells have the same number of positive and negative plates and nominal capacity as those with Design 7; this design was regarded as a backup of the standard cell design.

Five-cell subgroups for each of these designs were put on cycling on the VK-1 regime. The status of these cells is summarized in Table 6. Again recognizing the limitations of small number statistics, the main result bears out the design expectations: the extra separator layer used in Designs 6 and 8 appears to delay cell failure in cycling. The significance of this finding is supported by the essentially identical life capability of Design 6 and 8 cells, which have identical separator configurations.

[*] Temperature influence was not investigated for the discharged-stand cell.

[†] For detailed cell design specifications, refer to Reference No. 6.

[‡] See footnote in Table 3.

Table 6

CYCLING RESULTS: CELL DESIGN VARIATION GROUP*

(Status as of October 31, 1972)

<u>Design 7 ($6b^+/5b^-$) subgroup: total cells (in battery)</u>		5
No. of cells still cycling		2
Wet life, all cycling cells	(days)	1171
Cycle life, all cycling cells	(cycles)	910
No. of cells failed in cycling		3
Range and average of wet life	(days)	477-1112 [858]
Range and average of cycle life	(cycles)	348- 851 [641]
<u>Design 6 ($4b^+/\ell/5b^-$) subgroup: total cells (in battery)</u>		5
No. of cells still cycling		4
Wet life, all cycling cells	(days)	1171
Cycle life, all cycling cells	(cycles)	964
No. of cells failed in cycling		1
Wet life, (days)		1077
Cycle life, (cycles)		874
<u>Design 8($6b^+/\ell/5b^-$) subgroup: total cells (in battery)</u>		5
No. of cells still cycling		4
Wet life, all cycling cells	(days)	1171
Cycle life, all cycling cells	(cycles)	922
No. of cells failed in cycling		1
Wet life, (days)		1141
Cycle life, (cycles)		892

---

*Cycling is on the VK-1 regime, with all cells at laboratory temperature (nominally 24 ^{o}C).

Temperature-Battery/Cell Group (Cycling Regime: VK-1)

In the early phase of cell testing under Contract NAS 3-10928 at the Astropower Laboratory, the storage temperature of charged-stand cells was found to affect capacity retention of cells in the expected direction--increasingly better retention with decreasing temperature. An influence of temperature on cell wet stand and cycle life was suspected but enough testing information was not obtained to permit any conclusions regarding temperature as a factor. Similarly, although indications were obtained that operation of cells as batteries* was detrimental to cell cycle life, more information on this factor appeared desirable.

Generation of additional information on both factors was the major objective in testing cells in the so-called Temperature-Battery/Cell Group. The cycling results obtained with this group are given in Table 7. The major trends may be summarized as follows:

(1) Operation of cells in batteries appears to reduce cell wet and cycle life expectancy, presumably because of the additional stresses (excess voltage and/or overcharge) imposed on the remaining cells if one of the cells in a battery has lower voltage and charge acceptance during impending failure.

(2) Cycling of cells below room temperature appears to have a somewhat beneficial effect on wet stand and cycle life, whether cells are cycled singly or as a battery. However, this conclusion is weakened by the observation that cells from the 32°C battery group had better average cycle life than those from the 24°C battery. These findings must be considered in the light of small number statistics and the fact that impending failure of a single cell in a battery can impose very high stresses on all remaining cells. No comparison is possible for single cells inasmuch as the 32°C subgroup did not include single cells.

Plate-Lock Cell Group (Cycling Regimes: VK-3 and 100% DOD)

During environmental testing of cells under Contract NAS 3-10928, it was shown† that application of high shock loads to cells caused the electrode packs to shift partly into the void space under the cell lids.

---

*As defined for this test program; see footnote on p. 7.

†For a discussion of this work, see Reference 6.

Table 7

CYCLING RESULTS: TEMPERATURE-BATTERY/CELL GROUP*
(Status as of October 31, 1972)

Subgroup at 10°C:	total cells	6
No. of cells cycled individually		2
No. of individual cells still cycling		2
Wet life, each cell	(days)	1184
Cycle life, each cell	(cycles)	1047
No. of cells cycled as a battery		4
No. of battery cells still cycling		2
Wet life	(days)	1184
Cycle life	(cycles)	992
No. of battery cells failed in cycling		2
Range and average of wet life	(days)	757-785[771]
Range and average of cycle life	(cycles)	572-598[585]
Subgroup at 24°C:	total cells	6
No. of cells cycled individually		2
No. of individual cells still cycling		1
Wet life	(days)	1184
Cycle life	(cycles)	1059
No. of individual cells failed in cycling		1
Wet life	(days)	661
Cycle life	(cycles)	541
No. of cells cycled as a battery		4
No. of battery cells failed in cycling		4
Range and average of wet life	(days)	554-701[591]
Range and average of cycle life	(cycles)	429-576[466]
Subgroup at 32°C:	total cells	3
No. of cells cycled as a battery		3
No. of battery cells still cycling		1
Wet life	(days)	1143
Cycle life	(cycles)	974
No. of battery cells failed in cycling		2
Range and average of wet life	(days)	837-848[842]
Range and average of cycle life	(cycles)	668-679[673]

*Cycling is on the VK-1 regime.

Although no catastrophic cell failures were caused by environmental testing and the electrical performance of cells with shifted packs was satisfactory, an epoxy plate lock and heat sealing of bag tops (to localize electrodes within bags) were added as design features to one group of cells. Testing of this group was continued under the current program.

The breakdown of cells in the Plate-Lock Group into subgroups--corresponding to the experimental factors examined--is shown in Table 8, together with the results obtained in cycling these cells. Several trends are discernible in the test results obtained with cells cycled on the VK-3 regime:

(1) Plate locking tends to degrade the wet and cycle life of cells; the effect is not very large but definitely discernible.

(2) Extended curing of the epoxy cement used for plate locking appears to reduce the degrading effect of plate locking on cell life.

(3) Environmental testing does not seem to degrade wet and cycle life of plate-locked cells.

Examination of test data for cells cycled on the once-per-month, 100% DOD regime shows the same trends. However, the data provided by the control group (D) do not yet permit evaluation of the plate-lock factor inasmuch as two equipment-induced cell failures effectively reduced this subgroup to a 3-cell group. As more cells fail with time and cycling, meaningful information also on this factor can be expected to develop.

Group of Extra Cells (Cycling Regimes: VK-1 and 100% DOD)

In this group, several cells of varying backgrounds were collected, with cell design as the major experimental factor being tested. The designs* ranged from the early Design 2 (which had only the zinc negatives bagged) to a modification of Design 5 which employs bags for all electrodes plus an extra separator layer between the bagged electrodes. The cycling results obtained with this group are given in Table 9; the major trends can be summarized as follows:

* For details of the cell designs tested in this program, see Reference 6.

Table 8

CYCLING RESULTS: PLATE-LOCK GROUP*

		VK-3	100% DOD
Subgroup A (epoxy plate lock, normal cure, not environmentally tested), total cells		4	5
No. of cells still cycling		0	3
Wet life	(days)	-	816
Cycle life	(cycles)	-	23
No. of cells failed in cycling		4	2
Range and average of wet life	days)	223-274 [245]	605-635 [620]
Range and average of cycle life	(cycles)	265-403 [326]	17
Subgroup B (epoxy plate lock, normal cure, environmentally tested), total cells		3	5
No. of cells still cycling		0	3
Wet life	(days)	-	824
Cycle life	(cycles)	-	23
No. of cells failed in cycling		3	2
Range and average of wet life	(days)	244-285 [264]	536-793 [664]
Range and average of cycle life	(cycles)	281-404 [342]	18
Subgroup C (epoxy plate lock, extended cure, environmentally tested), total cells		4	5
No. of cells still cycling		0	3
Wet life	(days)	-	822
Cycle life	(cycles)	-	23
No. of cells failed in cycling		4	2
Range and average of wet life	(days)	253-319 [292]	520-789 [704]
Range and average of cycle life	(cycles)	289-468 [412]	20
Subgroup D (control: no plate lock, environmentally tested), total cells		4	5
No. of cells still cycling		0	2
Wet life	(days)	-	852
Cycle life	(cycles)	-	24
No. of cells failed in cycling		4	3†
Range and average of wet life	(days)	307-323 [318]	755
Range and average of cycle life	(cycles)	457-497 [480]	21

*All cycling is at laboratory temperature (nominally 24 °C).

†Two of these cells exploded on cycle 10 (wet life: 418 days) due to equipment malfunction; their wet and cycle life is not included in the data of the table.

Table 9

CYCLING RESULTS: GROUP OF EXTRA CELLS*
(Status as of October 31, 1972)

Design 2 subgroup	total cells	2†	VK-1 regime
No. of cells failed in cycling		2	
Average wet life	(days)	646	
Average cycle life	(cycles)	283	
Design 3 subgroup	total cells	5‡	
No. of cells still cycling		2#	
Range and average of wet life	(days)	1313, 1313 [1313]	
Range and average of cycle life	(cycles)	909—968 [939]	
No. of cells failed in cycling		3	
Range and average of wet life	(days)	996-1159[1084]	
Range and average of cycle life	(cycles)	636-799[724]	
Design 5 subgroup (VK-1)	total cells	3##	
No. of cells still cycling		3	
Wet life, all cells	(days)	1275	
Cycle life, all cells	(cycles)	913	
Design 5 subgroup (100% DOD)	total cells	2	100% DOD regime
No. of cells still cycling		1	
Wet life	(days)	1285	
Cycle life	(cycles)	151	
No. of cells failed in cycling		1	
Wet life	(days)	884	
Cycle life	(cycles)	136	
Design 7 cell (with SWRI type GX separator)	total cells	1	
No. of cells still cycling		1	
Wet life	(days)	802	
Cycle life	(cycles)	38	

* Cell cycling is at laboratory temperature (nominally 24°C).

† Cells HS-47-2,8 were cycled to failure at Astropower Laboratory.

‡ Cells were on 7-month stand prior to cycling (2 cells on charged stand, 3 cells on float-charged stand).

\# One cell each from among charged stand and float-charged stand cells.

\## Cells were on 7 to 9 month stand prior to cycling (one cell each on charged stand, float-charged stand and discharged stand).

(1) As expected, cells of Design 2 (built with fewer separator layers for a primary-type application) failed much earlier in cycling. The extra layer of semiflexible separator between the bagged electrodes of Design 5 appears to improve cycle life over that of Design 3 cells which had no extra layer.

(2) Although Design 5 zinc negatives have a lower capacity than those of Design 3, this feature so far has not led to low capacity failures; because of the rather shallow cycles of the VK-1 regime applied to these subgroups, nominally low capacity will not become a failure mode until all capacity has declined to 10-15% of its original value.

(3) A comparison* of the limited data for Design 3 and Design 5 cells cycling on the VK-1 regime with the data in Tables 5 and 6 suggests that a 7 to 9 month wet stand--even in the charged or float-charged conditions--does not degrade wet life and cycle life noticeably.

Cell Performance Versus Cycling Regimes

Wet life and cycle life data averaged by regime for the cells tested in this program are given in Table 10. Although such a comparison represents somewhat of an oversimplification inasmuch as there are significant variations (in terms of cell design and/or test parameters) within some of the groups, several trends are nevertheless apparent:

(1) On the rational basis of total capacity discharged per unit area of plate over the life of a cell, the Viking cells put on cycling immediately after their fabrication and formation have the highest cycling performance of all cell groups. The reduced performance of Viking charged-stand and float charged-stand cells is again noted, as is the similar average performance of these cell groups.

(2) Although the average number of cycles to failure was only 408 on the VK-3 regime, the rational cycling performance data (total Ahr per unit area of plate) for this regime were comparable to, or higher than, those for the presumably less stressful VK-1 regime, suggesting that a 35% depth of discharge may be less detrimental to cycling performance than extended standing of cells in a high average state of charge.

---

*Although there are differences in design, these differences are not considered large enough to invalidate a comparison in terms of parameters other than cell design.

Table 10

CONDENSED AVERAGE PERFORMANCE OF FAILED CELLS[a]

	FAILED CELLS									LIVE CELLS	
	1	2	3	4	5[b]	6	7	8[c]	9[c]	10	11
	3-Plate Cells (2) 21.5% DOD (3) 10.5% DOD Prorated VK-1 Regime	Temperature Battery/Cell Group VK-1 Regime ~10% DOD	Various Extra Cells VK-1 Regime ~10% DOD	Average for the 9 Cells in Columns 2 and 3	100% DOD Once per Month Charged Stand Between Cycles	VK-3 Cells 35% DOD	Charged Stand Category VK-2 Regime 7.5% & 15% DOD	Float Charged Stand Category VK-2 Regime 7.5% & 15% DOD	Discharged Stand Category VK-2 Regime 7.5% & 15% DOD	Discharged Stand Category VK-2 Regime 7.5% & 15% DOD	Cells Cycling Since Activation and no Stand Period VK-2 Regime 7.5% & 15% DOD
No. of Cells	5	6	3	9	5	6	6	6	1	8	4
Wet Life Days	1070	664	1084	802	629	285	972	1000	908	1137	982
Cycle Life	627	524	724	590	17	408	435	412	319	812	1683
Total Ahr Discharged per Cell	721	2090	2900	2360	700	5710	1960	1850	1436	3650	7570
Total Ahr Discharged per Electrode	721	418	580	472	140	1142	392	370	287	730	1515

[a] From the group given failure analysis at SRI, except for (live) cells listed in Columns 10 & 11 for comparison.

[b] The cells are from the NHS-114 series only. (Plate Lock & Environmental Test Group).

[c] Includes 2 cells in Column 8 and 1 cell in Column 9 that failed the reconditioning process (marginally) but cycled with others passing the reconditioning process after the 21+ month stand period (at the request of the NASA project manager).

[d] These cells, having no stand period were cycled immediately after activation, whereas the cells listed in Column 10 did stand 21+ months prior to cycling on the VK-2 regime. Data, as of 31 October 1972.

(3) Wet life, by itself, is not a suitable index of cell performance as noted in columns 2 and 5 of Table 10. These data indicate that, for similar wet life, the cells undergoing 100% DOD (with charged stand for a month between cycles) experience a much more stressful situation than, for example, the cells of the temperature/battery/cell group undergoing only 10% DOD: the output of the latter group is about 3-fold greater than the former.

(4) More frequent cycling favors a higher Ahr output over the life of cells (at least at low depths of discharge) as indicated by comparisons of columns 1, 3, and 11 which include data for cells with comparable wet lives and nearly identical depths of discharge.

Cell Testing Results:

Failure Analysis

The work statement for Task I of this program called for analysis of all cells that were tested to failure in this program. Failed cells were to be disassembled, the cause of failure to be determined by appropriate techniques of examination, and failure analysis data to be transmitted to the NASA project manager.

In the course of this program, a joint decision with the NASA project manager was made that analysis of some cells failed in testing at SRI would be done at NASA-Lewis. Complete data on all failed cells analyzed at SRI were transmitted to the NASA project manager as appendices to the Monthly Progress Reports.

Procedure

The detailed failure analysis procedure used in this program was adopted in a joint decision with the NASA project manager. Generally, it follows procedures used at NASA-Lewis but certain refinements in technique and diagnostic tests (such as the catalytic gassing test for zinc identification) were added at SRI as the work progressed. The basic procedure was as follows.

(1) A small hole was drilled through the cell lid to permit venting of internal gas pressure.

(2) Saw cuts were made around the cell peripheries (two cuts parallel to, and just below the lid, one cut parallel to the electrodes in the narrow faces of the cell); cutting was stopped just before severing the cell walls to prevent damage to electrode packs. The top then was carefully cracked off and the electrode tabs snipped.

(3) Interplate potential differences were then measured for each adjacent positive-negative electrode pair. Subsequently, free electrolyte (if present) was drained, the case cracked open and the electrode pack removed (intact if possible) for examination.

(4) Electrodes (still in their bags) were removed one by one. All bags were thoroughly inspected, and unusual features were examined under a 20-power binocular microscope.

(5) Suspected metallic shorts anywhere on the negative and positive bags were probed with an ohmmeter, and metallic deposits were tested for identity by placing a drop of KOH over them and contacting the deposit with a platinized platinum wire. Gas evolution (observed under the microscope) was taken as an indication of zinc; the test can be used to show absence of silver in macroscopic quantities by allowing the catalytic dissolution process to go on until all of the zinc is dissolved.

(6) Bagged silver electrodes were then soaked in hot water, and the electrode plates were pulled from their bags and closely examined.

(7) Because zinc electrode bags tended to adhere tightly to their electrodes, these bags were slit at their edges and carefully peeled away from the zinc plates. Zinc electrode faces then were closely examined and probed for dry and (or) hard areas.

(8) All pertinent observations were then recorded on failure analysis sheets. These failure analysis data formed the basis for the following results.

Inventory of Failed Cells

Of the 141 cells transferred to SRI in December 1970 as part of the novation of Contract NAS 3-10928, three were failed. An additional 82 failed between that time and the end of this program on October 31, 1972. Twenty-eight of these cells were transferred to NASA-Lewis for analysis; of the remaining 57 cells, 48 were subjected to failure analysis at SRI. Table 11 shows a complete inventory of failed cells, broken down by cell-testing groups and subgroups, and indicating whether and where failure analysis was performed.

At least one failed cell from each of the six test groups--including every major subgroup--was analyzed at our laboratories. Although there is still a limited backlog for analysis, conclusions on major failure modes were possible for all groups from the analyses already performed.

Faults and Failures

In any cell-failure analysis program, the first step toward eventual diagnosis of specific failure modes and suggestion of a possible failure mechanism consists of a physical and electrical examination of cells for significant faults. Pragmatically, we can define a significant fault to be any deviation from the physical appearance (exterior and interior) or electrical behavior of new cells which could cause--or contribute to--cell performance degradation and failure. Some faults are clearly related to cell failure while others ultimately might have caused cell failure if no other faults had been present. The major faults and failures found for the failed cells analyzed in this program are presented below.

Leaks were observed for a large percentage (34 out of 48 total) of failed cells. Three areas of leakage were noted: around terminal posts, around the pressure gages installed on some of the cells, and at the junction of cell lids to their respective cases. Since at least some cells were cycling after more than two years of continuous or intermittent leaking, it is apparent that even readily visible* leaks do not

*Using the standard phenolphthalein leak test.

Table 11

INVENTORY OF FAILED CELLS

Cell Group	No. of Cells	No. of Cells Analyzed at SRI	No. of Cells Transferred to NASA	No. of Cells in Backlog at SRI
3-Plate Pilot	6	5	0	1
Viking				
Charged Stand	15	9	6	0
Float-charged Stand	14	8	6	0
Discharged Stand	5	3	1	1
Design Variation	5	1	0	4
Temp-Battery Cell				
$10^{\circ}C$, Battery	2	1	1	0
$24^{\circ}C$, Battery	4	4	0	0
$24^{\circ}C$, Cell	1	0	1	0
$32^{\circ}C$, Battery	2	1	1	0
Plate Lock				
VK-3 regime	16	6	10	0
100% DOD regime	9	5	1	3
Extra				
Design 2, VK-1	1	1	0	0
Design 3, VK-1	3	3	0	0
Design 5, 100% DOD	2	1	1	0
All Groups	85	48	28	9

necessarily lead to early cell failure. Loss of electrolyte can be substantial, however; most failed cells did not contain any free electrolyte although, as a rule, they had moist plates and separators. A rough estimate based on volume and porosity of separators and battery plates in new Design 7 cells shows that these components can absorb about 75 ml of electrolyte. Assuming that there was no increase of absorbed electrolyte during aging, this suggests that cells found (after opening) to be without free electrolyte have lost 30% or more of their original electrolyte charge of about 110 ml. Inasmuch as the scope of our failure analysis did not include attempts to quantitatively recover cell electrolytes or characterize local resistance of separators in failed cells, there is currently no proof that loss of electrolyte was a factor in reducing wet and cycle life of the cells tested in this program. However, this possibility deserves some consideration because continued loss of electrolyte will eventually cause an increase in cell resistance and, quite probably, a nonuniform distribution of current and potential over the negative and positive plates. This condition, in turn, could promote dendrite penetration and capacity loss--two of the observed failure modes.

The importance of reliable seals--and the difficulty to achieve such seals--was recognized during cell development at Astropower Laboratory and led to the design of the triple "O"-ring, epoxy-reinforced seal used for the terminal posts of all cycling cells. The possibility that this relatively complex seal might still be inadequate had been anticipated by NASA-Lewis with the introduction of two additional seal designs; these were tested, together with the standard design, in a special Terminal Seal Test. The results are shown in Table 12. No clear superiority of the new NASA seals is evident from these data. The test may not be vigorous enough to provide a bigger spread between the inferior and superior terminal posts. More likely, however, these designs do not differ much in their capability to seal.

Table 12

TERMINAL SEAL TESTS

No. of Cases Originally on Test	No. of Cases that Failed	Av No. of Days on Test for Continuing Cases	Av No. of Test Days to Leak	Group No.*
1	1	--	516	Original
6	1	812	306	1 (A)
6	1	812	284	2 (B)
6	3	756	309	3 (C)
12	2	756	325	4 (D)

*Test groups and their parameters are described in Reference No. 6.

The other leak area of importance to cell design involved the lid-to-case seal.** Leaks at this seal were unexpected in view of its fabrication by a specially developed† ultrasonic welding technique that was followed by overpotting welds with epoxy resin. Occurrence of this type of leak implies failure of the ultrasonic weld and points to the need for modifications in seal fabrication. It seems possible that--if excessive pressure was occasionally applied--a thin weld line of highly viscous plastic resulted that retained residual stresses. This or other stresses leading to bond failure could probably be removed by an annealing step.

**Although another area of leakage--that of the screw fittings used for installations of pressure gages--also was frequent, it is not inherently associated with cell design. The fact that most of the lids with mounted gages had radial hair line cracks starting at the hole has implications for engineering applications of the plastic used for cell cases and lids.

†For details, see Reference No. 6

Bag splits were apparent upon disassembly of a majority (26 of 48) of the failed cells examined at SRI. In all instances of bag splits, the edges of bagged zinc electrodes were bulging, suggesting that the glued edge seams of the bags split under the influence of mechanical pressure exerted by the cycling zinc electrodes. Development of significant pressures is suggested also by our observation that cracks had formed in the bulged area of the coating of many zinc electrode bags. The bulged areas were just beyond the original zinc electrode edges and also beyond the projected edges of the silver electrode; they corresponded to the small void space that exists around new bagged zinc electrodes because of the technique used in shaping bags around these electrodes. Apparently, cycling eventually fills this space; eventually, seams can part and zinc masses can grow through the gap, leaving the bag around the silver electrode as the only barrier to zinc penetration on charging.

In every instance where bags had seam splits (even in cells where only a single bag was split), the free spaces between the tapered bag edges and the cell case edge and(or) bottom became filled with zinc, a situation conducive to failure by zinc shorting. In fact, an electric short between the extruded zinc mass and an adjacent silver electrode was noted in a number of instances. In others, the electric failure mode had indicated shorting but no short was found in the failure analysis--either because shorts were physically broken in disassembly or chemically removed by zinc dissolution. There is little doubt that bag splits and the associated extrusion of zinc were important factors in the ultimate failure of several cells.

Slumping of zinc electrodes--and the associated loss of negative capacity--tend to be major problems in extended cycling of all types of alkaline cells using zinc negatives and conventional separators. However, this fault (often referred to as "shape change") was found surprisingly infrequently in cells that failed during this program, thus confirming earlier observations* of this favorable characteristic exhibited by Astropower Laboratory silver-zinc cells.

---

*See reference 6.

Only one cell among the large group of Viking cells (from the Discharged Stand subgroup) showed slight slumping. The only other cells showing noticeable slumping were all from the Temperature-Battery/Cell group--one each from the cell subgroups cycled as batteries at $10^{o}C$, $24^{o}C$, and $32^{o}C$; the cell with the greatest degree of slumping came from the battery cycled at $32^{o}C$. In this connection, it is interesting to note that, compared to cells tested singly, cells cycled in batteries were quite probably exposed to more overcharging stresses that might promote slumping and(or) other types of cell failure.

Erosion (or shedding) of zinc electrodes was observed in ten of 48 cells analyzed--a significant percentage. Zinc electrode slumping--either in the form of the almost universal "edge" effect discussed above, or as the more extensive redistribution of active material observed in a few instances--was invariably accompanied by erosion-type loss of zinc from some areas of the negative plates. However, not all cases of erosion were associated with slumping: active material lost from zinc plates frequently was found in the void spaces exterior to electrode bags, often with no electrical connection remaining to zinc electrodes. Although migration of material through splits in bags undoubtedly accounted for much of this effect, deposits of "mushy" (that is, relatively soft, microcrystalline) zinc external to bags occasionally were observed to form before obvious bag splits could be seen.*

Erosion of zinc electrodes can cause, or contribute to, capacity loss of the negative plates. However, a corresponding correlation was not observed in this program, probably because only very extensive (>80% to 90%) capacity loss would lead to formal cell failure by low capacity. Therefore, observation of electrode erosion in our failure analyses was mainly used diagnostically; whenever erosion was observed, it indicated that active material had been lost from the zinc electrode and might be contributing to a failure-inducing, electrically "soft" or "hard" short.

---

*With cells using transparent polysulfone cell cases.

ZN-3 FACING AG-4

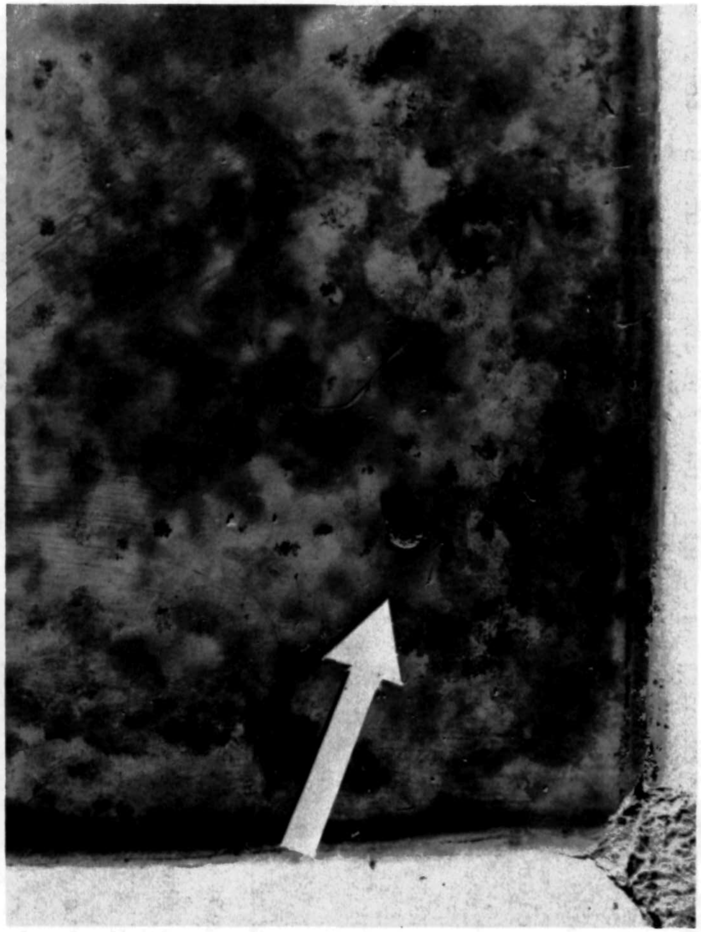

AG-4 FACING ZN-3

SA-1377-33

FIGURE 2 TYPICAL ZINC NODULE CAUSING CELL FAILURE (CELL NHS-114-30)

Zinc penetration and shorting were the faults associated most frequently with failure of cells in this program. Two physically and electrically different types of zinc shorts were found. The most frequently encountered type consisted of a single hard nodule of zinc (usually 1 to 2 mm in diameter); an example is shown in Figure 2. As a rule, this nodule formed a bridge between a negative and a positive bag* and made electrical contact with both plates. Separation of the plates in an attempt to further disassemble the cell pack tended to rip out the nodule from one of the electrodes, leaving a hole in the bags and, occasionally, a crater in either or both the zinc and the silver electrodes. This general type of zinc nodule short was usually observed in cells subjected to relatively high current, deep discharges such as those applied in the 100% DOD regime or in the reconditioning cycles following standing periods.

The second type of zinc short was associated with the development of several fern-like, dendritic growths of zinc crystals between bags. Electronic contact of the dendrite structures to one or the other electrode (usually the zinc negative) could frequently be demonstrated, but contact to both electrodes could not normally be shown because the dendrites tended to adhere preferentially to one of the electrodes upon separation of the bagged electrodes. This type of zinc shorting is assumed to occur via relatively fine dendritic filaments penetrating both separator bags to their electrodes and connecting them with the fern-like structures. Several attempts to find such filaments with a low power microscope were unsuccessful, probably because of insufficient resolution. However, an electric proof of such shorts was frequently available in that the voltage between electrodes so shorted rose rapidly after some displacement of the electrode bags with respect to each other, presumably because this resulted in a breaking of the shorting filament(s).

Shorts of a similar kind are likely to be involved also in connecting the zinc masses extruded from splits in the negative electrode bags with the silver positive--another relatively frequently observed fault of cells failed by shorting.

---

*No preferred location of the nodule on bag faces was evident.

Silver deposition in separators is a recognized problem in secondary alkaline cells that use silver positives and conventional cellulosic separators. Besides representing an irreversible loss of positive plate capacity, the metallic silver deposited in separators by chemical reaction involving dissolved silver oxide can eventually cause cell failure by shorting.*

As shown in Table 13, the failed cells examined in this program frequently had significant amounts of metallic silver deposited in finely divided form throughout the separator bags especially on the silver positives. Although these deposits represent a loss in positive plate capacity, capacity loss per se was not an important cause of failure for cells cycling on the regimes used in this testing program.

Regarding the possibility that the silver deposits may have caused (or contributed to) cell shorting, electrical probing even of obviously attacked, blackened silver electrode bags did not reveal any metallic shorts if bags were free from zinc nodules or dendrites. Accordingly, cell shorting by the metallic silver deposits, formed in semiflexible separators by the reaction of their partly organic coating with dissolved silver oxide, does not appear to be a failure mode for the cells examined by us. The silver analysis of electrode bags nevertheless yielded interesting results that are discussed further below, together with some comments regarding formation and effects of silver deposits.

Nominally low capacity without evident or suspected zinc shorts was the exclusive cause of failure for only five of the 48 cells analyzed at SRI. To put this finding in perspective, it must be remembered that

---

*Silver shorting is particularly important (relative to other failure modes) in silver-cadmium cells with cellulosic separators.

Table 13

SILVER CONTENT OF SEPARATORS FROM FAILED CELLS

Cell No.	Design	Regime	Temperature* (°K)	Temperature* (°C)	Cycle Life	Wet Life	Ahr Discharge Per Plate	Separator Identity†	Silver Content mg/cm²	Comments
HS-15-1-1	$1b^+/2b^-$	VK-1‡	297	24(C)	630	1058	882	Zn-1: case	0.05	Pure white color, facing case. Asbestos side is unstained.
HS-15-1-1	$1b^+/2b^-$	VK-1	297	24(C)	630	1058	882	Zn-1: Ag-1	1.07	Very pale gray color suggesting some silver deposition.
HS-15-1-1	$1b^+/2b^-$	VK-1	297	24(C)	630	1058	882	Ag-1: Zn-1	20.5	Very dark, almost black 3420-09 separator, coating tender.
HS-51-1	$3(5b^+/6b^-)$	VK-1	297	24(C)	799	1159	639	Ag-3: Zn-3	21.5	All bag surfaces are darkly stained.
HS-61-2	$7(6b^+/5b^-)$	VK-1	297	24(C)	430	555	344	Zn-2: Ag-3	0.85	A large light colored mottle analyzed.
HS-61-2	$7(6b^+/5b^-)$	VK-1	297	24(C)	430	555	344	Ag-3: Zn-2	11.8	Med. colored mottle opposite sample from the Zn-2 bag.
HS-82-2	$7(6b^+/5b^-)$	VK-1	305	32(C)	679	848	543	Zn-4: Ag-4	3.26	Specimen taken above slump, opposite Ag_2O coated Ag electrode.
HS-82-2	$7(6b^+/5b^-)$	VK-1	305	32(C)	679	848	543	Ag-4: Zn-4	21.1	Specimen taken above slump, opposite Zn-4 specimen.
HS-82-2	$7(6b^+/5b^-)$	VK-1	305	32(C)	679	848	543	Zn-4: Ag-4	2.09	Specimen taken over slump, opposite discharged Ag electrode.
HS-82-2	$7(6b^+/5b^-)$	VK-1	305	32(C)	679	848	543	Ag-4: Zn-4	15.9	Specimen taken over slump, opposite Zn-4 specimen.
HS-59-6	$7(6b^+/5b^-)$	VK-2	297	24(S)	699	1107	629	Ag-4: Zn-4	10.7	Charged stand cell; on stand ~ 25 months.
HS-59-12	$7(6b^+/5b^-)$	VK-2	305	32(S)	1	732	<4	Ag-2: Zn-2	10.9	Charged stand cell, failed its first reconditioning cycle.
HS-59-19	$7(6b^+/5b^-)$	VK-2	283	10(S)	480	1035	432	Ag-5: Zn-5	4.4	Float charged stand cell; on stand ~ 25 months.
HS-59-26	$7(6b^+/5b^-)$	VK-2	305	32(S)	1	745	<4	Ag-3: Zn-3	19.2	Float charged stand cell; on stand ~ 25 mo.; failed reconditioning cycle.
HS-66-11A	$8(6b^+/5b^-)$	VK-2	297	24(S)	2	756	<4	Ag-4: Zn-3	4.34	Discharged stand cell; on stand ~ 25 mo.; failed reconditioning cycles. Has layer of unsupported separator between bags.
NHS-114-6	$7(6b^+/5b^-)$	VK-3	297	24(C)	336	250	941	Ag-2: Zn-1	32.7	Delivered ~4700-Ahr discharge in its lifetime. Darkest bag and darkest area selected for analysis.
NHS-114-6	$7(6b^+/5b^-)$	VK-3	297	24(C)	336	250	941	Zn-2: Ag-2	0.06	Rather light colored bag surface.
NHS-114-6	$7(6b^+/5b^-)$	VK-3	297	24(C)	336	250	941	Ag-2: Zn-2	24.5	Sample approx. opposite the sample Zn-2:Ag-2.
NHS-114-28	$7(6b^+/5b^-)$	100% DOD	297	24(S)	17	620	595	Ag-1: Zn-1	16.4	
NHS-114-28	$7(6b^+/5b^-)$	100% DOD	297	24(S)	17	620	595	Ag-1: case	1.55	Although the coating was darkly stained, it had only one-tenth the silver that the other working face of the bag had.
HS-54-6	$5(4b^+/\ell/5b^-)$	100% DOD	297	24(C)	136	884	~915	Zn-2: Ag-1	2.19	This design had a coated asbestos layer between bags, with the coating facing the Ag electrode; capacity on last cycle was only 3.24 Ahr.
HS-54-6	$5(4b^+/\ell/5b^-)$	100% DOD	297	24(C)	136	884	~915	Ag-1: Zn-2	40.9	
HS-54-6	$5(4b^+/\ell/5b^-)$	100% DOD	297	24(C)	136	884	~915	§	4.20	

* Letters in parenthesis indicate whether test temperatures apply to cycling (C) or standing(S) conditions. All standing cells were cycled (if capable) at room temperature; for these cells,

† As an example of the notation used, Ag-4:Zn-3 means that the sample was taken from the bag surrounding silver electrode No. 4 on the side facing zinc electrode No. 3.

‡ Regime modified by prorating currents down to capacity of 3-plate cells.

§ Sample cut from extra layer facing Ag-1.

these failures all were from the Viking cell group for which "failure by low capacity" is defined as the inability to deliver a specified minimum capacity after the third reconditioning cycle.* This was a more severe capacity test than those implicit in the VK-1, -2 and -3 continuous cycling regimes. Accordingly, many if not all of these low-capacity failures probably would have cycled on the VK-2 regime applied to Viking cells passing the reconditioning step. In agreement with the NASA project manager, this assumption was tested on three low-capacity cells and confirmed by achieving 232, 319 and 667 cycles, respectively. Inasmuch as shorting by zinc nodules or dendrites was the cause of their eventual failures, these cells were not included in the group of low-capacity failures.

A substantial number of cells that failed on various cycling regimes had low capacity in addition to other symptoms of failure. Specifically, of the sixteen cells showing this second type of low capacity, six had definite zinc nodule shorts, the remainder gave indications of zinc filament-type shorts. It is likely, therefore, that the low capacity of these cells was due, at least in part, to zinc shorts not massive enough to prevent charging but sufficient to drain away much of the cell charge.

To provide some perspective as to how frequent--and, hence, how important--the various faults and failures discussed in the foregoing are for the cells tested and analyzed in this program, a statistical breakdown is given in Table 14.

---

*After standing for 21 to 25 months, Viking cells were discharged at 7 A; low capacity (but not failure) was diagnosed if the delivered capacity was less than 21 Ahr. Two complete charge-discharge cycles were then applied; a cell was declared failed if it failed to deliver 21 Ahr plus a 40-second pulse of 12A with the cell voltage maintained above 1 V .

Table 14

CELL FAILURE ANALYSIS: STATISTICAL BREAKDOWN OF FAULTS* AND FAILURES†
(for cells failed before October 31, 1972)

Total number of cells analyzed at SRI	48
<u>Faults</u>	
Leaks	34
Split bags	26
Zinc nodule shorts (confirmed)	28
Zinc dendrite shorts (probable)	15
Low capacity	21
Zinc electrode slumping	4
Zinc electrode erosion	10
<u>Total Faults</u>	138
<u>Physical and(or) Formal Causes of Cell Failure</u>	
Zinc nodule short	28†
Zinc dendrite or filament short	15†
Nominally low capacity (Viking standing cells only)	5‡
<u>Total Failures</u>	48

---

*Faults may or may not be associated with cell failures; most cells had several faults.

†The most probable physical cause of cell failure, based on failure analysis results.

‡Failure to pass capacity test in reconditioning procedure.

Failure Modes: Breakdown by Cell Test Group

The overall failure statistics given above indicate that zinc nodule and dendrite(filament) shorting together accounted for nearly all failures in each cell test group. However, there were sufficient systematic differences in the fault and failure patterns of cells from different groups to warrant a breakdown of failure analysis findings; this breakdown by cell test group is shown in Tables 15 through 21. The major findings from the analysis of these tables can be summarized as follows:

1. Zinc nodule shorts were the almost exclusive failure mode of cells subjected to 100% DOD with charged stand between periodic discharges. This failure mode is also dominant for Viking cells of the charged and float-charged stand subgroups that failed during stand or early in subsequent cycling, and for the Temperature-Battery/Cell group. Inasmuch as several more cells from other groups failed early by this mode, failure analysis has established zinc nodule shorts as the major cause for early cell failures. Zinc nodule shorts were not observed in the few failed cells from the Viking discharged-stand category.

2. Shorts associated with presence of dendritic and mossy zinc (and ascribed to zinc filament penetration) are the dominant failure mode for those cells from the Viking and other groups that attained at least several hundred cycles on the VK-1 and VK-2 regimes and are the exclusive failure mode for cells cycling on the VK-3 regime.

3. Nominally low cell capacity by the criteria applied to the Viking cell group was the cause for the five remaining failures; these included primarily the four cells from the discharged-stand group that failed in the reconditioning step. Two of these failures may not be representative inasmuch as the cells had been subjected to significant periods ($3\frac{1}{2}$ and $7\frac{1}{2}$ months) of charged stand at $52^{\circ}C$

before being put on the routine 21 to 25 month discharged stand; a third one showed generally atypical behavior for this group (see 7., below). Our experience strongly suggests that all cells failed due to nominally low capacity would have been capable of extended cycling on the VK-2 regime.

4. The survival rate and cycling capability of charged-stand and float charged-stand Viking cells in the reconditioning step are greatly decreased at stand temperatures of 32^{o}C and above.

5. Bag splits were common in all cell groups with the exception of the Viking charged-stand and float charged-stand categories and the Plate-Lock Cell subgroup cycled on 100% DOD. However, no correlation is apparent between bag splits and a particular failure mode.

6. All 3-plate cells (lids sealed with RTV silicone adhesive only) developed leaks. A substantial percentage of the cells in all other groups also were leaking but no direct correlation is apparent between cell leakage and a particular failure mode.

7. Half of the cells showing zinc electrode erosion, and (with one exception) all cells showing electrode slumping were from batteries of the Temperature-Battery/Cell group. The exception was a cell from the Viking discharged-stand category; this cell also had significant erosion--both atypical faults for the Viking cell group.

Table 15

CELL FAILURE ANALYSIS:
3-PLATE PILOT CELLS*
(Status as of 31 October 1973)

Cell No.	Cycle Life	Wet Life (d)	Leaks† ‡	Bag Splits	Slumping ‡	Erosion	Failure Notations
HS-15-1-1	630	1085	+	+	-	-	External mossy zinc shorting at bottom bag edges and probably low capacity.
HS-15-1-2	555	984	+	+	-	-	External zinc deposits near bottom. Low capacity.
HS-16-1-1	835	1288	+	+	-	-	Zn nodule shorts, plus external mossy Zn deposits.
HS-16-2-1	633	1085	+	-	-	-	Low capacity, probable occasional transitory shorts.
HS-16-2-2	480	937	+	+	-	-	Elec. behavior suggests a short. External Zn deposits, top and bottom

* Cycling was on VK-1 regime, modified by prorating currents down to the capacity of 3-plate cells; cell temperature was nominally 24°C.

† Three-plate cells had lids sealed to cases with silicone RTV adhesive instead of regular (ultrasonic weld plus epoxy) seals.

‡ Here and in the following tables, the symbols "+" and "-" indicate that a particular type of fault was observed or not observed, respectively.

Table 16

CELL FAILURE ANALYSIS:
VIKING, CHARGED WET STAND CATEGORY*
(Status as of 31 October 1972)

Cell No.	Stand. Tempera- ture (°C)	Cycle Life†	Wet Life(d)	Leaks	Bag Splits	Slumping	Erosion	Failure Notations
HS-59-2	10	209	861	-	+	-		Zn nodule short between plates.
HS-59-3	10	143	813	slight	-	-	-	Zn nodule short between plates.
HS-59-6	24	699 [761]	1107 [1140]	slight	-	-	-	Zn dendrite slow short and low capacity.
HS-59-7	24	0	752	slight	-	-	-	Low capacity and Zn nodule short and low capacity prior to recondition cycle.
HS-59-8	24	474 [663]	994 [1112]	slight	-	-	-	Some Zn dendrites between bags and low capacity.
HS-59-9	24	610	1062	slight	+	-	-	Many Zn dentrites and shorting nodules and low capacity.
HS-59-10	24	476 [630]	994 [1088]	slight	-	-	-	Many adherent Zn dendrites between bags and low capacity. Coating cracks noted over cemented areas.
HS-59-12	32	0	722	Heavy	-	-	-	Low capacity before reconditioning. Could not be reconditioned.
AH-39-1	42	0	698	-	+	-	-	Zn nodule short between plates, low capacity before reconditioning.

*Cycling is on VK-2 regime after 21 to 25 months stand at various temperatures.

†The cycle and wet life data given in this table refer to the first failure of a cell; for most cells, this was also the ultimate failure because they could not be made to cycle thereafter. However, for a number of cycling cells capable of accepting charge but failing to maintain a voltage above 1.0 V during discharge additional cycles were obtained by the following procedure: (1) a discharge half-cycle was skipped and the cell returned to its normal cycling regime; (2) the procedure was repeated after each of the next two failures to maintain 1.0 V during discharge; (3) a reformation charge was applied after the fourth such failure and the cell put back on cycling; (4) after the next failure, the cell was permanently removed from cycling. The numbers in brackets represent the ultimate cycle and wet life so achieved.

Table 17

CELL FAILURE ANALYSIS:
VIKING, FLOAT CHARGED STAND CATEGORY*
(Status as of October 31, 1972)

Cell No.	Stand. Tempera- ture (°C)	Cycle Life‡	Wet Life	Leaks	Bag Splits	Slumping	Erosion	Failure Notations
HS-59-15†	10	3(232)	771(911)	+	-	-	-	Zn nodule short between plates. Also low capacity prior to reconditioning.
HS-59-18	10	152	869	-	-	-	-	Zn nodule short between plates.
HS-59-19	10	480	1035	+	+	-	-	Zn nodule short between plates, and much external Zn deposits. Definitely not low capacity. Capacity check prior to reconditioning yielded 45.2 A hr.
HS-59-21†	24	3(471) [677]	756(1032) [1136]	slight	-	-	-	Many adherent dendrites between bags; low capacity.
HS-59-22†	24	560 [650]	1076 [1126]	+	-	-	-	Many adherent dendrites between bags; low capacity.
HS-59-26	32	0	745	-	-	-	-	Low capacity.
HS-59-27	32	0	742	slight	-	-	-	Low capacity.
HS-61-14	32	379	974	+	-	-	-	Zn dendrite short. Also low capacity.

*Cycling is on VK-2 regime after 21 to 25 months stand at various temperatures.

†These cells failed in the last reconditioning cycle but were put on VK-2 cycling at the request of the NASA Project Manager. Numbers in parentheses refer to cumulative cycle and wet life until first failure during cycling on VK-2.

‡See last footnote on Table 16.

Table 18

CELL FAILURE ANALYSIS:
VIKING, DISCHARGED WET STAND CATEGORY*
(Status as of October 31, 1972)

Cell No.	Stand. Temperature (°C)	Cycle Life	Wet Life(d)	Leaks	Bag Splits	Slumping	Erosion	Failure Notations
HS-66-11A	24	0	756	-	-	Slight	+(significant)	Low capacity
AH-39-3	24	0(319)†	699(908)†	-	+	-	-	Low capacity (shorting) mossy Zn dendrites between bag faces
AH-39-4	24	0	699	+	+	-	-	Low capacity

*Cycling is on VK-2 regime after 21 to 25 months stand.

†Cell failed in first reconditioning cycle and was put on VK-2 cycling at the the request of the NASA Project Manager; numbers in parentheses refer to cumulative cycle and wet life.

Table 19

CELL FAILURE ANALYSIS:
TEMPERATURE-BATTERY/CELL GROUP*
(Status as of October 31, 1972)

Cell No.	Temperature (^{o}C)	Cycle Life	Wet Life	Leaks	Bag Splits	Slumping	Erosion	Failure Notations
HS-61-1	24	429	554	Slight	+	-	-	Slow short; wouldn't charge. Much external mossy Zn. Low capacity.
HS-61-2	24	430	555	Slight	+	-	Slight	Zn nodule short.
HS-61-3	24	576	701	+	+	-	+	Small Zn nodule short plus much external Zn.
HS-61-4	24	430	555	-	+	Slight	Slight	Slow short. Wouldn't charge. Much external Zn deposits.
HS-61-10	10	598	785	+	+	Slight	+	Zn nodule short plus much external Zn deposits
HS-82-2	32	678	832	+	+	+	Slight	Zn nodule short between plates.

*All cells are of Design 7; cycling is on VK-1 regime at various temperatures.

Table 20

CELL FAILURE ANALYSIS: PLATE LOCK CELL GROUP*
(Status as of October 31, 1972)

Cell No.	Cycle Life	Wet Life(d)	Leaks	Bag Splits	Slumping	Erosion	Failure Notations
Cells Tested on VK-3 Regime							
NHS-114-6	336	250	-	+	-	-	Probable small short. Couldn't charge.
NHS-114-9	261	223	+	+	-	-	Elect.short in cell. Much external Zn deposits.
NHS-114-13	404	285	Slight	-	-	+	Couldn't charge. Much external Zn may have shorted.
NHS-114-23	457	307	+	+	-	-	Evidence of large dendrites between plates.
NHS-114-36	497	323	+	+	-	-	Probable short via much external Zn deposits
NHS-114-38	491	322	-	+	-	-	Feathery Zn dendrite shorts between bag faces and at edges; low capacity.
Cells Tested on 100% DOD Regime							
NHS-114-1	18	635	-	+	-	-	Zn nodule short between electrodes.
NHS-114-2	16	605	-	-	-	Slight	Zn nodule short between electrodes.
NHS-114-20	14	536	?	-	-	-	Zn nodule short between electrodes. Cell exploded on stand.
NHS-114-28	17	620	-	-	-	-	Zn nodule short between electrodes.
NHS-114-34	21	747	-	-	-	-	Zn module short between electrodes.

*Cycling is performed at laboratory temperature (nominally 24°C)

Table 21

CELL FAILURE ANALYSIS:
DESIGN VARIATION AND EXTRA CELL GROUPS*
(Status as of October 31, 1972)

Cell No.	Design	Regime	Cycle Life	Wet Life	Leaks	Bag Splits	Slumping	Erosion	Failure Notations
HS-66-2	7†	VK-1	348	477	Slight	+	-	Slight	Much external zinc; indication of electrical short.
HS-47-8	2‡		283	646	Slight	-	-	-	Zn nodule short.
HS-51-1	3‡		799	1159	Heavy	+	-	-	Zn dendrite short through Ag and out to massive Zn.
HS-51-2	3‡		738	1098	Heavy	+	-	-	External heavy deposits of Zn at bottom. Massive Zn shorts.
HS-51-3	3‡		636	996	Heavy	+	-	-	External heavy deposits of Zn at bottom. Massive Zn shorts.
HS-54-6	5‡	100%# DOD	136	884	Slight	-	-	-	Zn dendrite at faces; no external Zn; low capacity (3.24 A hr)

* Cycling is at laboratory temperature (normally 24°C)

† From Design Variation Group

‡ From Extra Cell Group

\# Prior to transfer to SRI, the cell was cycled at rates varying from once per day to once per two weeks. In the 4-month period prior to transfer cycling rate averaged ~once per 3-days. At time of transfer, the cell had accumulated 129 cycles. The charge input is at 1.5A to 2.00V. The discharge is at 6A to 1.00V, then 2A to 1V .

Discussion

In judging the significance of the findings of the cell testing program and their implications, it is well to remember that the large fluctuations associated with the small number statistics governing the results of this test program tend to introduce considerable uncertainties, especially in attempts toward a more detailed analysis. However, as will be shown, the test program has provided (and continues to provide) meaningful answers to the most important questions pursued.

Major Testing Objectives and Cell Failure Modes

The major objective of the silver-zinc cell development and testing program initiated at Astropower Laboratory--and continued with the remaining testing at SRI--was the demonstration that the use of largely inorganic separators imparts long stand and cycle life to silver-zinc cells. Although all cell test groups discussed in previous sections were designed to contribute information toward this objective, the Viking cell group has a somewhat special role in that it addresses the central questions of how extended stand--and the electric/electrochemical and temperature conditions of cells during stand--affect cell life. In this connection, the much higher survival rate of cells standing in the discharged state and their subsequent, better cycle life capability are key findings. The results of the failure analysis (Table 18) indicate that failures in this cell test category, whether encountered during reconditioning or in subsequent cycling, are never due to zinc nodule shorts--the primary failure mode associated with early cell failures. In particular, nominally low capacity was the only apparent fault with the few cells failing the reconditioning procedure after about two years' discharged stand. Furthermore, half of these cells had actually been subjected to lengthy charged stand at elevated temperatures before their discharged stand period--a procedure that might have contributed to their eventual failure. The successful attempt to cycle one of these cells suggests that all of the Viking discharged-stand cells could have cycled on the VK-2 regime.

In contrast, a significant percentage of the Viking cells standing on charged and float-charged stand (see Tables 16 and 17) failed by zinc nodule shorts in the reconditioning cycles or within the first few hundred cycles thereafter. Inasmuch as formation of zinc nodules at least during open circuit charged stand appears unlikely, the possibility must be considered that the shorting nodules were formed predominantly during the reconditioning cycles. One possible reason why this occurred only in charged- and float charged-stand cells is that the greater availability of dissolved silver oxide in charged cells caused a correspondingly larger attack on the organic phases of the semiflexible separator bags during the extended stand period. Separators so weakened might not be able to prevent formation of zinc nodule shorts in the reconditioning cycles. Silver analysis data in fact suggest* that separators are significantly more attacked in charged-stand and float charged-stand cells.†

---

*See Table 13: compare silver bag analyses for early cell failures HS-59-6 and -12 (charged stand) and HS-59-26 (float charged stand) with HS-66-11A (discharged stand).

†A hypothetical failure mechanism may be sketched as follows: zinc dendrites are growing through a few large pores (or faults) in the zinc electrode bag. If these dendrites face an intact silver electrode bag, the probability for individual zinc dendrites to find a large pore or fault in that bag is very small, and dendrites tend to grow parallel to, and between bags instead. If the silver bag has been heavily attacked, on the other hand, the probability is much increased for at least one or perhaps a few zinc dendrites to line up with large pores or faults in the silver bag. Where this occurs, the current density and overpotential will be increased locally, thus further increasing the tendency for the zinc dendrite(s) to grow; this effect will increase with increasing penetration and favor growth of the dendrite that has penetrated farthest toward the silver electrode. The zinc dendrite(s) may also grow in circumference by mechanically displacing some of the weakened separator structure. Eventually (possibly even within a few cycles if separators are sufficiently weakened), a massive zinc nodule short can form and bridge to the silver positive, causing irreversible cell failure.

As expected, attack by silver oxide is less in cells standing at a lower temperature (Table 13, cell HS-59-19); at the same time, the survival rate and subsequent cycling capability of such cells is increased (Table 5). Increased standing temperature, on the other hand, is highly detrimental: all except one of the charged-stand or float charged-stand cells in the $32^{o}C$ and $42^{o}C$ subgroups failed in the reconditioning step, either by zinc nodule shorts or by low capacity. As expected, their silver electrode bags had the highest silver content (for a given wet life) of all separators analyzed.

Another interesting finding is that, to date, there are no failures among the four Viking cells put on cycling immediately after the initial formation cycles. In considering possible benefits for cell life of shallow cycling versus discharged stand, it must be remembered that four of five failed discharged-stand cells failed due to nominally low capacity, with the further qualification that two of these cells had a non-representative history. Because of the shallow depth of discharge of the VK-2 regime, this failure mode will not be observed in the Early Cycling category of cells until cell capacities will have declined to a much lower level than 21 Ahr. Thus, a cell failing the reconditioning step may not yet be failing on the VK-2 regime. Substantially longer cycling of live cells will be required to decide whether a real difference exists in the wet life and cycle life capabilities of immediately cycled cells and cells standing in the discharged condition prior to cycling.

In further scrutiny of the major failure patterns versus group behavior, it is to be noted that zinc nodule shorts are the exclusive failure mode of plate-locked cells cycled on the 100% DOD regime. Nearly all of the wet life of these cells is spent in the charged stand condition, and the charge-discharge cycling is to 100% completion--conditions not unlike those encountered by the charged-stand category of the Viking cells subjected to the reconditioning cycles. It is suggested that the failure mechanisms are correspondingly similar: inability of the separator--weakened by long wet life in a charged cell--to withstand penetration by shorting nodules that tend to form in deep cycling. On the other hand, plate-locked cells failed during cycling on the VK-3 regime did not exhibit any zinc nodule shorts despite the fact that its 35% DOD makes this regime the most stressful of the three continuous cycling regimes and resulted in a relatively low cell cycle life. The correspondingly short wet life and small extent of separator degradation in these cells may be the explanation for this behavior.

<u>The Temperature-Battery/Cell</u> group is the only other test group with a significant number of failures by zinc nodule shorts. At first glance, this observation appears to deviate from the pattern because these cells are cycled continuously on the low-stress VK-1 regime. However, attention is drawn to the fact that every one of the cells failed by zinc nodule shorts is from a cell subgroup cycled as a battery. Thus, this type of failure appears to be associated not only with weakened separators failing in deep discharges but also under the stresses (such as overcharge and gassing) that can result for some of the cells in a battery, especially later in life when cell imbalances have developed. Note also that cells cycling on the VK-1 regime tend to be in an almost fully charged state most of their lives--a condition favoring high levels of separator-degrading silver oxide in the cell electrolyte.

It is noteworthy that failed cells from the Temperature-Battery/Cell group were significantly inferior to the cells from other groups which were cycled on the VK-1 regime in other respects also: as a group they had the lowest wet and cycle lives, showed split bags in every cell, and included most of the few incidences of zinc electrode erosion and slumping. If we attribute these small-sample observations largely to operation of cells in batteries, the conclusion is that cycle and wet stand life tend to suffer if cells encounter uncontrolled charge (and overcharge), especially later in their wet lives when separators are likely to be weakened.

The second major failure mode for all cell groups and test conditions--dominant for cells that did not fail by zinc nodule shorts in their first 800 to 900 days of wet life--is shorting by relatively fine (filament-type) dendrites. As a rule, this type of short could not be demonstrated directly with disassembled cells but was inferred from several independent observations. Its electrical characteristic ranged from that of fairly massive shorts (probably due to multiple shorting by zinc dendrites) which tended to prevent cells from being charged at all, to slow shorts that were usually associated with and at least partially responsible for, low cell capacity. Several Viking cells with slow shorts were made to deliver additional cycles by skipping a few discharges, see Tables 15 and 16.

Filament shorts were found quite universally for cells from every test group and every continuous cycling regime when the failed cell had achieved typically 400 to 500 or more cycles on the VK-1 and VK-2 regimes, and about 250 or more cycles on the VK-3 regime. This type of short apparently forms during continuous cycling at low to moderate rates and depth of discharge. It is almost always associated with presence of zinc external to the separator bags, either in the form of mossy zinc extruded at the seams of split bags, or, in the absence of bag splits, as zinc dendrites growing along separator surfaces in the narrow space between negative and positive bags. The latter type was observed in about one-third of all dendrite shorts, suggesting that zinc dendrite shorting through separator bags is the most probable ultimate failure also of cycling cells with intact bags.

Other Testing Objectives

Turning to the specific objectives pursued with the smaller cell test groups and subgroups, the cycling results obtained in the Design Variation and Extra Cell groups show that cycle life and wet life increase with increasing number of separator layers between positives and negatives, as expected whenever shorting is the dominant failure mode. However, since zinc bag splits and extrusion of zinc into the void spaces around bags were quite common, it is probable that the extra sheet of separator was less effective in increasing cycle life than a complete, intact bag would have been. This conclusion is supported by the test results* obtained in the Three-Plate Pilot Cell group: Cell HS-16-2-2, which had a separator sheet-covered silver positive and was found to have a split zinc electrode bag, had the shortest cycle life among the cells of this group; a similar cell (HS-16-1-1) with a bagged silver electrode had nearly double the cycle life.

The Plate-Lock group cycling results indicate that plate-locking tends to reduce cell wet and cycle life although extended cure of the epoxy cement used in the plate lock appears to alleviate this effect somewhat. An interesting feature of cells in this group was that the voltage "spike" for the silver (I) - silver (II) transition was absent in the cycling curves† for two aging cells with normally cured epoxy plate lock--in sharp contrast to the behavior of nearly all other cells. It appears possible that a component (such as an amine) released from the epoxy may have influenced this silver oxide phase transformation by adsorption but it is not clear to what extent such adsorption could have a negative effect on cycle life. Environmental testing appears to have no effects on the wet and cycle life of plate-locked cells.

---

*See Table 15.

†See Section on Cycling Curves, below.

The main finding from testing the Temperature-Battery/Cell group--the inferior performance of cell cycled as batteries--has already been mentioned above. The temperature factor appears to be less significant in comparison, showing only a slight superiority of cells and batteries cycled at $10^{o}C$ over those cycled at 24 and $32^{o}C$, respectively. This is in contrast to the significant temperature influence on Viking cells standing on charged- and float charged-stand. A rather speculative explanation is that the favorable influence of $10^{o}C$ during standing and the apparently negative influence of this temperature on cycling have compensated each other for the Viking cells. More information on the temperature factor on cycle life is clearly desirable.

Bag Splits

This fault deserves special discussion not only since it was found so frequently in the Astropower-type silver zinc cells tested under this program but because the suggestion had been made that bag splits may be a major cause of premature cell failure.

An immediate comment is that bag splits were not in any way related to zinc nodule shorts, the dominant mode of early cell failure. Bag splits were observed only in a minority of cells so failed, and the mechanism of their failure must involve zinc penetration through bags--especially through weakened bags as discussed above.

The extent to which split bags may have shortened the cycle and wet life of cells failed by filament-type zinc dendrite shorts is more difficult to assess. Almost all cells on the VK-1 and VK-3 regimes that failed by this mode also had split bags, and a short from the extruded zinc mass to the silver electrode was shown or suspected in a number of instances. On the other hand, the only three cells cycling on VK-1 not showing split bags had no more than average cycle and wet life. Compared to the cell groups cycling on the VK-1 and VK-3 regimes, Viking standing cells that had passed the reconditioning step and failed in cycling on the VK-2 regime showed a far smaller incidence of bag splits--even after eliminating the early (zinc nodule-caused) failures from the comparison. However, over their entire cycle life these Viking cells as a group delivered only about 10% more total charge per unit of plate area than the cells that had failed on the generally similar VK-1 regime. The failed VK-3 cells, on the other hand, delivered 2-1/2 times more charge although their bags were invariably split. It appears that split bags are at most a minor factor in reducing the life of cells on continuous cycling regimes.

The incidence of bag splits also does not appear to correlate with that of any other faults such as low capacity or leakage, nor with specific treatments such as heat sterilization, plate-locking, or environmental testing. However, the small statistical sample available for some of these correlations should be kept in mind.

As mentioned above, there was much lower incidence of bag splits in the cycling Viking cells compared to cycling cells from other groups; this observation is of interest in relation to causes and possible cures for the bag splitting problem. The differences in the cycling regimes do not provide an explanation of this finding. An obvious possibility, however, is in the manual cell building process: most Viking cells analyzed to date are from one series (HS-59) which might have experienced an uncontrolled difference of a fabrication or materials parameter favorably affecting bag cementing. Another possibility centers on the different treatment of cells prior to cycling. According to this hypothesis, the 2-year stand period (especially on charged- and float charged-stand) had weakened and softened separators to the point where the mechanical stresses exerted by the working zinc electrode in subsequent cycling resulted in straining of the bags rather than transfer of stresses to the cemented bag seams.

Silver deposition

Silver shorting was not among the established causes for failure of cells tested in this program. However, the silver analysis* data of Table 13 can be used to show that the amount of silver found deposited in the separator bags of failed cells often was a significant fraction of the silver content of positive electrodes. For example, the silver lost from silver electrode No. 4 in Cell HS-82-2 is approximately 42.4 mg/cm^2,† or about 12% of the silver loading (23×10^3 $mg/66\ cm^2 \approx 350\ mg/cm^2$) of a representative new positive electrode. The largest deposits found in silver analysis (see Table 13) represent up to 25% of silver electrode loadings. In view of the uncertainties introduced by spot analysis, and considering that the effective positive capacity is typically only about 75% of that calculated from silver loading, it appears possible that silver deposits in semiflexible separators accounted for much of the irreversible capacity loss experienced by Viking charged-stand and float charged-stand cells in their 21-to 25-month standing period. This interpretation does not seem applicable to capacity loss of the failed discharged-stand cells; however, the capacity lost by some of these cells may be due in part to their charged-stand history prior to the routine discharged-stand period.

---

*Analysis was by conventional wet chemical techniques.

†The calculation is based on the data given in Table No. 13. It uses the average of two areas analyzed for silver and zinc bags and assumes that comparable amounts of silver would have been found in the separators on each side of the silver electrode.

The distribution of silver in the electrode bags offers some clues on how the deposits might have been formed. First, the deposits were in the form of black, microdispersed stains in which silver was apparently not sufficiently contiguous for metallic conductivity, suggesting that attack took place in many isolated locations. Second, although the degree of blackness was not a reliable indicator for the amount of silver,* it was nonetheless apparent that more silver was deposited in the asbestos support than in the inorganic/organic coating. This finding was somewhat unexpected because the pseudo-plasticizer--the organic phase thought susceptible to attack by dissolved silver oxide--is used in the coating only. A partial explanation might be that silver oxide reacts primarily with hydrolysis products† rather than with the plasticizer itself; these products are somewhat soluble and would tend to migrate toward a sink constituted by the zone in which the reaction with silver oxide takes place. Also, reaction of silver oxide with the resin coating‡ of the asbestos fibers may have contributed to making the silver concentration larger in the asbestos support than in the coating. A third possibility--silver deposition in separators by a zinc shuttle mechanism**--does not appear to be consistent with the experimentally found silver distribution.

---

*Some very darkly stained samples were found to contain less than 2 mg/cm^2; other samples with a silver analysis of over 10 mg/cm^2 showed medium-dark staining only. Also, zinc electrode bags stained to the same shade as the adjacent silver electrode bags showed nevertheless a tenfold lower silver analysis.

†The pseudo-plasticizer is an ester of a polyol and an organic acid; experience at Astropower Laboratory has shown that the ester undergoes hydrolysis in strong base.

‡Although this resin was found to be unreactive in bulk form, it might well be sufficiently reactive when finely dispersed on the surface of asbestos fibers.

**This mechanism has been invoked to explain silver track shorting of the type found occasionally in rigid inorganic separators. It proposes a cyclical growth of zinc dendrites during charge, followed during discharge by separation of the dendrite from the zinc electrode and electrochemical dissolution of the dendrite in a local cell reaction with silver oxide, causing deposition of a metallic silver track in the growth path of a zinc dendrite.

As mentioned earlier and shown in Table 13, the amount of silver deposited in separators increased significantly with increasing cell standing temperature. However, the data are insufficient to estimate the magnitude of temperature coefficients which could have indicated which step--diffusion or the chemical reaction itself--was controlling the rate of the silver deposition process.

Two other observations are of some interest; both are consistent with (although not a conclusive proof of) a mass transport-limited reaction. First, separators from cells cycling on the VK-3 and 100% DOD regimes had much larger silver deposits than those from cells on VK-1 and VK-2 regimes, in that order. In explanation, the more extensive volume changes associated with the deeper 100% DOD and VK-3 cycles would tend to promote convective mixing and mass transport of silver oxide; this effect should be smallest for Viking cells (VK-2 regime) since most of their wet life was spent standing. Second, separators from cells on the VK-1 regime showed an approximately linear increase of their silver deposits with cell wet life. Again this behavior would be expected for a diffusion-limited reaction as long as the rate-controlling concentration gradient is not changing appreciably.* This condition appears to be met for the silver oxide concentration gradient: during stand (or averaged over a number of cycles), the positive plate provides a constant-concentration source, the reaction zone with the plasticizer an approximately zero-concentration sink of silver oxide. Similar considerations apply to the alternate possibility--a reaction rate limited by diffusion of the plasticizer. As more analytical data for failed cells become available, firmer conclusions should emerge.

---

*Near zero concentration of silver oxide in the "reaction zone" within a separator would be expected if (1) the reaction itself is faster than mass transport (the assumption being tested in this model), and (2) only a small part of the plasticizer has reacted. The latter assumption is consistent with the findings for cells cycling on the VK-1 regime: typically, silver deposits were 20 mg/cm^2 whereas complete reaction of the plasticizer should result in a silver deposit of about 150 mg/cm^2. (Basis of estimate: complete oxidation of a compound with the approximate composition $(CH_2)_n$ to carbon dioxide).

Cycling Curves

For nearly all cells tested in this program, individual cycling curves of the type shown in Figures 3 through 14 were obtained throughout the cell life. The primary purpose in recording these curves was to document the basic cycling information (type of cycle; cycle life) for each cell* and to judge impending failures--and, once they occurred, their general type--from the electrical behavior of cells. Although a detailed analysis of the large number of cycling curves obtained is beyond the scope of this program, some of the features of these curves will be discussed here.

Figure 3 shows a representative set of curves for a Viking cell (1691 cycles as of October 31, 1972 , and continuing to cycle) at three stages of its life. Note the two different cycles of the VK-2 regime and the fact that the cell began its cycle life with a relatively low average state of charge (after delivering 21 Ahr in an initial performance test, see also Ref. 6.) Because of a slight excess charge in each cycle, the cell's average state of charge gradually increased as shown by the earlier rise to the silver (II) voltage plateau in cycles 400 and 401. The curves for these cycles also begin to show the voltage spike associated with the silver (I) oxide--silver (II) oxide transition which is generally displayed by alkaline cells using silver positives.

As shown in Figure 3, this spike had become higher, and the preceding voltage rise had become much more rapid as the cell had acquired about 1700 cycles; these features were shown by most of the cells tested in this program. In particular, the increasingly rapid voltage rise was universally† observed and could be used as a qualitative indicator for

---

* In a few instances where cells were tested as batteries, only the battery voltage was recorded but the voltages of individual cells were then monitored at least occasionally.

† Unless a cell already had sufficiently extensive shorting to prevent charge acceptance.

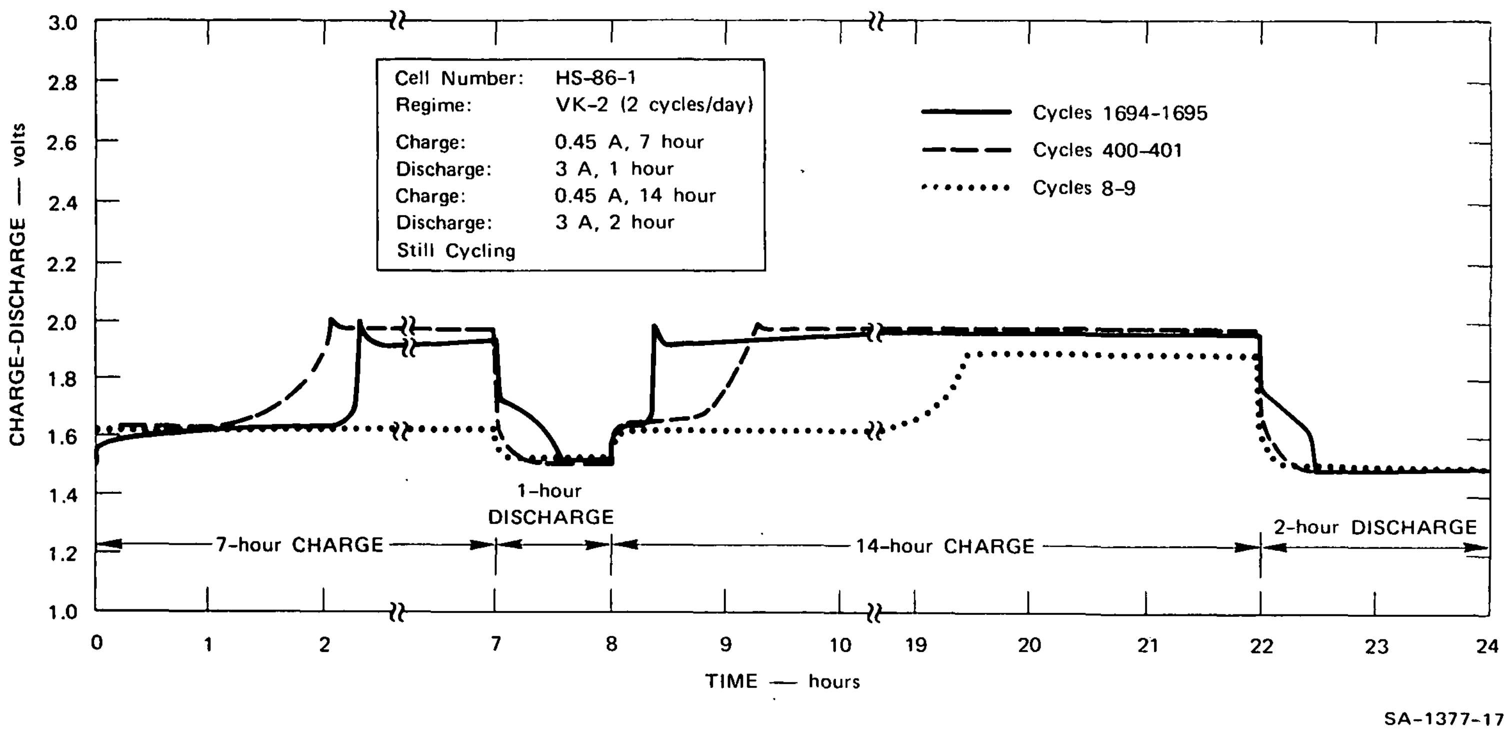

FIGURE 3 CYCLING CURVES (VIKING, EARLY CYCLING CATEGORY)

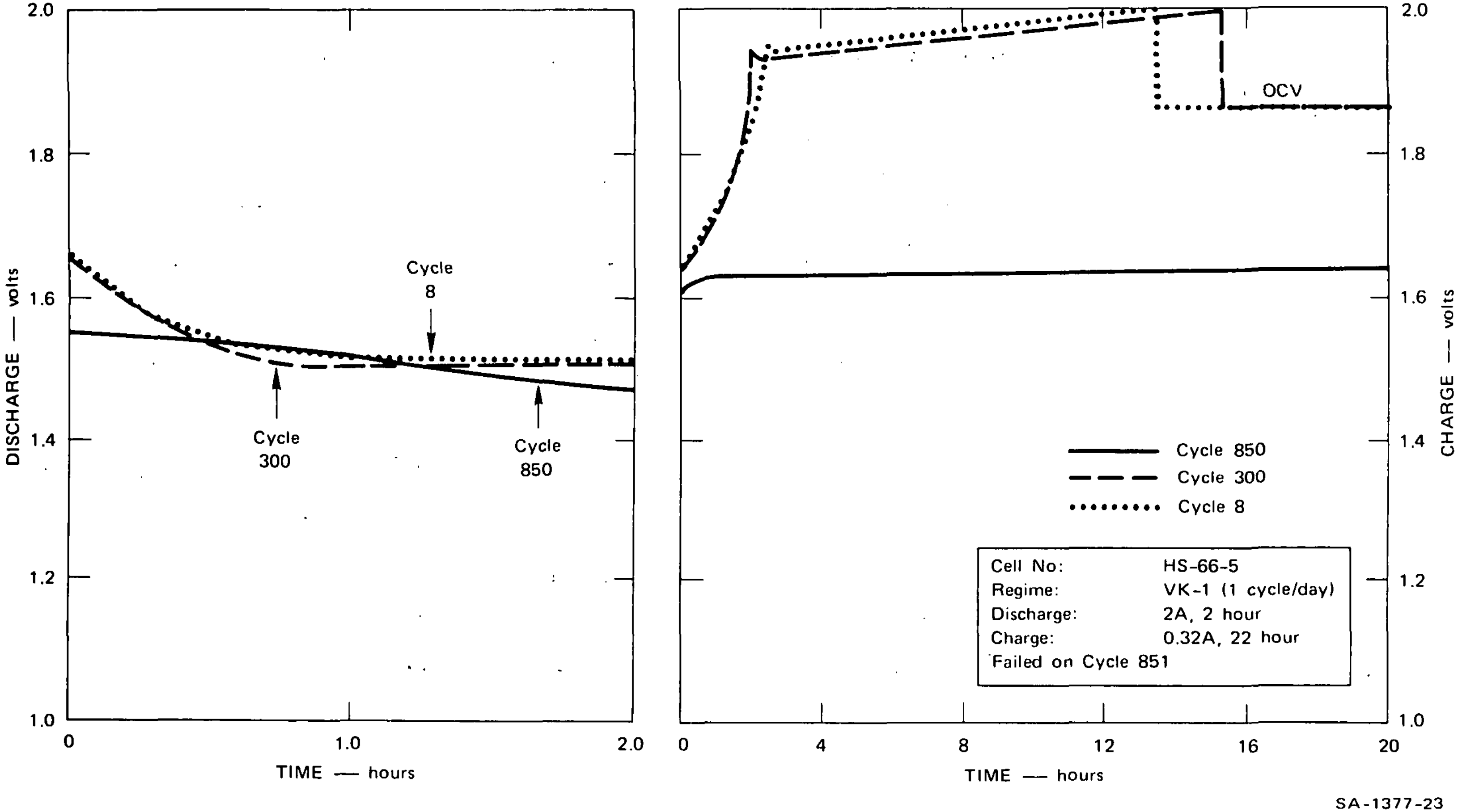

FIGURE 4 CYCLING CURVES (CELL IN A BATTERY WITH FOUR OTHERS)
(DESIGN VARIATION, DESIGN 7 SUBGROUP)

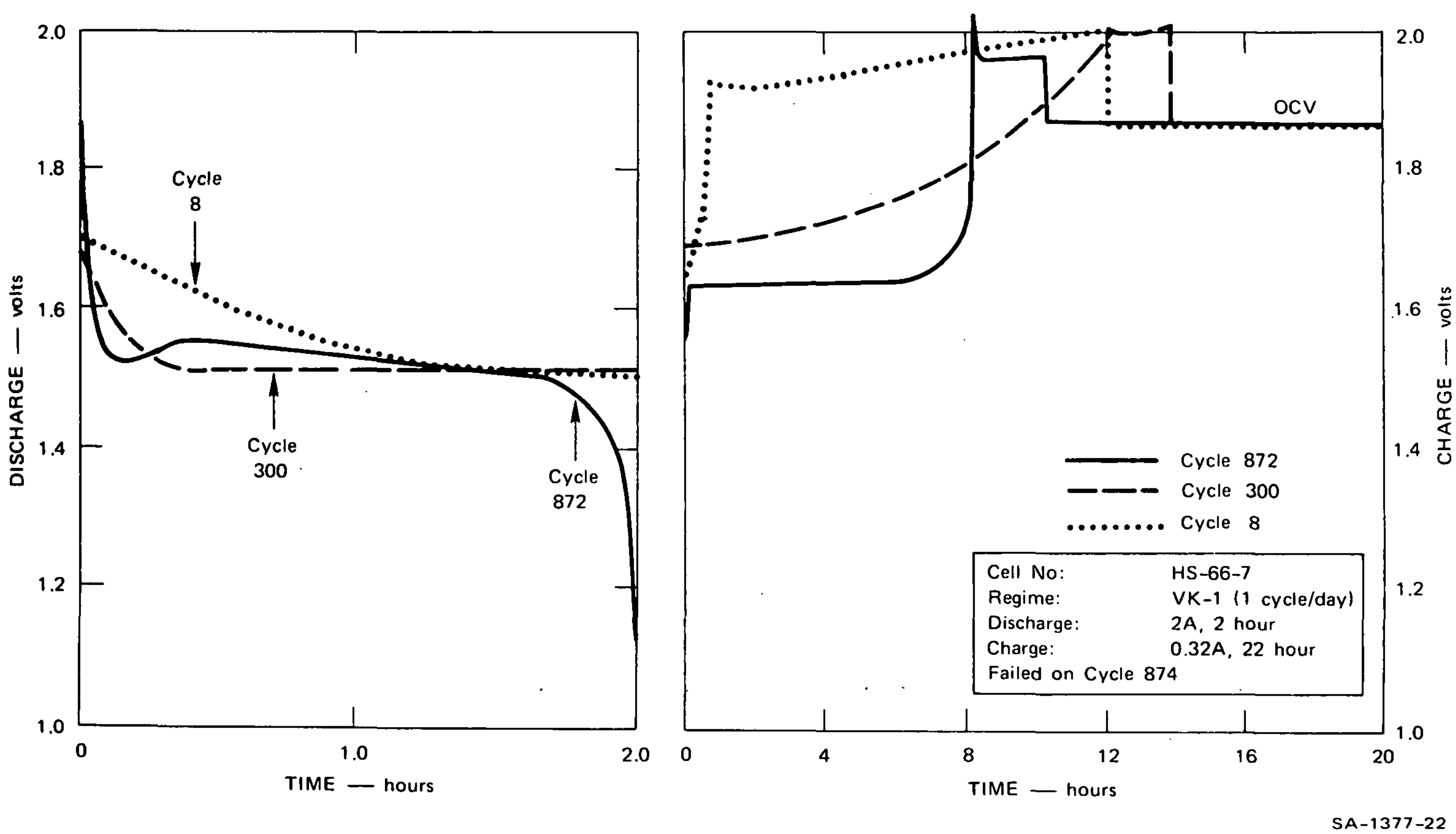

FIGURE 5 CYCLING CURVES (CELL IN A BATTERY WITH FOUR OTHERS) (DESIGN VARIATION, DESIGN 6 SUBGROUP)

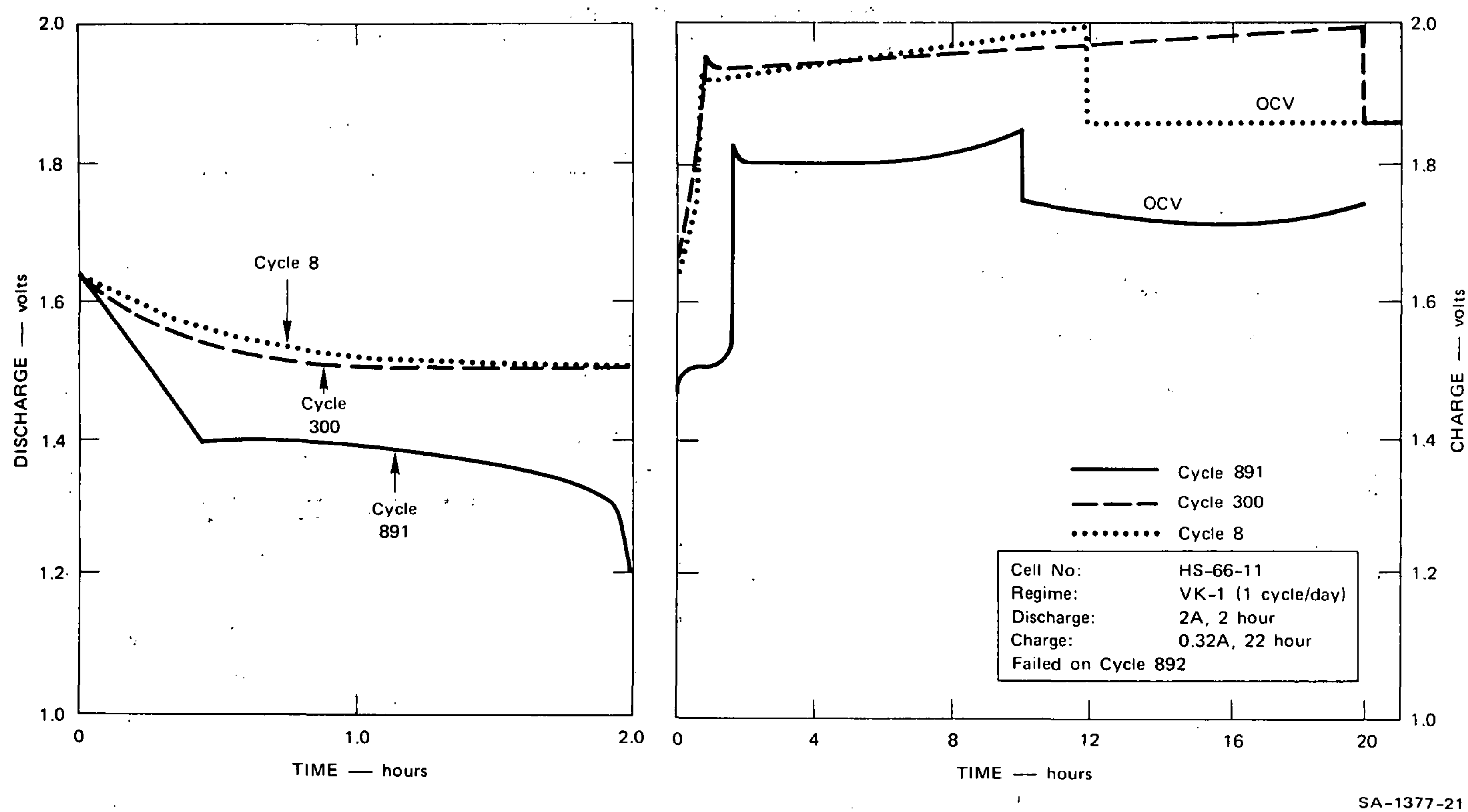

FIGURE 6 CYCLING CURVES (CELL IN A BATTERY WITH FOUR OTHERS) (DESIGN VARIATION, DESIGN 8 SUBGROUP)

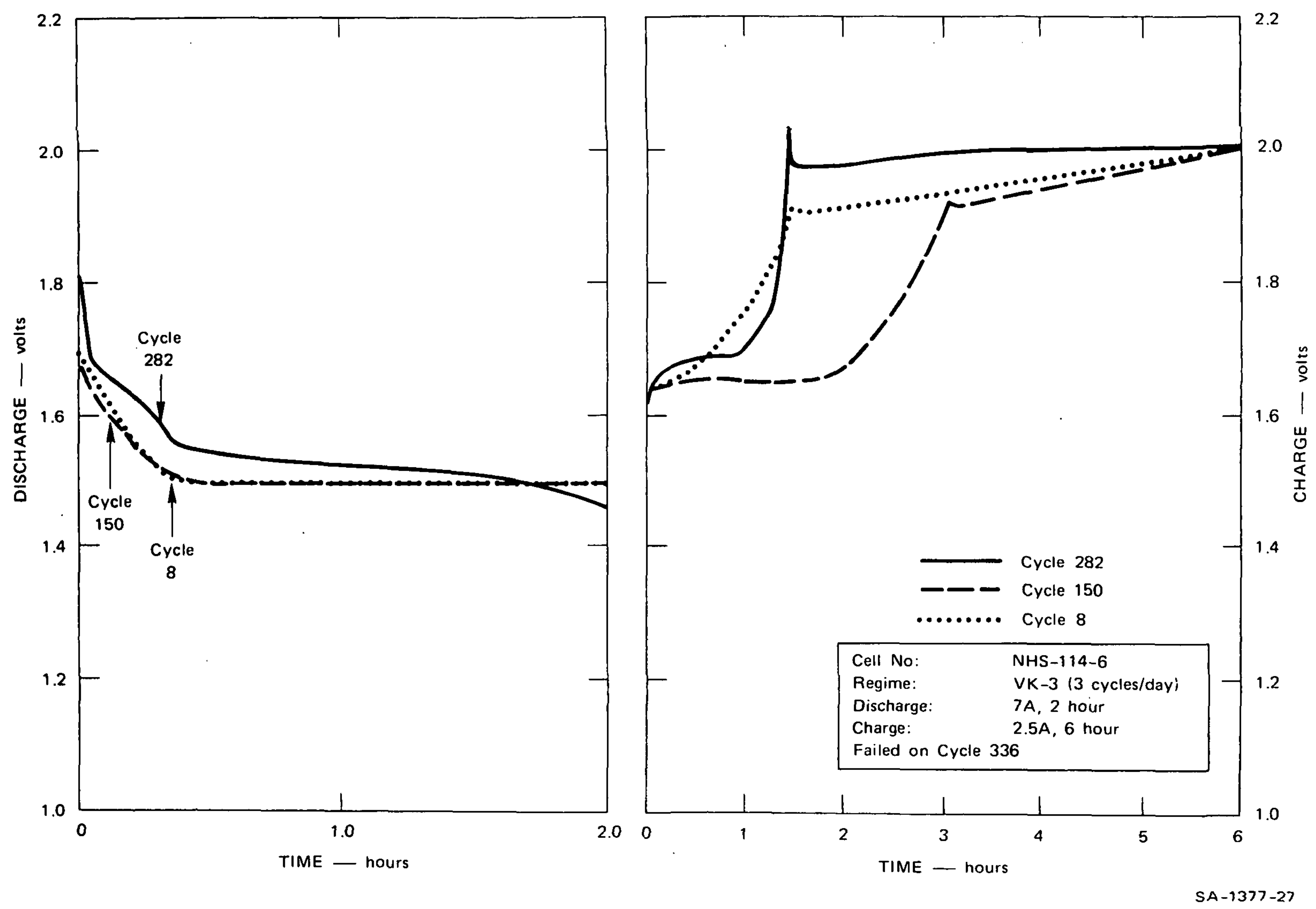

FIGURE 7 CYCLING CURVES (PLATE LOCK, SUBGROUP A)

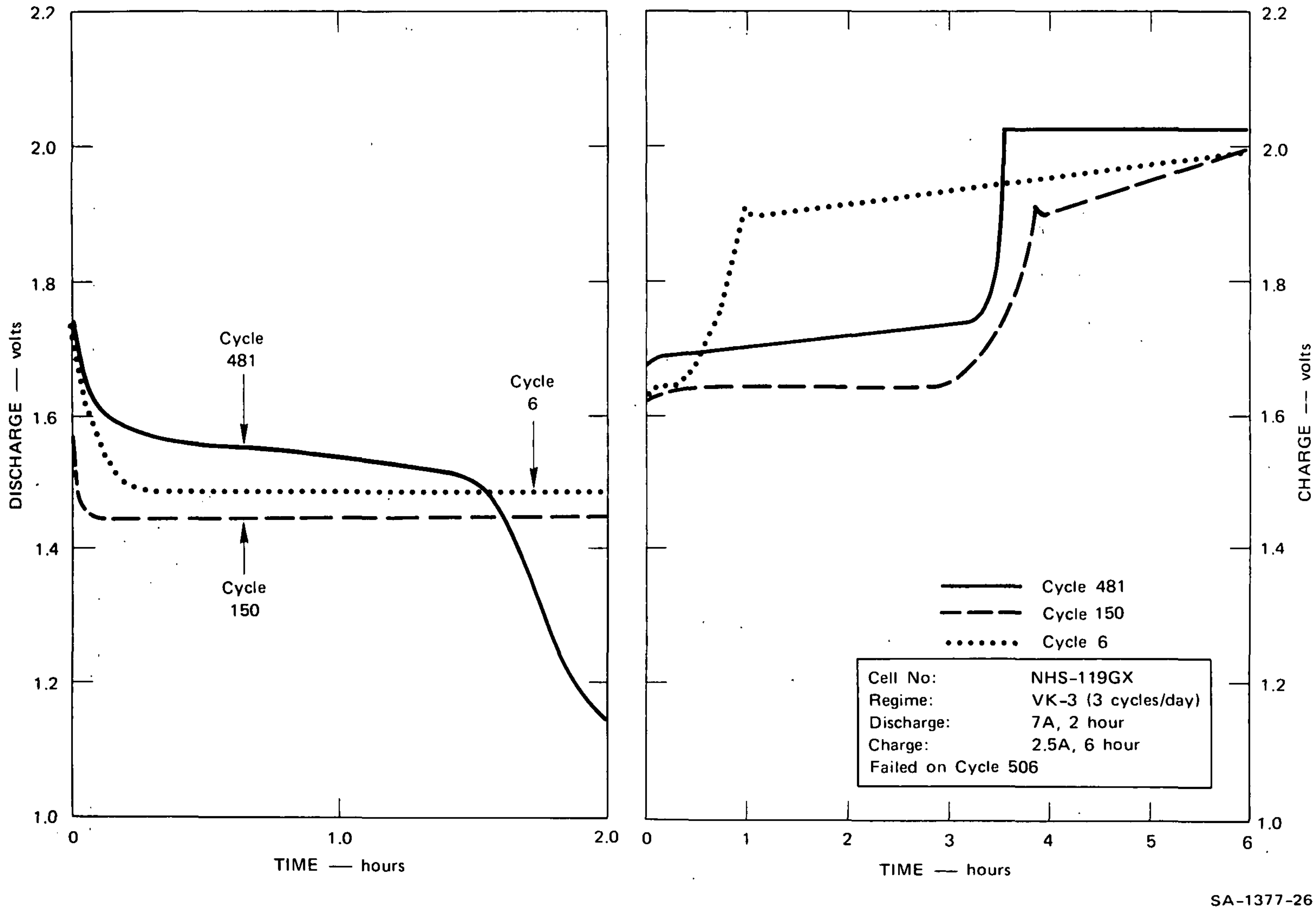

FIGURE 8 CYCLING CURVES (PLATE LOCK, SUBGROUP B, SWRI TYPE GX SEPARATOR)

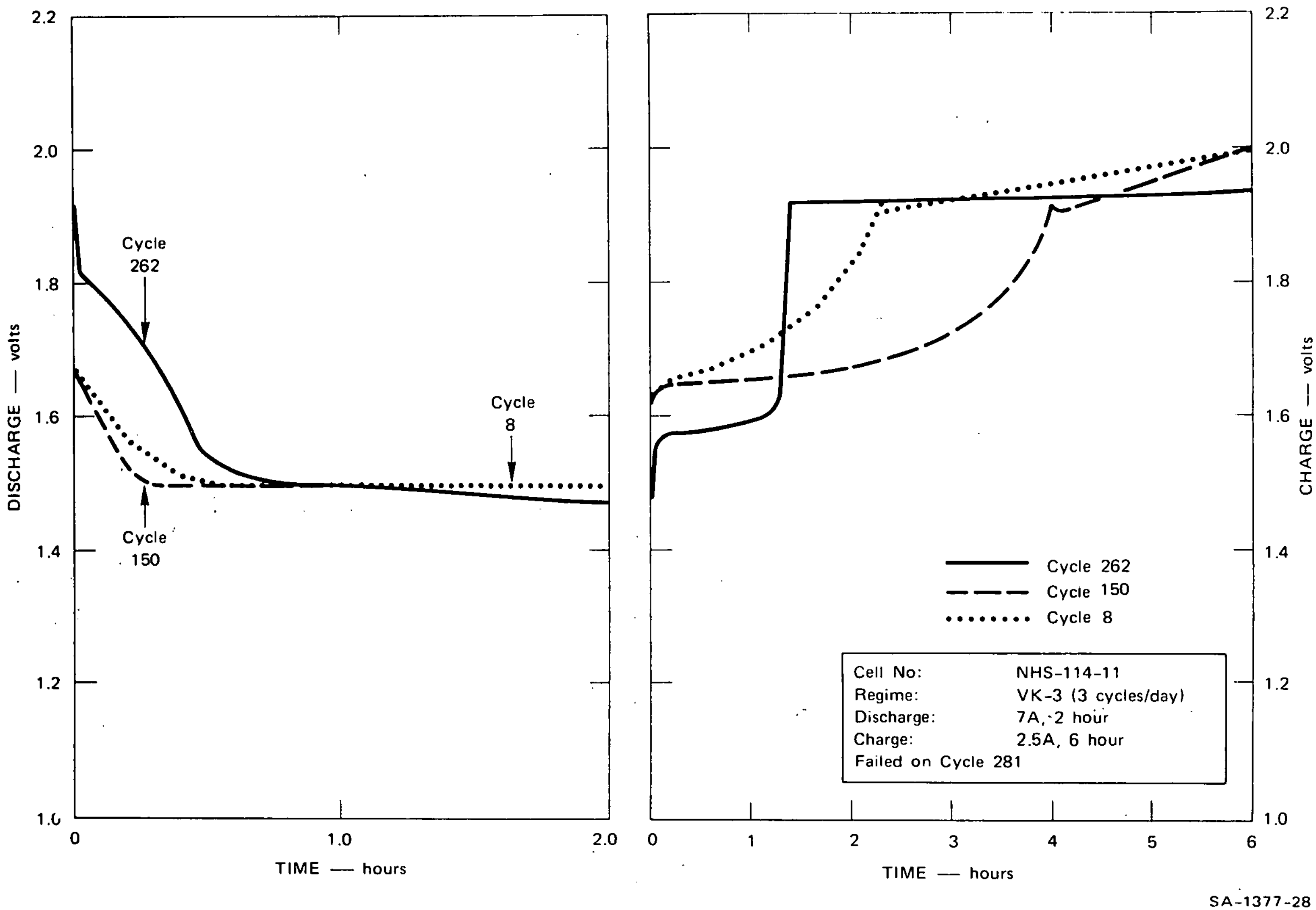

FIGURE 9 CYCLING CURVES (PLATE LOCK, SUBGROUP B)

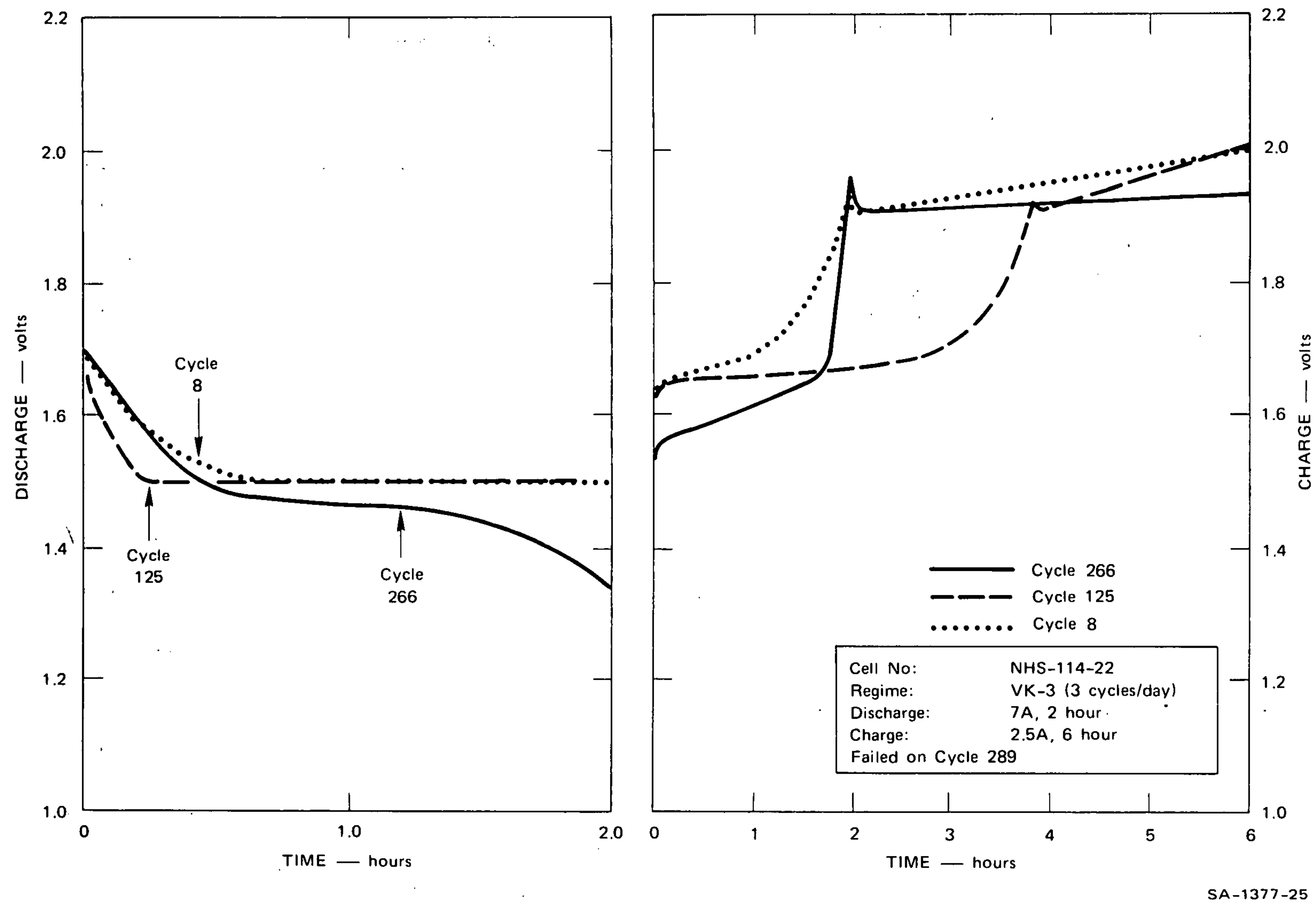

FIGURE 10 CYCLING CURVES (PLATE LOCK, SUBGROUP C)

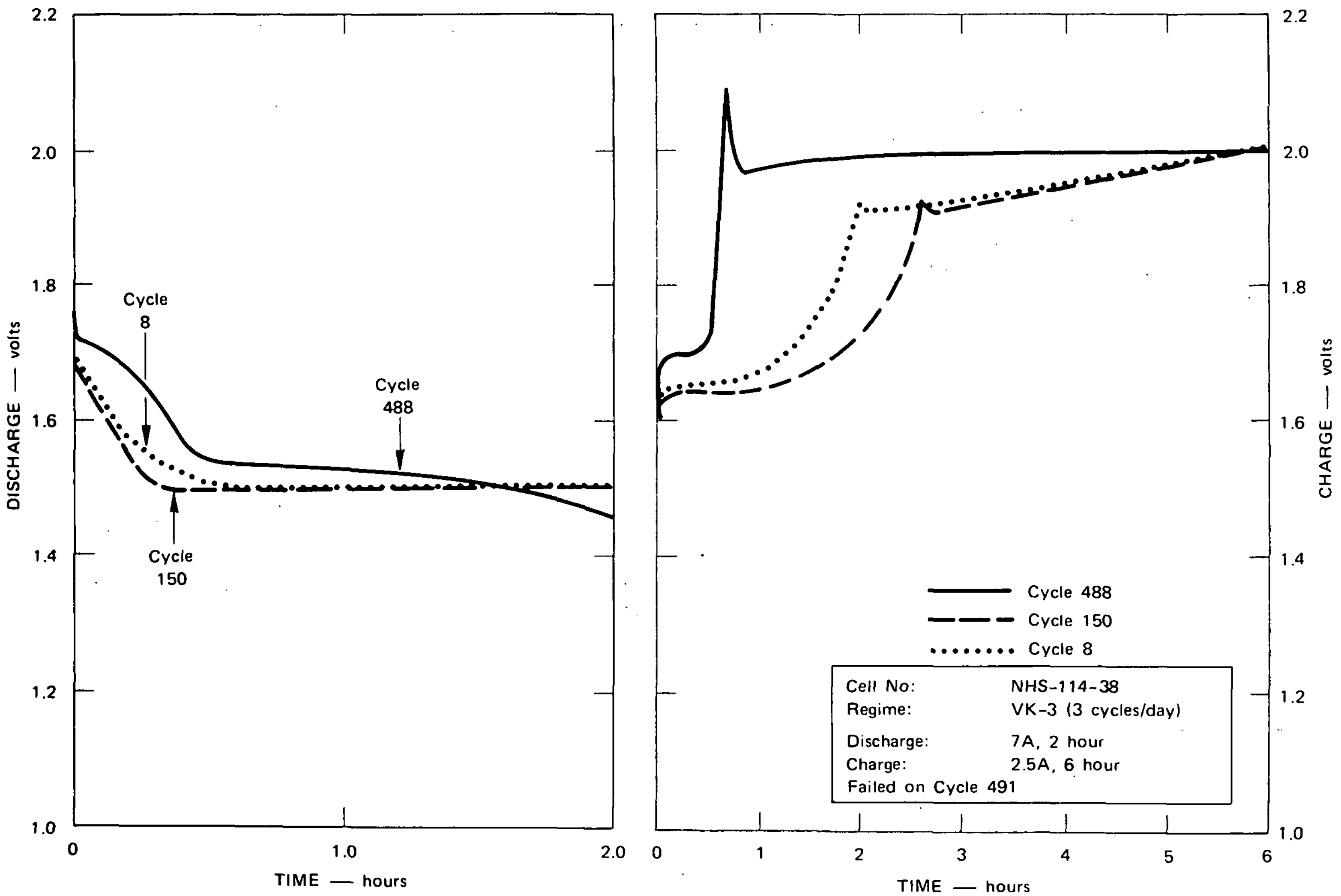

SA-1377-24

FIGURE 11 CYCLING CURVES (PLATE LOCK, SUBGROUP D)

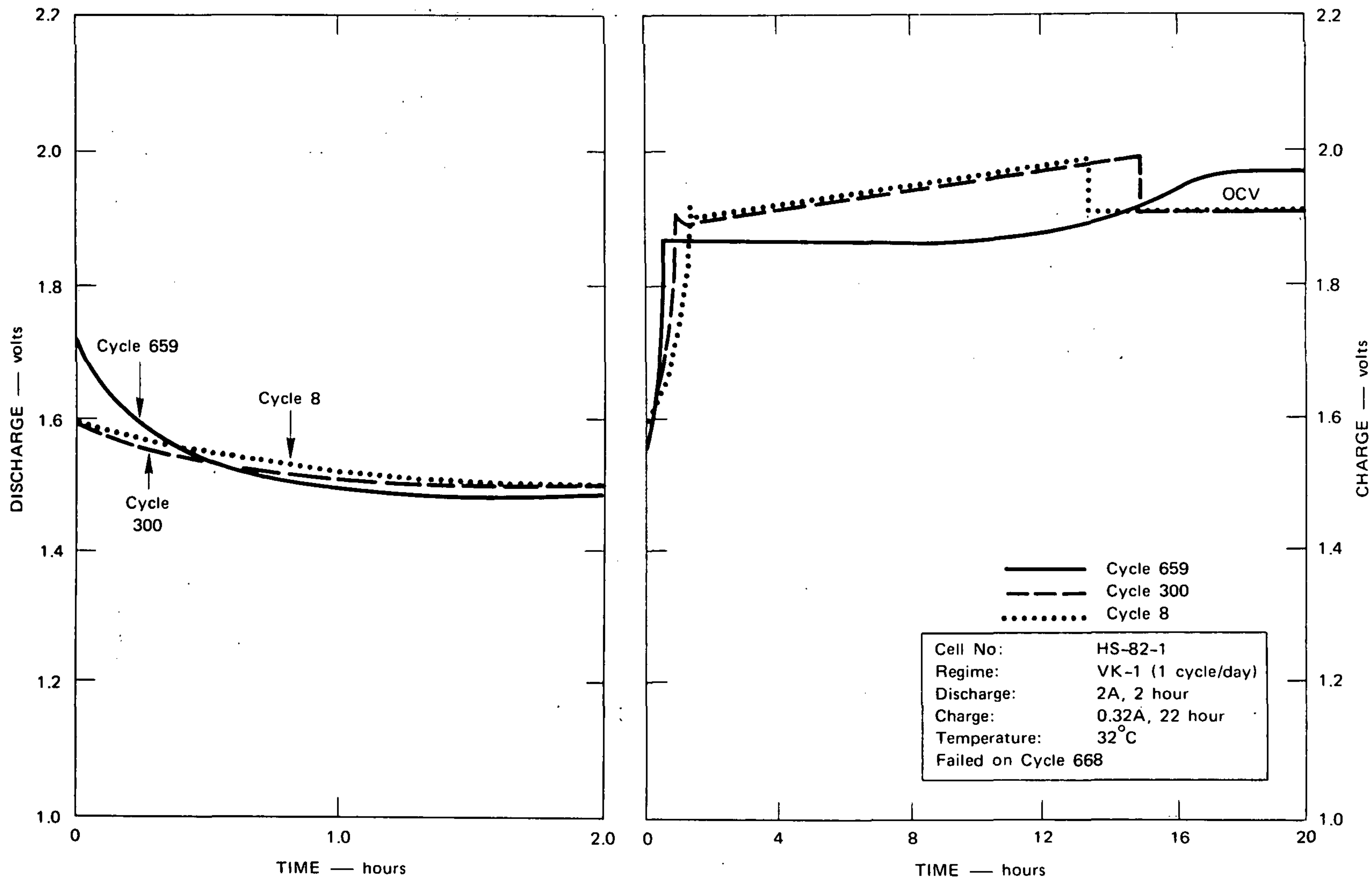

SA-1377-20

FIGURE 12 CYCLING CURVES (CELL IN BATTERY WITH THREE OTHERS) (TEMPERATURE/BATTERY/CELL GROUP)

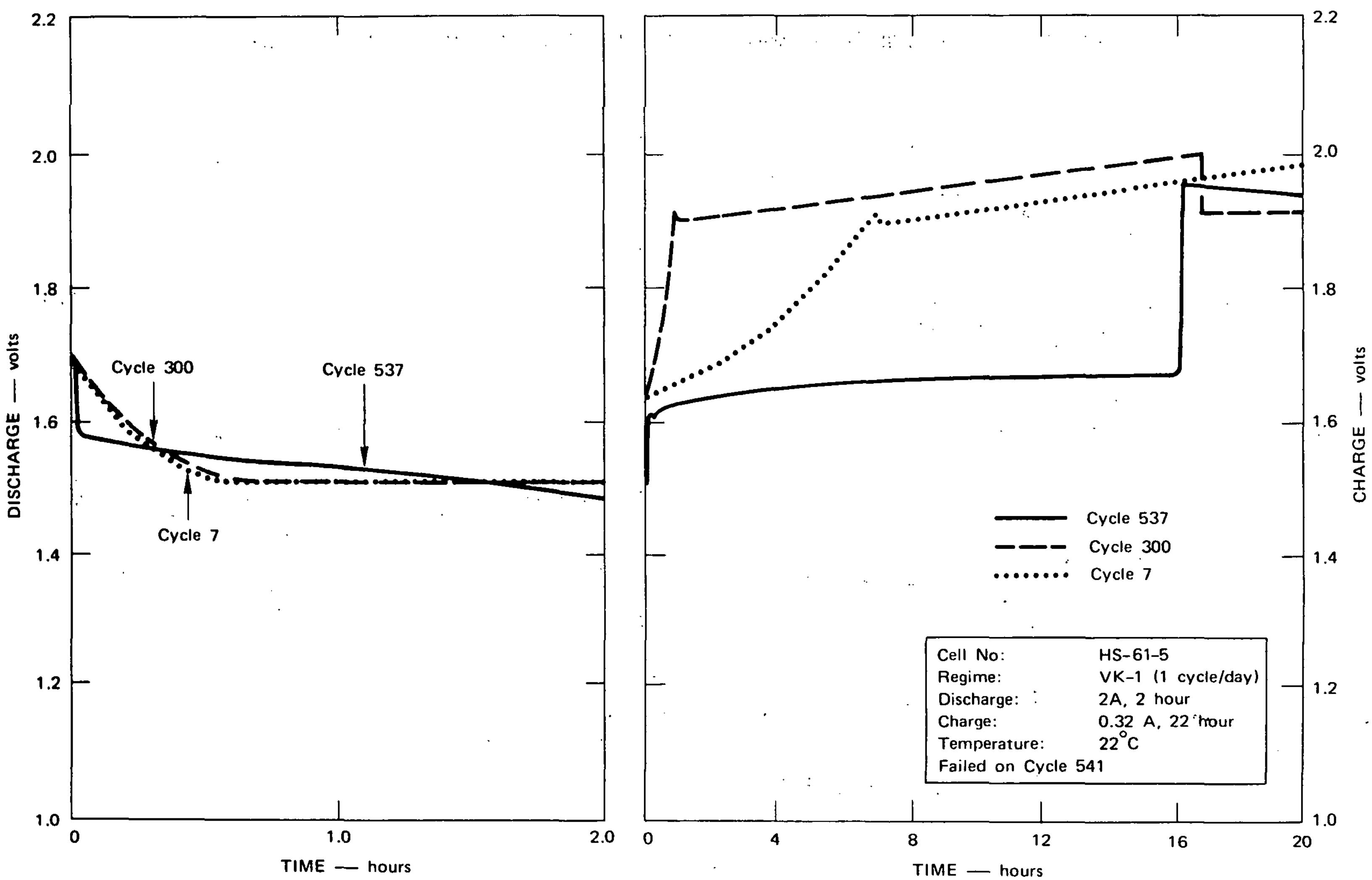

SA-1377-18

FIGURE 13 CYCLING CURVES (SINGLE CELL) (TEMPERATURE/BATTERY/CELL GROUP)

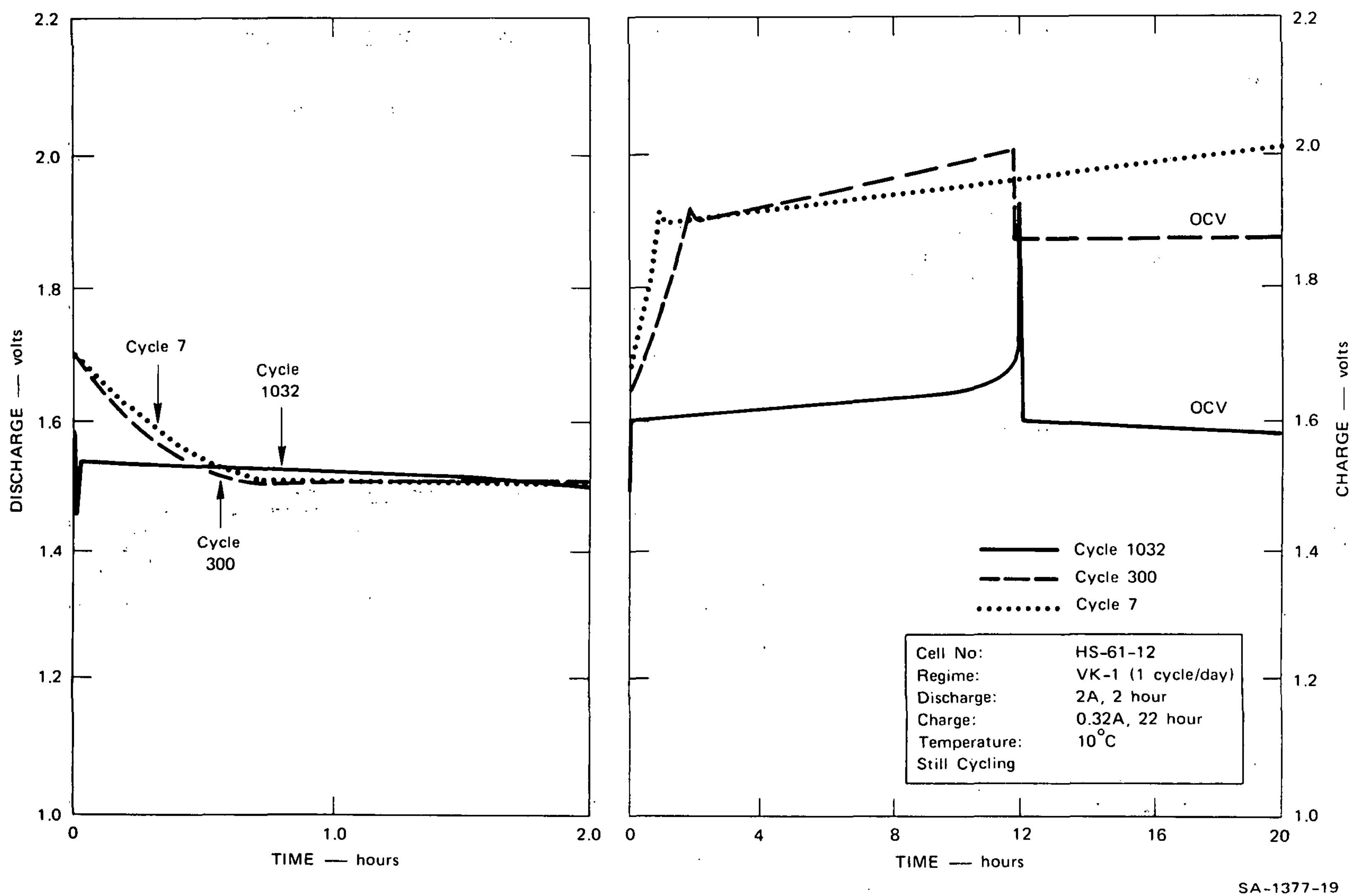

FIGURE 14 CYCLING CURVES (SINGLE CELL) (TEMPERATURE/BATTERY/CELL GROUP)

the state of health (age) of a cell. Two phenomena are thought to be responsible for the observed effect, (1) a decrease in effective capacity of the silver electrode which will effectively increase the relative rate of charging represented by a constant current, and (2) the development with cycling of a more uniform silver crystallite size which will lead to a more uniform state of charge throughout the electrode and, hence, a more nearly uniform conversion of silver (I) to silver (II) during charging.*
The rate of voltage rise might lend itself as a semiquantitative test of silver capacity (obtained automatically in each cycle), of value in determining whether and to what extent cells are positive limited.

Figures 4 through 6 represent updates of similar curves given in Ref. 6 for several cells, cycled as batteries, in the Design Variation group. The electrical behavior of a significantly shorted cell is evident in Figure 4 for cycle 850; as expected, the cell failed in the next cycle. Note that in cycle 850 the remaining cells forming a battery with this failing cell will have experienced an average of (2.00-1.68)/4 = 0.08 V above the customary cutoff voltage of 2.00 V per cell. This and similar events in other battery cell groups represent a very significant overcharge condition that may explain the generally inferior performance of cells cycled in batteries.

Figure 5 shows a cell about to fail (in cycle 872) due to inability to maintain a voltage above 1.00 V during discharge. This behavior was often associated with slow shorts. It is apparent that shorting is not yet sufficient to prevent the cell from being charged in cycle 872, but charge acceptance is degraded as suggested by the relatively late voltage rise.

---

*A fairly uniform, rapid conversion of the lower silver oxide into silver (II) oxide may also explain the flatness of the silver (II) plateau during charging, and presence of a significant silver (II) plateau in discharging aged cells (see Figure 3).

A significantly shorted cell very close to failure is shown in Figure 6 (cycle 891); again, this behavior probably has caused overcharge conditions in the other cells of the battery. The voltage behavior in the discharge curve of cycle 891 suggests partial cell recovery from a significant shorting condition.

Figures 7 through 11 show cycling curves for cells from the various subgroups of the Plate Lock group. Noteworthy features include the exceptionally high voltage spikes for cells from subgroups A (Figure 7), C (Figure 10), and D (Figure 11), and their conspicuous absence in subgroup B cells (Figures 8 and 9). A possible explanation, involving adsorption of organic compounds leached from the normally cured epoxy plate locks in subgroup B cells, was advanced above. A minor feature is apparent in the discharge curves of Figure 8: the cell with SWRI type GX separator exhibits an increase of the internal resistance between cycles 6 and 150. This is in contrast to the behavior of cells with the standard semiflexible separators which show consistently low levels throughout most of their lives.*

Three more sets of cycling curves are shown in Figures 12 through 14. Again, they show typical features, including a very steep voltage rise near the end of cell life (Figures 12 and 13.) The late voltage rise, declining voltage on the upper silver plateau, and sloping discharge curve in Figure 13, cycle 537 all suggest impending failure by shorting; the exaggerated spike in Figure 14 (cycle 1032) is caused by the switch to open circuit triggered by the voltage spike.

---

*An estimate of the internal resistance is no longer possible later in cell life when sloping discharge curves begin to indicate shorting or other faults.

TASK II - SEPARATOR RESEARCH AND DEVELOPMENT

The Work Statement for Task II specified exploration of inorganic formulations to produce chemically stable, nongassing, long-life separators suitable for alkaline batteries, notably the silver-zinc, silver-cadmium, and nickel-zinc systems. Primary interest was to be on development of semiflexible or flexible formulations, but rigid separators comprising formulations beyond the 3420-09 and 3420-25 compositions also were to be fabricated and characterized. The latter compositions were to serve as baseline materials for improvement of rigid and semiflexible separators. Promising formulations were then to be evaluated in Task III by application of separator screening techniques.

Other stipulations under Task II included investigation of changes in separator formulation, determination of the effects of constituent parts on separator properties, and utilization of fabrication techniques lending themselves to eventual mass production of separators. However, in the course of the work, agreement was reached with the NASA Project Manager that--in the interest of providing clear comparisons with established inorganic separator materials and concentrating on the inorganic phase as the major variable--separator fabrication techniques would be limited to those used previously at Astropower Laboratory in the fabrication of the 3420-25 separator.

Selection of Inorganic Base Materials

In accordance with the Work Statement, the classes of materials chosen for study included olivines, zirconias, monticellite, and titanias. From these basic classes, a total of twenty specific materials were to be obtained--through purchase from commercial sources and(or) by preparation via suitable chemical modifications of selected class members--for incorporation into separator formulations.

The rationale in selecting these classes was as follows: Olivines were included because (1) the olivine-based 3420-09 separator, although prone to gassing in contact with zinc, appears to impart excellent cycling behavior to silver-zinc cells, and (2) other members of the olivine class can be expected to be nongassing. The suitability of zirconia was established through the success of the zirconia-based 3420-25 separator in cells that were still on test after 26 to 43 months of wet life. Monticellite was included because, as an iron-free modification of the olivine class, it appeared to have potential as a nongassing, low-cost separator base material. Finally, although titania itself is not sufficiently stable in caustic, a titania-based material was used in all Astropower silver-zinc cells as a part of the successful zinc electrode-separator composite.

Selection and Preparation of Inorganic Separator Stock Materials

The inorganic stock materials initially considered for separator development are listed in Table 22, together with their code designations used in this program. As shown in the table, of the 17 materials actually used, six (codes JC, K, M, N, P, R) were obtained commercially. These six materials were used as is, and two of them (N', R') were obtained by further diminution of the commercial powders. A total of 11 materials (A, B', C', D', E', F', G', HP', L', Q, S') were obtained by high-temperature synthesis; five of these were chemical modifications made by doping corresponding stock materials with a small amount of an inorganic cation. The doping step was performed on fully reacted

Table 22

LETTER CODE ASSIGNMENTS TO THE INORGANIC SEPARATOR MATERIALS

Code Letter	Material	Used in Separators: Rigids	Used in Separators: Semiflexibles
	Olivines		
A	3420-09*	+	+
A'	3420-09*	-	+
B'	Synthetic, substituted olivine*	+	+
C'	Synthetic, substituted olivine*	+	+
D'	Synthetic, substituted olivine*	+	+
E'	Synthetic, substituted and doped olivine*	+	+
F'	Synthetic, substituted and doped olivine*	+	-
G'	Synthetic, substituted and doped olivine*	+	-
W'	Natural iron olivine	-	-
	Titanias		
H, J, JC	Commercial magnesium titanate	+	+
HP'	Synthesized pure magnesium titanate	+	-
K	Commercial calcium titanate	+	+
L'	Doped pure magnesium titanate*	+	+
	Zirconias		
M	C.P. zirconium dioxide (commercial)	+	+
N	Commercial zirconium spinel	+	-
N'	Commercial zirconium spinel	+	+
P	Commercial calcium zirconate	+	+
Q, Q', Q'-X	3420-25*	+	+
R	Commercial zirconium dioxide, "Zircoa-B"	+	+
R'	Commercial zirconium dioxide, "Zircoa-B"	+	+
S'	Doped commercial calcium zirconate*	+	+
	Monticellites		
T'	Monticellite ($CaMgSiO_4$), not used	-	-
U'	Substituted monticellite, not made	-	-
V'	Doped, substituted monticellite*, not made	-	-

*These are proprietary materials.

The prime (') refers to the fact that a commercial or as-received material is further milled for an extended time, or that a synthesized material is milled for a time such that most of the product is smaller than 5 micrometer particle size, and approaching 1-2 micrometer size.

materials to minimize uncontrolled loss of dopant during the extended firing times at the high temperatures required for synthesis of most materials.

The objective in preparing these separator stock materials was to obtain dry powders of small particle size (generally, less than 5 micrometers*) and adequate purity (preferably at least 95% for purchased or reacted materials); these became the stock for sintering rigid porous disks and for compounding the dipping slurries used to make semiflexible separator sheets.

Inasmuch as absence of the gassing tendency of separators was to be one of the major criteria for their suitability, the zinc-gassing test (described in more detail under Task III) was applied routinely as soon as possible after preparation of each candidate inorganic stock material. In practice, the selection criteria of anticipated, low semiconductivity and catalytic activity proved correct to the extent that all materials developed show little or no gassing when in contact with zinc.† Experience at Astropower Laboratory with the 3420-09 separator had shown that formulating inorganic stock materials with binder systems into semiflexible separators further reduces the gassing tendency, presumably by reducing the extent of contact between zinc- and binder-coated ceramic particles.

As a result, most or all of the materials developed were expected to qualify, with respect to freedom from gassing, for incorporation into rigid and semiflexible separator formulations. The last two columns of

---

* Representative particle size analyses for selected inorganic stock materials are shown in Table 23.

† Although reproducible gassing rates were observed for all materials examined in the zinc-gassing test, the rates for many of these were lower than that of the successful 3420-25 stock material. For several materials, the gassing rate actually was below that of the zinc powder blank.

Table 23

FISHER SUBSIEVE ANALYSIS ON SELECTED INORGANIC SEPARATOR STOCK MATERIALS

Sample Code	Diameter (Micrometers)
JC	0.87
R	1.90
E'	0.65
B'	1.06
S'	4.98
R'	0.62
M	1.0

Table 22 show which of these were actually fabricated into rigid separator disks, and which materials were incorporated into semiflexible separators after screening tests had been performed on these disks.

Olivines

Previous research findings have shown that the tendency of the otherwise very promising 3420-09 separator to gas when in contact with zinc was caused by the catalytic activity of the iron content in natural olivine. This finding led to the concept of iron-free olivines for nongassing separators. In an internal research program, such olivines were synthesized and shown to be essentially nongassing. In addition, techniques for doping of inorganic materials were developed that appeared to have an inhibiting effect on zinc dendrite penetration through separators containing such materials. The materials and techniques developed at Astropower Laboratory formed the basis for much of the separator development work performed at SRI under this program.

All olivines were synthesized from oxide or carbonate starting materials of reagent (or, in a few instances, USP) purity. Typically, dry mixing for 15 to 30 minutes, followed by wet mixing in a ball mill resulted in a homogeneous mix which was dried and ground to a powder. Fugitive binders were added in appropriate solvent, followed by drying and granulation on screens. The granular material was then pressed into 50x12-mm or 38x12-mm slugs at about 1.38×10^4 N/cm^2 (20,000 psi). Firing in an electric furnace for several hours at selected temperatures developed the desired ceramic structures. Selection of appropriate reaction temperatures and times was accomplished by performing pilot runs on small 9.6-mm diameter pellets in a tube furnace. X-ray diffraction analyses on the pellets guided the selection of temperature required for at least 95% conversion to the desired species. None of the syntheses required temperatures above 1623^oK (1350^oC).

The fired reaction products were broken up in a mortar and milled in a ball mill to a diameter below 5 micrometers. Preparation of 3420-09 stock was an exception to these procedures in that this material was milled for a shorter period of time, in accordance with the standard procedure developed at Astropower Laboratory. This yielded a separator stock material with a particle size ranging between 3 - 15 micrometers.

Zirconias

Except for 3420-25 material and the doped calcium zirconate (code S'), the other zirconium compounds came directly from commercial sources. The zirconium spinel (codes N and N'), apparently a frequently used material in ceramic and glass wares, had a stated nominal composition of ZrO_2 39-41%, SiO_2 20-22%, Al_2O_3 18.5-20.5%, and ZnO 17-21%. Nominal size was stated to be less than 44 micrometers, with 0.5% retained on a 325-mesh screen. The calcium zirconate (code P) had a stated nominal composition of ZrO_2 65.0-67.0%, CaO 28.0-30.0%, SiO_2 3.0-4.0%, Al_2O_3 0.5% max, and TiO_2 0.5% max. Particle size range was 0.5 to 3.0 micrometers, with less than 0.1% retained on a 325-mesh screen.

Monticellites

Attempts were made to obtain monticellite ($CaMgSiO_4$) from commercial sources. However, one source of pure monticellite (prepared by the hydrothermal method) had stopped supplying that material, and another source could supply only a material of 30% purity (mixed with calcite and idiocrase). Therefore, synthesis of monticellite was attempted at our laboratories.

Despite variation of starting materials, firing temperatures, and reaction times, no material obtained exceeded 90% purity. Although the presence of other phases might not have influenced separator behavior, a joint decision was reached with the NASA Project Manager to eliminate monticellite-based separator stock materials in the interest of concentrating program efforts on fully characterized materials.

Titanias

Four titania-derived materials were explored, two of which were synthesized. Commercial magnesium titanate (codes H, J, and JC) had a nominal analysis of TiO_2 38.0-42.0%, SiO_2 9.0-12.0%, Al_2O_3 4.0-5.0%, and MgO 39.0-43.0%. 99% passed through a 325-mesh screen; particle size range was stated to be 0.5 to 3.0 micrometers. Commercial calcium titanate (code K) contained TiO_2 55.0-58.0%, SiO_2 1.0-2.0%, Al_2O_3 0.5% max, and CaO 39.0-41.0%; particle size range was similar to that of the magnesium titanate.

Although efforts were made to procure chemically pure magnesium titanate from commercial sources, material of adequate purity could not be obtained. Therefore, the pure material was successfully synthesized by firing an intimate mixture of the pure oxides at 1523 $^{\circ}$K (1250 $^{\circ}$C) for six hours.

Preparation of Rigid Ceramic Disks

The Work Statement for this program specified that all inorganic separator materials developed be tested also in the form of rigid, porous ceramic disks of the general type developed at Astropower Laboratory.

Experience had shown that disks with porosities in the range of about 20% to 30% combined adequate conductivity and mechanical strength with promising performance as separators in silver-zinc cells. This guideline and the fabrication techniques used at Astropower Laboratory were used in preparing rigid separator disks under this program.

The basic technique for preparing this type of inorganic separator includes preparation of pressing granulations from inorganic stock materials and binder systems, pressing of granulations into "green" disks, and firing of the green disks to obtain rigid, porous sinters of appropriate porosity. These steps are discussed in the following.

Preparation of Pressing Granulations and Green Disks

With the exception of the reference material 3420-09,* all inorganic separator materials were in the form of fine powders as a result of the final step in preparing the stock materials.

The stock materials were mixed with a solution of fugitive binders and (or) lubricants, and the resulting thick pastes were dried under stirring to form an easily crumbled mass. This method of drying minimized segregation of the binders. Early preparations using Carbowax 4000 as combined binder and lubricant resulted in fragile green disks. A water-soluble resin was substituted for the Carbowax as the binder, and paraffin was added as lubricant. Increased green strength was noted, and all subsequent pressing granulations used this modified binder/lubricant system.

From the dried mass, the minus 60 plus 100-mesh fraction was collected. Use of this relatively narrow size fraction prevented size

* This material was available in the form of a spray-dried, coarsely granular powder already incorporating the binder. Green disks were pressed directly from this powder.

segregation and permitted uniform loading of the 25.4-mm-diameter die. Granulations then were pressed at approximately 6.9×10^3 N/cm^2 (10,000 psi) to produce compacted green disks. In a few instances 1.38×10^4 N/cm^2 (20,000 psi) were applied in an attempt to eliminate specimens with edge cracks or full cracks after firing.

Firing Procedure and Results

A "Globar"-heated tube furnace was used in firing green disks to produce rigid, porous ceramic samples. The general procedure was to conduct a few test firings for each new formulation to establish a time-temperature relationship that resulted in disks of the desired porosity range (24 to 29%). Good yields of usable rigid disks were then obtained by the following procedure. A stack of disks (usually 3 to 8) was loaded on a flat ceramic setter. Starting at the cool end of the tube, the setter was pushed inwards about 4 cm every few minutes to gradually warm the disks. As soon as fumes of the binder were observed, the setter was allowed to remain in that zone until all the volatile matter had disappeared. Then the setter was advanced in increments of about 2 cm each and held for 2 to 3 minutes until the disks reached a temperature within 200-300°K of the peak firing temperature. At that point, the setter was pushed into the center of the hot zone, and the firing time base started. After the requisite time at peak firing temperature, the setter was pushed into a zone that was about 200-300°K cooler. When the stack and setter had cooled to the lower temperature, the setter was again pushed to a cooler region, 400-600°K below the firing temperature. Finally the setter was pushed into the cold zone of the tube (temperature about 420 to 570°K). After about 5 minutes in this zone the samples were pulled out, placed on a ceramic slab and cooled to room temperature.

Separate firing tubes were used in firing the doped materials to avoid contamination of undoped materials by traces of the slightly volatile dopant. The zirconia setters, ground flat to give correspondingly flat disks, were changed with every formulation to avoid possible contamination from previous firings. In some cases it was necessary to add flat ceramic slabs as weights on top of a stack of disks to minimize warping.

Several materials were prone to warping or cracking, especially those incorporating the synthetic olivines F' and G'; the commercial magnesium titanates, H, J, and JC; the modifications of the 3420-25 material Q, Q', and Q'X; and the zircoa-B materials, R and R'. However, adequately flat disks of the desired porosity ultimately were produced from every formulation in sufficient numbers to permit performance of all screening tests selected for Task III. Firing conditions, the range of porosities obtained, and the yields of disks are summarized in Table 24.

Preparation of Semiflexible Wafers

As stated previously, a joint decision had been made with the NASA Project Manager to concentrate on inorganic materials as the main parameter in separator development, at the expense of experimentation with changed binder/plasticizer formulations. Therefore, the formulation and preparation technique developed at Astropower Laboratory for the successful 3420-25 semiflexible separator was adopted as the general technology base for preparing semiflexible separators under this program. However, the SRI approach differed from standard Astropower Laboratory procedure in one important respect: The coating formulations were prepared on the basis of an equal volume (rather than equal weight) percentage of the

Table 24

FIRING CONDITIONS FOR RIGID CERAMIC DISKS

Class	Material Code No.	No. of Disks Fired	Time Ranges (Min)	Approx. Temp. Ranges Explored (^oK)	Preferred Temperature Estimated	Porosity Range(%)	No. of Intact Disks Retrieved
O	A	15	-45-	1470 - 1520	~ 1500	22.9-27.4	11
L	B'	12	-45-	1450 - 1470	~ 1460	21.0-26.4	12
I	C'	25	15-30	1350 - 1450	~ 1360	0.0-30.8	21
V	D'	22	-45-	1410 - 1520	~ 1520	24.5-32.7	14
I	E'	24	30-45	1440 - 1470	~ 1450	18.4-28.2	24
N	F'	12	20-45	1340 - 1370	~ 1370	27.9-31.0	11
E	G'	29	30-45	1520 - 1590	~ 1590	16.5-31.1	4
S	W'	24	30-45	1440 - 1520	not detd.	1.5-23.8	24
T	H	25	30-45	1520 - 1670	~ 1560	0.0-35.0	13
I	HP'	9	-45-	1350 - 1570	~ 1350	16.9-25.9	9
T	J	17	-45-	1470 - 1520	not detd.	28.8-38.0	17
A	JC	22	-45-	1520 - 1660	~ 1520	16.2-28.0	13
N	K	11	-45-	1370 - 1510	~ 1370	0.1-26.2	6
I	L'	12	-45-	1350 - 1370	~ 1370	.3-29.5	11
A							
S							
Z	M	21	13-45	1600 - 1670	not detd.	21.3-26.2	8
I	N	24	30-45	1470 - 1545	~ 1530	24.4-35.7	21
R	N'	24	-45-	1500 - 1670	~ 1620	20.2-40.3	24
C	P	14	-45-	1510 - 1590	~ 1580	24.4-34.0	13
O	Q'X	41	-45-	1470 - 1630	~ 1520	19.9-30.3	34
N	Q	15	-45-	1500 - 1620	~ 1545	13.9-36.7	14
I	Q'	37	-45-	1490 - 1540	~ 1540	27.4-34.1	31
A	R	42	-45-	1500 - 1620	~ 1570	25.3-33.9	19
S	R'	30	-45-	1470 - 1520	~ 1510	19.5-32.0	26
	S'	11	-45-	1530 - 1570	~ 1540	18.4-27.3	10

inorganic material, with the 3420-25 formulation serving as the reference. It was felt that this procedure provided a better comparison of the materials inasmuch as geometric factors were expected to be more nearly equal. A consequence of this was that the SRI formulation (A') of the 3420-09 baseline material differed somewhat from the corresponding Astropower formulation (A).

Preparation of Coating Slurries

The preparation of the slurries followed established procedures. All inorganic powders were screened through a 325-mesh screen to remove tramp material and agglomerates. A slurry was made up from inorganic material, resinous binder, plasticizer, and solvent, and mixed in a ball mill for 15 - 16 hours. This was followed by another screening through a 325-mesh sieve to remove agglomerates of ceramic material or undissolved polymer, or chips from the mill-mixing media. After these steps, a viscosity adjustment was made if necessary, and the slurries were bottled for subsequent use in the dipping operation. The compositions and procedures essentially followed those cited in U.S. Pat. No. 3,625,770. No extraordinary problems were encountered in the preparation of the slurries.

Coating Procedure

Several procedures had been developed at Astropower Laboratory for fabrication of semiflexible separators incorporating inorganic materials. One of the most successful was to coat one side of specially prepared sheets of fuel cell asbestos with the type of slurry described above. The silver-zinc cells under test at SRI (Task I) have separators of this type; in this particular instance, the coating was formed by dipping bags, properly sealed at three edges, into the slurry.

Although the basic Astropower procedure did yield useful semiflexible separators, the manual dipping technique and certain aspects of slurry handling tended to create problems in achieving high quality, uniform coatings. To eliminate the influence of the corresponding variability of separators from the results of this program, a mechanical dipping machine was built and used at SRI in making semiflexible separators. After considerable experimentation to determine optimum values for immersion rate, residence time, and withdrawal rates of separator bags, coatings of the desired thickness (typically, 100-150 micrometers) could be made reproducibly.

Provided that the relative humidity was kept below about 60%, these coatings were free of striations, bubbles, and other defects and had nearly uniform thickness over the entire surface of dipped bags. Each bag yielded two sheets, each sheet in turn six wafers for the screening tests under Task III. Additional bags were dipped to provide strips for tensile and flexibility tests.

TASK III - SEPARATOR EVALUATION BY SCREENING METHODS

The Work Statement for this Contract specified evaluation of the tests generally used for screening separators in terms of probable performance in batteries. The tests to be evaluated included those described in the standard reference book* for separator testing, with the following as a minimum:

(1) Pore size distribution

(2) Absorptivity

(3) Permeability

(4) Resistivity

(5) Wet strength

(6) Compatibility

(7) Oxidation resistance

(8) Silver and zinc penetration.

Tests expected to correlate significantly with separator performance in battery cells were to be recommended for application to the rigid and semiflexible separators developed in this program. The results of these activities are described in the following sections.

---

*The Air Force Screening Test Manual for Silver-Zinc Batteries, edited by Cooper and Fleischer, Reference 7.

Evaluation of Separator Screening Tests*

In this initial subtask, we were to evaluate the commonly used separator screening methods and recommend those that appear to correlate best with separator behavior in silver-zinc cells.

Conclusions and recommendations from our analysis and evaluation of screening methods as described in the Cooper-Fleischer booklet and used in various laboratories over approximately the past ten years are given below for the major characteristics relating to separator function. The discussion uses a test sequence different from the listings given above and in the Work Statement; however, all tests listed, plus several additional ones, are discussed.

Electrical Resistance

Electrical resistance of a battery separator (equilibrated with the particular battery electrolyte) is a key criterion for separator suitability: thus, its measurement serves as a preliminary screening test. In practice, DC and AC techniques have been used, apparently with equal success. The measurement, as a rule, is carried out by a differential technique (with and without the test specimen in the resistance cell). With some minor variations, the basic approaches and resistivity cells discussed by Lander and Weaver and by Salkind and Kelley in the standard reference have been widely used. These techniques are invariably compromises in which adequate precision is sought while permitting ready exchange and rapid measurement of test samples. To achieve acceptable results, care is necessary in uniformly filling separators with electrolyte, reproducibly positioning the sensing electrodes, and controlling (or determining) the electrolyte temperatures and composition.

---

*Screening methods, as used here, are defined broadly to include (1) techniques used to characterize separators in terms of relevant physical characteristics (characterization tests), and (2) tests that attempt to simulate the behavior of separators in actual cells (screening tests).

After several modifications at SRI, the conventional cell and technique previously used at Astropower Laboratory gave satisfactory results in our separator screening program; this is discussed more fully in later subsections of Task III.

Chemical Stability (Compatibility)

Immersion tests are used routinely in separator development programs to screen candidate materials with respect to stability to the chemical environment in actual cells. Several different degrading factors, including KOH electrolytes of various concentrations, and electrolytes containing dissolved silver oxide, oxygen, or other oxidizing agents, have been used. Change of weight or porosity, loss of strength, extent of depolymerization, amount of metallic silver deposited, and the formation of degradation products have been used successfully as measures for the extent of degradation of the various separator materials. Tests invariably are run at elevated temperatures to accelerate degradation effects.

A criticism of several past programs is that (1) insufficient information was obtained on the temperature dependence of degradation, and (2) excess electrolyte was used in degradation tests. The first of these shortcomings makes it difficult to extrapolate degradation effects from elevated to battery operating temperatures. The second precludes realistic simulation of separator conditions in battery cells, including possible attainment of "degradation equilibria" and change of electrolyte conductivity due to extensive reaction; the latter considerations are particularly relevant for inorganic separators. These shortcomings were eliminated from our screening program by carrying out degradation tests at several temperatures and electrolyte-to-separator volume ratios. Furthermore, in addition to weight loss, porosity and resistivity after KOH immersion were determined as more specific measures of degradation, with a view to learning more about extent and functional consequences of separator degradation.

Mechanical Characteristics

Mechanical properties such as flexibility, tensile strength, and dimensional stability bear directly on handling of separators in battery fabrication and affect their mechanical integrity over the life of a battery. Although measurements of tensile strength and separator dimensions are performed quite routinely in most separator development programs, there are no numerical values--or even ranges of such values--that could serve as acceptability criteria. This is particularly true for developmental silver-zinc cells with noncellulosic membranes. These cells are essentially built by hand and vary significantly in design, with correspondingly different mechanical requirements for the separators. Nevertheless, characterization of separators in terms of their key mechanical parameters is of considerable value in any technology-oriented development program.

Regarding the materials to be developed in our program, there is a fundamental mechanical difference between rigid and semiflexible inorganic separators. For rigid separators, little dimensional change is expected upon contact with electrolyte, and tensile strength is of little interest. The relevant characteristic for fabrication of, and use in, batteries is the modulus of rupture. Semiflexible separators can be characterized in terms of their dry and wet dimensions and their tensile strength. In view of the longer-range objective to develop separators of increased flexibility, a simple but reasonably repeatable test of the degree of flexibility would be of considerable utility.

Open Porosity (Volume of Open Pores)

Porosity has intrinsic importance as a key separator characteristic, and also for possible correlations with other indices of separator performance. Porosity data permit (1) calculation of pore tortuosity when combined with separator resistance data, and (2) determination of "open" vs. "closed" pores when combined with determination of apparent (geometric) and true (bulk) density of separators.

Inasmuch as open, continuous pores are of prime interest for separator function, techniques depending on intrusion of a liquid are preferred for determination of separator porosity. Water impregnation of evacuated samples is easily performed and should give representative results for the open porosity of reasonably wettable materials. Mercury intrusion at high pressures [e.g. 4.1×10^4 N/cm^2 (60,000 psig)] will give the volume of open pores down to approximately 100 Å. Comparison of water and mercury porosity data can give some indication regarding the extent of wettability of separator materials and, for wettable specimens, whether a separator contains an appreciable volume of micropores.

Regarding the materials of our program, the rigid separators appear to be readily wettable. Accordingly, little or no difference should exist between porosities determined by water impregnation (under vacuum) and by electrolyte absorption. Vacuum impregnation seems preferable because the possibility of errors caused by trapped gas is eliminated and a meaningful comparison with mercury porosity data (also obtained with evacuated samples) appears possible and should indicate whether a separator has a significant micropore volume. For our semiflexible separators that are formulated from inorganic materials and organic binder systems, water intrusion and total intrusion of mercury will give average values only of the multiphase structure. This increases the importance of an independent characterization of porous structure.

Average Pore Size and Pore Size Distribution

There is universal agreement that these characteristics must play a central role in the function and performance of battery separators. However. a survey of the state of the art shows that there is no firm--much less quantitative--understanding of how pore size and distribution (geometric and size) affect separator performance, or what would constitute a preferred set of specifications. This is so partly because different battery systems often require different functions in a separator. For example, systems with essentially insoluble reactants and products do not require that the separator be permselective; on the other hand, permeability to gas may be required.

The present understanding of separator functions in silver-zinc batteries is limited to relatively simple ideas such as desirability of uniform distribution of pores (to ensure uniform utilization and distribution of active materials) having very small diameters (to provide selective retardation of silver oxide and zincate diffusion and suppress zinc dendrite growth). Quantitative support for these hypotheses is not available; for example, no attempt seems to have been made to establish whether any of the available separator materials offer some degree of selective retardation. There is also some question whether these simple ideas apply to all types of separators.

The first step in improving the understanding of the role of pore size and distribution--and thus in permitting use of these data to screen (or even design) suitable separators--is a more complete characterization of materials. This need has been recognized, and at least six different techniques have been used over the past 5 to 10 years for determination of separator pore size and(or) pore size distribution, including

Water (or electrolyte) permeability
Mercury porosimetry
Electron microscopy
Gas adsorption
Gas permeability
Liquid phase diffusion .

Water (or electrolyte) permeability is used quite routinely since the equipment is simple to set up and use. Based on the assumption of laminar flow, the Hagen-Poiseuille law may be used to calculate an average pore size from measured permeation rates with liquids of known viscosity. In interpreting the results, it should be remembered that the technique yields the average pore size for hydraulic flow. Although it is often tacitly assumed that this average also applies for the major diffusion and migration processes across battery separators, this assumption will be seriously in error whenever the pore size distribution is relatively broad and (or) the separator contains a limited number of larger pores or pinholes. The hydraulic flow per unit area (flux) increases with the square of pore diameter while the flux of ions (via migration and diffusion) and molecules (via diffusion) in first approximation is independent of pore diameter. As a result, measurement of the hydraulic permeability tends to exaggerate the influence of larger pores (or defects). While this actually enhances the value of this technique for detection of large pores and other flaws (for example, in a quality control step), additional means of characterizing pore size clearly are required to permit meaningful interpretation of permeability measurements.

Mercury porosimetry has been used in a few instances to provide information on average pore size and pore size distribution in separators. A knowledge of these characteristics is highly desirable because the presence of an appreciable number of large pores can be expected to significantly influence (presumably degrade) separator functions and performance. Although the technique has some limitations due to uncertainty of the mercury-separator contact angle and the compressibility of porous organic materials, mercury porosimetry does produce important information on porous structures* not readily available from other techniques, and its use to characterize separators is strongly recommended, especially in conjunction with other techniques such as measurement of water intrusion and permeability.

---

*This information can include indications regarding unusual pore shapes (such as ink-bottle pores) available from a more refined analysis of static and dynamic (hysteresis) porosimetry data.

Electron microscopy is a powerful technique to obtain detailed information on the structure of porous and microporous materials. It has been applied successfully to characterize pores in several types of battery separators. High resolution microscopy is required for micropores such as those found in radiation-grafted polyolefins. Whenever a resolution of about 200 Å is adequate, scanning electron microscopy is preferable because larger areas and greater depth of field can be scanned with minimal sample preparation. Since electron microscopy is the only method among those listed above to give direct evidence of the basic geometry in porous structures, it complements all other techniques and should be considered indispensable in any more fundamentally oriented separator development program.

Gas adsorption, gas permeability, and liquid phase diffusion all have been used with some success to determine pore size distribution and average pore size in separators. From our review of past work we conclude that these techniques could have advantages in special situations (for example, separator quality control tests could be based on gas permeability measurements). However, they do not seem to offer sufficient information beyond that available from the tests discussed above to justify their application in programs designed primarily for developing and screening separator materials.

Penetration by Zinc Dendrites

The most obvious function of separators in silver-zinc cells is to retard shorting of cells by zinc dendrites. Presumably, this is accomplished by the tortuous electrolyte path in porous separators. Another likely function of separators in reducing the dendrite problem is to promote a uniform current density distribution (thus minimizing dendrite-favoring areas of increased overvoltage) and, quite probably, retard zincate diffusion (thus increasing the effective throwing power of the electrolyte-electrode system).

There seems to be general agreement and some experimental evidence that both concepts point to the need for separators having very small pore size. However, there is also some evidence that dendrites can eventually penetrate through pores as small as 10 Å. Another separator function postulated for some materials is the gradual release of surface-active compounds that can retard dendrite growth. Not surprisingly in view of this complex situation, no model for the dendritistatic functions of a separator is available that could be used to design effective separators. Accordingly, extensive screening of candidate materials is used to empirically select dendritistatic separator materials.

Apparently, the only test for dendritistatic functions used in separator development programs is the zinc penetration test developed by Dalin and Solomon, which is described in the Cooper-Fleischer booklet. Although correlation of test results with separator behavior in cells has been claimed, quantitative evidence has not been presented. Previous test experience in inorganic separator screening, although probably not supported by sufficient cell tests, was inconclusive: the figures-of-merit (e.g., in minutes per mil penetration) obtained at Astropower Laboratory* were not outstanding although the separators had very good dendritistatic properties in cell tests.

Lander comments that one of the reported problems with the zinc dendrite penetration test as specified in the Cooper-Fleischer booklet is the buildup of zinc in the back of test samples. This effect is responsible for mechanically induced or accelerated failure of separators in the test; he suggests that a cycling test would avoid the problem. Perhaps a more relevant argument for cycling than this criticism (it might be argued that this effect, to some extent at least, simulates the situation in a battery as mossy zinc develops on the negative plate) is that cycling is the normal mode of battery operation, and that a zinc penetration test should attempt to simulate this condition. For example, inorganic separators with relatively large pores might function not so much by preventing dendrite penetration <u>into</u> separators as by limiting

---

*See Reference 8.

penetration through separators because of cyclic growth and dissolution of dendrites. This behavior is not simulated in the established zinc penetration test.

Another criticism of the test as now performed is that a high and unchanging concentration of zincate ion is present at the separator surface facing away from the zinc electrode. This does not simulate the situation in batteries especially during extended overcharge--the condition most conducive to dendrite growth. For the zinc dendrite penetration test to be more representative and, hence, more useful, it should be modified by simulating typical charge-discharge cycles and realistic concentrations of zincate ion in the cell electrolyte.

Silver Diffusion (Silver Oxide Transport)

Resistance of a separator to silver oxide transport is generally considered an important criterion for separator suitability, and silver diffusion tests patterned after the one described in the standard reference have been used quite routinely to characterize experimental separator formulations. A wide range--at least from 2.5×10^{-4} g/hr x cm^2 (1.6×10^{-3} g/hr x in.^{2}) to 2.5×10^{-2} g/hr x cm^2 (1.6×10^{-1} g/hr x in.^{2})--has been reported (see, for example, reference 7, p. 114, and reference 9) for the diffusion of silver oxide through membranes that appear to qualify as reasonably practical separator materials. This is rather surprising inasmuch as 2.5×10^{-2} g/hr x cm^2 would correspond to a self-discharge rate of about 6 mA/cm^2 (in the order of a C/7 rate). Some doubt may be expressed whether these data have any significance for separator characterization and screening--either because they might be in error* or because, for very permeable separators, the effective transport rate

*Compare, for example, a diffusion rate of 1.6×10^{-1} g/hr x in.^{2} (given in reference 9) with the upper limit for the diffusional flux R_d, estimated by using the standard relationship for the diffusive mass transport of silver oxide to the zinc negative is controlled by processes other than diffusion through the separator. Because of this, and also since silver diffusion rates might be calculated directly from a known(or estimated) diffusion coefficient and the mass transport characteristics of the porous structure, there is some question whether measurement of silver diffusion through candidate separators is worthwhile.

Direct measurement of silver diffusion is, however, useful for several reasons. The specific barrier property of the separator will show up if the diffusion measurement is performed in conjunction with other tests; this is important for conventional cellulosic membranes which constitute a partial chemical barrier to silver oxide transport. Equally important, any beneficial specific retardation caused by microporosity and (or) ion exchange properties of new materials would be discovered in the diffusion measurement. Even if no special barrier effect is present, an independent characterization of separator mass transport characteristics is very desirable, especially if the characterization test is basically simple.

---

rate

$$R_d = \frac{M_w P D c_o}{\tau^2 h} \left(\frac{g}{cm^2 x sec}\right)$$

and the following representative values:

Molecular weight of silver oxide	M_w	= 232 g/mole
Separator porosity	P	= 40% (high assumption)
Diffusion constant of silver oxide	D	= $10^{-5} cm^2/sec$ (high assumption)
Concentration of silver oxide	c_o	= $2.5x10^{-7} mole/cm^3$ (high assumption)
Pore tortuosity	τ	= 1.0 (low assumption)
Separator thickness	h	= $4x10^{-3}$cm (reference 9)

It follows that $$(R_d)_{max} = \frac{232x0.4x10^{-5}x2.5x10^{-7}}{4x10^{-3}} \approx 6x10^{-8}\left(\frac{g}{cm^2 xsec}\right)$$

$$\approx 1.4x10^{-3}\left(\frac{g}{in^2 xhr}\right)$$

that is, two orders of magnitude lower than the experimental silver transport rate given in reference 9.

Such appears to be the case regarding the diffusion tests described in the standard reference and used in subsequently published work. The required sensitive analysis for silver usually is done in the diffusion cell, either polarographically or via counting of a radioactive Ag^{110} tracer. The latter technique has the advantage that silver deposited in the separator by chemical reaction with the organic material is conveniently determined by the same counting apparatus. However, major criticisms of the tests as used in most of the previous work may be raised. First, stirring of the "receiving" compartment is generally performed to permit chemical analysis. Although no problems would be anticipated for microporous materials, our experience in other R&D projects has been that hydraulic flow caused by stirring can introduce large errors in measuring diffusion rates through membranes that have pores in the micrometer range. It seems possible* that this effect is responsible for some of the unusually large silver "diffusion" rates reported in the literature. On the other hand, if stirring is omitted or performed only occasionally, a stagnant diffusion layer will form

---

*The possibility that in stirred solutions hydraulic flow may become the major mode of silver oxide transport (at sufficiently large pore diameters) can be appreciated by calculating, for example, the differential pressure across the separator sufficient to cause a hydraulic flux (R_h) equal to ten times the diffusional flux (R_d). Using the expression for R_d from the footnote on the preceding page, and deriving the hydraulic flow of a solute through a separator from the Poiseuille equation, we set

$$R_h/R_d = \frac{PDc_oM_w}{\tau^2 h} \Big/ \frac{Pr_o^2 \Delta P c_o M_w}{8\eta\tau^2 h} = \frac{8\eta D}{r_o^2 \Delta P} = 10 \quad \text{(in cgs units)}$$

With representative assumptions ($D = 10^{-5}\ cm^2/sec$; $\eta = 10^{-2}$ Poise), the following pressure differentials are calculated:

r_o (micrometers)	0.1	0.32	1.0	10.0
ΔP (dynes/cm^2)	8×10^4	8×10^3	8×10^2	8
ΔP (cm H_2O)	80	8	0.8	8×10^{-3}

next to the separator and lead to lower diffusion rates than those representative for the separator itself.

Instead of using the accepted measurement techniques, we have proposed* to determine the flux of diffusing silver oxide by its potentiostatic reduction at a silver sheet or gauze electrode directly adjacent to the low concentration side of the separator. This approach would provide well-defined silver oxide concentration gradients and permit use of a simple measurement technique giving absolute flux data without further calibration. The proposed technique is particularly appropriate for materials such as our inorganic separators that are not expected to react rapidly with silver oxide.

Zinc Diffusion (Zincate Transport)

It is widely accepted that one of the most important functions of separators in silver-zinc cells is to retard the transport of zincate and that separators should be characterized in terms of their resistance to zincate transport.

A zinc diffusion screening test developed by Lander is described in the Cooper-Fleischer booklet and has been used in several separator development programs. Much of what has been said above for the silver oxide diffusion test also provides the rationale for recommending† that separator screening programs include a zincate transport measurement. This parallelism continues on the experimental side: potentiostatic reduction of zincate at a heavily amalgamated zinc (or platinum or gold) electrode directly adjacent to the separator is recommended as a potentially simpler, faster and more accurate analysis technique.

---

*In the interest of concentrating the technical effort on the separator materials investigation, no work on the proposed or any other technique for measurement of diffusion rates was performed.

†See second footnote on preceding page.

Recommended Tests

On the basis of the foregoing analysis, a series of tests was recommended for application to the separators developed in this program. These tests fall into two groups. The first group contains the tests considered essential for our separator development and screening program; it also includes the basic measurements required for separator characterizations. These measurements and tests were applied to the separators developed under Task II. The results are presented and discussed in some detail in the following sections; procedures and sequences used in the performance of measurements and tests are described in Appendices A and B, respectively.

The second group of recommended tests includes techniques for separator characterization that are considered very desirable but not essential for separator screening programs. In the interest of concentrating efforts on investigating the materials parameters of inorganic separators, the secondary tests were not applied in this program. However, their application, possibly together with other advanced techniques of investigation, is considered essential for any program directed toward an improved understanding of the mechanism(s) by which separators for silver-zinc cells function.

Primary separator measurements and tests:

- Weighing
- Measurement of dimensions and volume
- Water intrusion
- Electrical resistivity
- Degradation (chemical compatibility)
- Mercury porosimetry
- Water permeability
- Zinc gassing (inorganic separator stock)
- Zinc dendrite penetration
- Modulus of rupture (rigids)
- Burst strength (semiflexibles)
- Tensile strength (semiflexibles)
- Bending test (semiflexibles)

Secondary separator measurements and tests

- Electron microscopy
- Zinc dendrite penetration (during simulated cycling)
- Silver oxide transport (preferably by proposed SRI technique)
- Zincate transport (preferably by proposed SRI technique)

Results and Discussion

In accordance with the Work Statement for this program, candidate separator materials were first prepared and studied in the form of rigid ceramic disks. The results obtained in applying screening tests* to inorganic materials in the form of rigid, porous disks are given in Tables 25, 26, and 27. After review of these results, sixteen candidate inorganic materials were selected for preparation and screening of semiflexible separator formulations; the test results for semiflexible separators are given in Table 28. The five separator stock materials not included represented variations of the other materials. Although these variations might have resulted in somewhat different properties for the basic material and its variation in rigid form, the differences were expected to be negligible after incorporation of the materials in semiflexible separators.*

Screening test results for rigid and semiflexible separator samples are discussed in the following sections, beginning with the discussion of tests related principally to the function of separators in cells. Test results related primarily to separator compatibility with the cell environment are discussed subsequently. Many of these results were obtained in routine tests but important information was also developed in supplementary tests.

Resistivity: Rigid Disks

As shown in Tables 25, 26, and 27, the specific volume resistivities of the rigid disks fell in a rather narrow range. This result is a direct consequence of selecting disks from a limited range of porosities (about 24 to 29 vol%) and shows that disks with generally similar

---

*Materials F' and G' are related to E' both chemically and in terms of performance as rigids and were therefore deleted from study as semiflexibles. Similarly, material HP is a more pure and more costly form of JC, and was deleted. The three Q materials differed only in source of fabrication or in particle size, and only Q was retained for study in the semiflexible formulation.

Table 25

SUMMARY OF RESULTS (RIGID DISKS)

Class	Density (g/cc)	Porosity Range (Water Intrusion) (v/o)	Resistivity (Normalized to 45 w/o KOH at 18°C) (ohm-cm)	Modulus of Rupture (N/cm^2)	Modulus of Rupture ($lbs/in.^2$)	Pore Size (μm)	Potassium Hydroxide Degradation (w/o)	Zinc Dendrite Penetration (min)	Zinc Gassing (cc/24hr)	Materials Selected for Semiflexible Testing
OLIVINES										
A	3.4	25-28	26	689	1000	0.4	2.4	>25 hr	6600	+*
B'	3.4	24-26	25	1516	2200	0.6	1.5	100	1.7	+
C'	3.4	26-28	27	758	1100	0.7	20	140	8	+
D'	3.4	24-25	27	1724	2500	0.8	2.5	90	2.4	+
E'	3.4	25-26	27	1655	2400	0.5	12	250	0.0	+
F'	3.4	28-29	21	896	1300	1.0	5.0	210	0.1	
G'	3.4	27-29	16	896	1300	0.8	3.3	230	0.5	
TITANIAS										
H,J,JC	3.8	26-27	29	1172	1700	0.7	0.3	110	2.1	+
HP'	3.8	27-28	16	896	1300	0.4	0.4	190	5.3	
K	4.0	26-27	20	1172	1700	0.3	0.7	190	4.5	+
L'	3.9	28-29	17	689	1000	0.6	0.9	160	0.7	+
ZIRCONIAS										
(M)†	5.6	23-24	26			0.6	Severe	150	64.1	+
N	4.6	24-26	30	1516	2200	0.8	7.0	140		
N'	4.6	25-26	29	2069	3000	0.3	6.4	160	0.6	+
P	4.5	25-27	25	1516	2200	0.7	2.1	240	2.9	+
Q	5.4	27-29	30	2413	3500	0.6	4.8	110		+
Q'	5.4	28-30	29	1103	1600	0.4	5.9	180	32	
Q'-x	5.4					0.5		150	3.5	
R	5.4	27-28	18	1172	1700	0.7	0.9	120	87	+
R'	5.4	24-26	24	345	500	0.3	3.7	190	12.4	+
S'	4.6	27-28	20	1241	1800	0.5	1.2	300	0.2	+

*Material A was selected for study in the semiflexible formulation made from both the unmilled stock (A) and the milled stock (A')

†Material M intended for semiflexible formulations only. Data in rigid formulation not required.

Table 26

SUMMARY OF RIGID DISK SCREENING TESTS, BATCH 2*

Material	Code	Batch	Porosities (By Water Intrusion) P_w (Volume %)				Weight Loss (KOH Degradation) L (Weight %)			Resistivities (Normalized to 45% KOH and 291°K) $\bar{\rho}_r$ (ohm-cm)					Pore Diameters (By Water Permeation) D_p (micrometers)			Pore Diameters and Tortuosities (By Mercury Porosimetry) D_m (micrometers), τ_b (based on D_p and D_m)						Tortuosities (By Porosity and Resistivity) τ_a (Based on P_w and $\bar{\rho}_r$)		Zinc Dendrite T (min)
										KCl	KOH	KOH	KOH	KCl				D_m	τ_b	D_m	τ_b	D_m	τ_b			
			V	393 a	393 b	353 b	393 b	393 a	393 b	V	393 a	393 b	353 a	353 a	V	393 a	353 b	V	V	393 b	393 b	353 b	353 b	V	353 b	V
OLIVINES																										
A	-1-C	2.11	25.6	-	26.9	-	-	2.4	-	-	-	20.1	-	-	-	0.35	-	-	-	0.40	-	-	-	-	-	-
	-3-B	2.12	26.8	-	-	28.1	-	-	1.3	-	-	-	14.1	49.2†	-	-	-	-	-	-	-	-	-	-	2.3	
	-3-C	2.13	27.7	28.4	-	-	0.55	-	-	-	23.7	-	-	-	-	-	-	-	-	-	-	-	-	-	-	-
	-3-D	2.14	27.2	-	-	-	-	-	-	-	-	-	-	-	0.36	-	-	0.45	1.3	-	-	-	-	-	-	-
	-3-A	2.24	26.6	-	-	-	-	-	-	25.9	-	-	-	-	0.31	-	-	0.40	1.2	-	-	-	-	1.6	-	-
B'	-3-A	2.11	-	-	26.2	-	-	1.4	-	-	-	17.5	-	-	-	-	-	-	-	-	-	-	-	-	-	-
	-3-B	2.12	24.5	-	-	25.3	-	-	1.1	-	-	-	13.8	501†	-	-	0.18†	-	-	-	-	0.55	3.1	-	7	-
	-3-C	2.13	24.5	25.4	-	-	0.89	-	-	-	20.5	-	-	-	-	-	-	-	-	-	-	-	-	-	-	-
	-3-E	2.14	-	-	-	-	-	-	-	17.2	-	-	-	-	-	-	-	0.60	-	-	-	-	-	-	-	-
	-3-D	2.21	25.1	-	24.9	-	-	1.6	-	-	-	17.6	-	-	-	0.37	-	-	-	0.60	1.6	-	-	-	-	-
	-3-F	2.22	25.0	-	-	25.5	-	-	1.0	-	-	-	17.4	235	-	-	-	-	-	-	-	-	-	-	4.8	-
	-3-G	2.23	25.7	26.5	-	-	0.90	-	-	-	23.3	-	-	-	-	-	-	-	-	-	-	-	-	-	-	-
	-3-H	2.24	26.0	-	-	-	-	-	-	29.6	-	-	-	-	0.45	-	-	0.60	1.3	-	-	-	-	1.7	-	102
C'	-10-A	2.11	26.4	-	45.0	-	-	22	-	-	-	8.9	-	-	-	-	-	-	-	-	-	-	-	-	-	-
	-10-B	2.12	26.7	-	-	37.0	-	-	11	-	-	-	13.1	14.5†	-	-	0.47†	-	-	-	-	0.55	1.2	-	1.4	-
	-10-C	2.13	26.8	30.3	-	-	3.5	-	-	-	204	-	-	-	-	-	-	-	-	-	-	-	-	-	-	-
	-10-D	2.14	26.5	-	-	-	-	-	-	27.4	-	-	-	-	0.41	-	-	0.70	1.7	-	-	-	-	1.7	-	140
	-10-F	2.21	27.8	-	41.8	-	-	16	-	-	-	12.3	-	-	-	-	-	-	-	-	-	-	-	-	1.5	-
	-10-G	2.22	27.9	-	-	37.8	-	-	11	-	-	-	13.8	15.4	-	-	0.46	-	-	-	-	0.60	1.3	-	-	-
	-10-H	2.23	27.8	31.9	-	-	5.0	-	-	-	174	-	-	-	-	-	-	-	-	-	-	-	-	-	-	-
E'	-6-A	2.11	25.6	-	31.6	-	-	17	-	-	-	15.2	-	-	-	0.30†	-	-	-	-	-	-	-	-	-	-
	-6-B	2.12	25.5	-	-	28.4	-	-	4.4	-	-	-	17.0	25.7†	-	-	0.33	-	-	-	-	0.40	1.2	-	1.7	-
	-6-C	2.13	25.0	25.6	-	-	1.7	-	-	-	38.4	-	-	-	-	-	-	-	-	-	-	-	-	-	-	-
	-6-D	2.14	25.6	-	-	-	-	-	-	26.6	-	-	-	-	0.32	-	--	0.45	1.4	-	-	-	-	1.6	-	101
	-6-E	2.21	25.9	-	29.4	-	-	8.2	-	-	-	14.3	-	-	-	0.22	-	-	-	0.35	1.6	-	-	-	-	-
	-6-F	2.22	25.7	-	-	28.5	-	-	4.1	-	-	-	14.4	205	-	-	-	-	-	-	-	-	-	-	4.8	-
	-6-G	2.23	25.9	27.7	-	-	2.4	-	-	-	30.0	-	-	-	0.30	-	-	-	-	-	-	-	-	-	-	-
ZIRCONIAS																										
N	-3-A	2.11	24.3	-	30.1	-	-	7.0	-	-	-	16.8	-	-	-	0.61†	-	-	-	0.80	1.3	-	-	-	-	-
	-3-B	2.12	-	-	-	29.7	-	-	5.6	-	-	-	15.9	208†	-	-	-	-	-	-	-	-	-	-	4.9	-
	-3-C	2.13	26.0	29.1	-	-	3.1	-	-	-	33.3	-	-	-	-	-	-	-	-	-	-	-	-	-	-	-
	-3-D	2.14		-	-	-	-	-	-	31.5	-	-	-	-	0.42	-	-	0.75	1.8	-	-	-	-	1.8	-	140
	-4-A	2.21	26.7	-	32.7	-	-	7.1	-	-	-	12.4	-	-	-	0.17	-	-	-	0.70	4.1	-	-	-	-	-
	-4-B	2.22	25.5	-	-	28.2	-	-	4.0	-	-	-	18.2	53.5	-	-	-	-	-	-	-	-	-	-	2.4	-
	-4-C	2.23	25.7	28.7	-	-	3.1	-	-	-	25.0	-	-	-	-	-	-	-	-	-	-	-	-	-	-	-
	-4-D	2.24	25.3	-	-	-	-	-	-	29.8	-	-	-	-	0.52	-	-	0.70	1.4	-	-	-	-	1.7	-	148
Q'	-3-A	2.11	-	-	37.1	-	-	5.8	-	-	-	20.7	-	-	-	-	-	-	-	-	-	-	-	-	-	-
	-3-B	2.12		-	-	33.7	-	-	4.2	-	-	-	62.7	22.3†	-	-	(0.18)	-	-	-	-	0.30	1.7	-	1.7	-
	-3-C	2.13	-	28.5	-	-	0.48	-	-	-	30.6	-	-	-	-	-	-	-	-	-	-	-	-	-	-	-
	-5-A	2.14	29.5	-	-	-	-	-	-	20.7	-	-	-	-	0.36	-	-	0.40	1.1	-	-	-	-	1.5	-	60
	-2-A	2.21	29.0	-	36.9	-	-	5.9	-	-	-	53.0	-	-	-	0.28	-	-	-	0.40	1.4	-	-	-	-	-
	-2-B	2.22	27.9	-	-	34.6	-	-	4.9	-	-	-	62.8	18.9	-	-	-	-	-	-	-	-	-	-	1.6	-
	-2-C	2.23	28.4	30.2	-	-	0.88	-	-	-	25.6	-	-	-	-	-	-	-	-	-	-	-	-	-	-	-
	-2-D	2.24	28.9	-	-	-	-	-	-	24.9	-	-	-	-	0.36	-	-	0.35	~1.0	-	-	-	-	1.7	-	178

*Temperature (°K) and letters (a, b) used in column headingd have following meanings: V indicates the virgin disks before screening tests; letters following temperatures refer to values obtained after degradation tests, i.e., 393a indicates degradation at 120°C in a volume ratio of two to one, and 393b indicates degradation at 120°C in a volume ratio of 100:1, and similarly for other headings.

†These data were obtained using water which may have been contaminated with particulate matter.

Table 27

RESULTS - BATCHES 3 AND 4

Batch	Mat'l Class	Code	Porosity (volume percent) Virgin	Porosity Deg 393°K	Porosity Deg 353°K	KOH Wt Loss L, in W/O 393°K	KOH Wt Loss L, in W/O 353°K	Resistivity, $\bar{P}_r$ Virgin	Resistivity Deg 393°K	Resistivity Deg 353°K	Tortuosity, τ_a Virgin	Tortuosity Deg 393°K	Tortuosity Deg 353°K	Pore Size--H_2O Perm. (micrometers) Virgin	H_2O Perm. Deg 393°K	H_2O Perm. Deg 353°K	Pore Size--H_g Porosim. (micrometers) Virgin	H_g Porosim. Deg 393°K	H_g Porosim. Deg 353°K	τ_b	Zinc Dendrite T_p (mins.)	MOR N/cm^2	MOR lb/in^2	Zinc Gassing	Batch No.
Batch 3	Olivines	A-1-B	25.5					24.0			1.5			0.37							>25 hrs	696	1010	5 ml/min	3.3
		D'-8-A	24.6	26.3		2.5		26.6	22.0		1.6	1.5												2.4 ml/	3.1
		D'-8-B	24.7		25.7		1.3	25.8		23.3	1.6		1.5			0.50			0.75					day	3.2
		D'-8-C	24.8					28.1			1.7			0.53						1.5	89				3.3
		D'-8-D	24.7														0.75					1860	2700	↓	3.4
	Titanias	JC-7-A	27.1	27.2		0.3		27.2	28.4		1.7	1.7			0.47			0.70				978	1420	1.6 ml/	3.1
		JC-7-B	25.9		25.9		0.1	28.9		29.5	1.7		1.7			0.46								day	3.2
		JC-7-C	25.5					30.8			1.7			0.47						1.5	112				3.3
		JC-8-A	27.3														0.70					1419	2060	↓	3.4
		K-5-A	27.0	28.0		0.7		19.2	20.3		1.4	1.5												4.5 ml/	3.1
		K-5-B	26.7		27.3		0.5	21.0		20.6	1.5		1.5		0.20			0.25				1247	1810	day	3.2
		K-5-C	26.5					21.0			1.5			0.18						1.3	194				3.3
		K-4-D	27.2														0.25					1130	1640	↓	3.4
	Zirconias	M-5-A	23.3					25.7			1.5			0.44							148			64 ml/	3.3
		M-5-B	23.0																					day	3.3
		N'-6-A	25.5	34.6		6.4		28.2	14.3		1.7	1.4			0.16			0.2				496	720	0.6 ml/	3.1
		N'-6-B	26.2		35.1		6.7	28.4		14.8	1.7		1.4			0.17								day	3.2
		N'-6-C	25.6					30.7			1.8			0.16						1.4	160				3.3
		N'-6-D	25.5														0.25					1984	2880	↓	3.4
		P-4-E	25.7	28.9		2.1		27.7			1.7													2.9 ml/	3.1
		P-4-B	25.7		27.7		0.7	27.0		23.0	1.6		1.6			0.49		0.7				503	730	day	3.2
		P-4-C	25.9					21.6			1.5			0.56											3.3
		P-4-D	26.2														0.7			1.3		1502	2180		3.4
		P-3-A	26.7																						3.3
		P-5-B	24.1																		244			↓	3.3
		Q-6-A	25.4	31.0		4.8		33.1	21.6		1.8	1.6			0.16			0.3				469	680		3.1
		Q-6-B	25.6		31.4		3.6	32.1		21.2	1.8		1.6			0.23				1.9					3.2
		Q-6-C	25.1					29.7			1.7			0.32							111				3.3
		Q-6-D	25.7														0.55			2.0		2549	3700		3.4
		R-12-A	27.9	29.1		0.9		17.7	16.2		1.4	1.4												85 ml/	3.1
		R-12-B	28.0		28.8		0.4	17.0		16.8	1.4		1.4			0.57			0.7			455	660	day	3.2
		R-13-A	27.4					18.2			1.4			0.56						1.2	120			↑	3.3
		R-13-B	27.1														0.7					1171	1700	12 ml/	3.4
		R'-8-A	25.5	32.0		3.7		23.5	15.6		1.5	1.4			0.24			0.3				407	590	day	3.1
		R'-8-B	24.0		28.5		3.1	26.8		19.0	1.6		1.5			0.21									3.2
		R'-8-C	25.8					23.0			1.5			0.24						1.3	192				3.3
		R'-8-D	25.3														0.3					372	540	↓	3.4
Batch 4	Olivines	F'-5-A	28.3			5.3		20.4			1.5							0.9						0.1 ml/	3.1
		F'-3-A	28.7	31.2		4.2		18.3			1.4													day	3.1
		F'-5-B	28.3		30.4		3.0	22.3		16.2	1.6		1.4						0.9						3.2
		F'-5-C	28.5					22.2			1.6			0.29						3	210				3.3
		F'-5-D	28.4														0.95					903	1310	↓	3.4
		G'-12-A	28.7	29.3		3.3		15.6	15.2		1.3	1.3						0.9						0.5 ml/	3.1
		G'-12-B	28.5		28.6		0.1	16.2		15.9	1.3		1.3						0.7					day	3.2
		G'-13-A	27.6					18.4			1.4														3.3
		G'-11-A	28.7					13.9			1.2														3.3
		G'-10-B	27.5																						3.3
		G'-13-C	27.0														0.8					909	1320	↓	3.4
	Titanias	HP'-6-A	27.8			0.6		13.0			1.2							0.4						5.3 ml/	3.1
		HP'-5-A	27.1	27.3		0.2		17.2	14.5		1.3	1.2						0.4						day	3.1
		HP'-6-B	27.6		28.1		0.4	15.6			1.3		1.3						0.45						3.2
		HP'-6-C	27.5					15.5			1.3			0.35						1.2					3.3
		HP'-6-D	27.1														0.4					469	680	↓	3.4
		L'-3-A	28.6	29.8		0.9		16.4	16.7		1.4	1.4						0.55						0.7 ml/	3.1
		L'-3-B	28.6		29.3		0.6	17.1		17.1	1.4		1.4						0.6					day	3.2
		L'-5-A	28.6		28.7		0.5	17.2		15.3	1.4		1.3						0.55						3.2
		L'-3-C	27.8					17.1			1.4			0.31						1.8					3.3
		L'-5-B	28.4					18.4			1.4														3.3
		L'-3-D	28.3														0.55					655	950	↓	3.4
	Zirconias	S'-4-A	27.6	29.7		1.2		19.1	16.8		1.4	1.4						0.5						0.2 ml/	3.1
		S'-4-B	27.0		28.0		0.5	22.0		19.8	1.5		1.5						0.5					day	3.2
		S'-5-A	27.8					20.0			1.5			0.36						1.3	306				3.3
		S'-5-B	27.5														0.45					1206	1750	↓	3.4

Table 28

RESULTS OF SEMIFLEXIBLE SEPARATOR SCREENING TEST

Material	Test	Physical Properties: Wafer Thickness (mils)	Coating Thickness (mils)	Wafer Weight (grams)	Area Density (milligrams/cm^2)	Volume Mercury Intruded (μℓ at 15,000 psi)	Open Porosity by Mercury Intrusion (volume percent)	Zinc Dendrite: Zinc Dendrite Shorting Time Average of Five (minutes)	Zinc Dendrite Shorting Time Minimum Time Observed (minutes)	Zinc Dendrite Shorting Time Maximum Time Observed (minutes)	Mechanical Properties: Tensile, Dry (breaking load, grams)	Tensile, Wet One-Week Soak, RT, KOH (breaking load, grams)	Burst, Dry (burst pressure, inches Hg)	Burst, Wet with H_2O Initial (burst pressure, inches Hg)	Burst, Wet with H_2O One-Week Soak, RT, H_2O (burst pressure, inches Hg)	Burst, Wet with KOH One-Week RT Soak plus 48 Hours 353°K (80°C) (burst pressure, inches Hg)	Flex, Dry (cracking diameter, inches)	Flex, Wet One-Week Soak in KOH (cracking diameter, inches)	Permeability: Permeability, Fresh Equation B, based on h (pore diameter, microns)	Permeability, Soaked Equation B, based on h (pore diameter, microns)	Resistance: Resistivity, $\bar{\rho}_r$, h Initial (ohm-cm)	Resistivity, $\bar{\rho}_r$, h Soaked (ohm-cm)	Resistivity, $\bar{\rho}_r$, h Degraded (ohm-cm)	Resistivity, $\bar{\mathcal{R}}_r$, h Initial (ohm-cm^2)	Resistivity, $\bar{\mathcal{R}}_r$, h Soaked (ohm-cm^2)	Resistivity, $\bar{\mathcal{R}}_r$, h Degraded (ohm-cm^2)
	Mean Entire Population	15.8	5.21	0.2494	48.8	71.7	35.0	234	180	294	2740	665	61.1	20.4	24.0	11.8	0.73	0.15	0.044* 0.06	0.044* 0.053	41.8	32.6	21.2	1.67	1.31	0.847
	No. of Samples Tested per Material	24	36	16	16	32	24	5	1	1	2	2	2	2	2	3	2	2	2	2	3	3	3	3	3	3
Olivines	A	16.3	5.2	0.2604	51.0	74 71	34	89	75	110	2300	670	75	23	23	13	1.0	0.13	0.09	0.05	38	26	18	1.62	1.09	0.779
Olivines	A′	15.5	4.9	0.2236	43.8	64 67	33	160	90	230	3600	912	90	34	31	13	0.8	0.09	0.08	0.06	61	49	26	2.51	2.01	1.09
Olivines	B′	15.9	5.3	0.2350	46.0	73 72	35	250	170	310	3600	790	89	30	29	12	0.6	0.13	0.08	0.08	64	41	27	2.52	1.63	1.08
Olivines	C′	16.2	5.5	0.2375	46.5	69 72	34	280	210	340	2800	750	67	23	25	15	0.9	0.13	0.05	0.06	62	40	24	2.50	1.58	0.957
Olivines	D′	15.2	5.1	0.2323	45.5	65 69	34	290	250	340	3200	710	67	17	31	16	0.5	0.13	0.09	0.09	48	38	24	1.86	1.47	0.925
Olivines	E′	16.3	5.4	0.2396	49.6	65 71	32	330	290	410	2600	670	71	21	24	12	0.7	0.19	0.07	0.01*	35	25	19	1.51	1.25	0.812
Titanias	JC	17.5	6.0	0.2585	50.6	81 80	35	390	340	460	2000	530	57	10	18	7	0.7	0.13	0.01*	0.04*	29	28	16	1.27	1.23	0.689
Titanias	K	15.4	5.0	0.2342	45.9	67 70	34	160	140	180	3100	790	70	24	32	18	0.6	0.19	0.01*	0.05	49	37	22	1.90	1.44	0.859
Titanias	L′	14.5	4.8	0.2297	45.0	67 65	35	230	90	330	2900	600	52	26	32	10	0.6	0.25	0.01*	0.02*	35	33	23	1.30	1.25	0.855
Zirconias	M	14.8	4.8	0.2685	52.6	76 67	37	200	180	220	2200	520	47	17	21	9	0.6	0.13	0.009*	0.01*	34	27	20	1.37	1.09	0.795
Zirconias	N′	15.8	5.2	0.2523	49.4	75 74	36	200	170	260	2200	600	47	14	21	15	0.9	0.06	0.03*	0.04	25	21	14	1.01	0.865	0.579
Zirconias	P	15.7	5.6	0.2648	51.8	70 75	36	250	170	350	2700	550	59	20	21	9	0.5	0.19	0.09	0.06	29	29	21	1.18	1.17	0.835
Zirconias	Q	15.6	5.1	0.2659	52.1	71 76	36	200	140	260	2400	630	18[a]	19	21	12	0.8	0.06	0.03*	0.03*	55	28	29	2.10	1.07	1.09
Zirconias	R	15.9	5.3	0.2846	55.7	72 75	36	250	170	370	3000	760	53	22	23	10	0.8	0.38	0.02*	0.02*	36	34	21	1.46	1.37	0.852
Zirconias	R′	15.0	4.2	0.2370	46.4	73 69	36	180	140	210	2800	520	43	17	22	11	0.8	0.06	0.03*	0.05	31	30	17	1.16	1.13	0.663
Zirconias	S′	16.7	5.8	0.2652	51.9	75 80	36	290	250	320	2600	630	57	17	21	9	0.9	0.13	0.02*	0.02*	34	31	17	1.42	1.29	0.695

[a] Samples were wetted and data here should be rejected.

* Anomalous behavior during test.

porosities also have similar tortuosities. However, the results obtained in the preliminary Batch 1 test for a group of disks with different porosities indicate that pore tortuosity is not independent of porosity. Figure 15 displays this effect, which shows up as a decidedly nonlinear relationship between conductivity and porosity; the scatter of data over a band may be due (at least in part) to the imprecision of the resistance data of these first studies for which the resistance cell had not yet been modified (see Appendix A). The relationship expected for a porous body comprising straight pores (forming a 90° angle with the surface) is also shown in Figure 15. The experimental data show that the deviation from this simple model becomes very large at porosities below 15%, and the curvature of the plot indicates that tortuosity is increasing with decreasing porosity. For a given porosity, however, the range of conductivities is within the experimental uncertainty for all disks tested. Thus, although the disks represented ten different materials, no material appears to fall outside the band of data scatter, suggesting that all materials have a similar porous structure.

Preliminary evaluation of the resistance measurement technique with Batch 1 disks had suggested a better repeatability than that indicated by the ±20% scatter of the experimental data. To investigate this inconsistency further--especially also the possible role of chemical attack on separator resistance--six disks all of material H but having different porosities, were selected for a more detailed study of resistance and its possible changes as a result of various treatments applied to the disks. To examine the chemical factor, the electrolyte was alternated between 45 wt% KOH and 0.1N KCl; disks were cleaned by Soxhlet extraction between measurements. The results are shown in Table 29.

In examining the data, the more than proportionate decrease of conductivity with decreasing porosity is again noted. Further, even after normalizing the resistance data (using the conductivities of

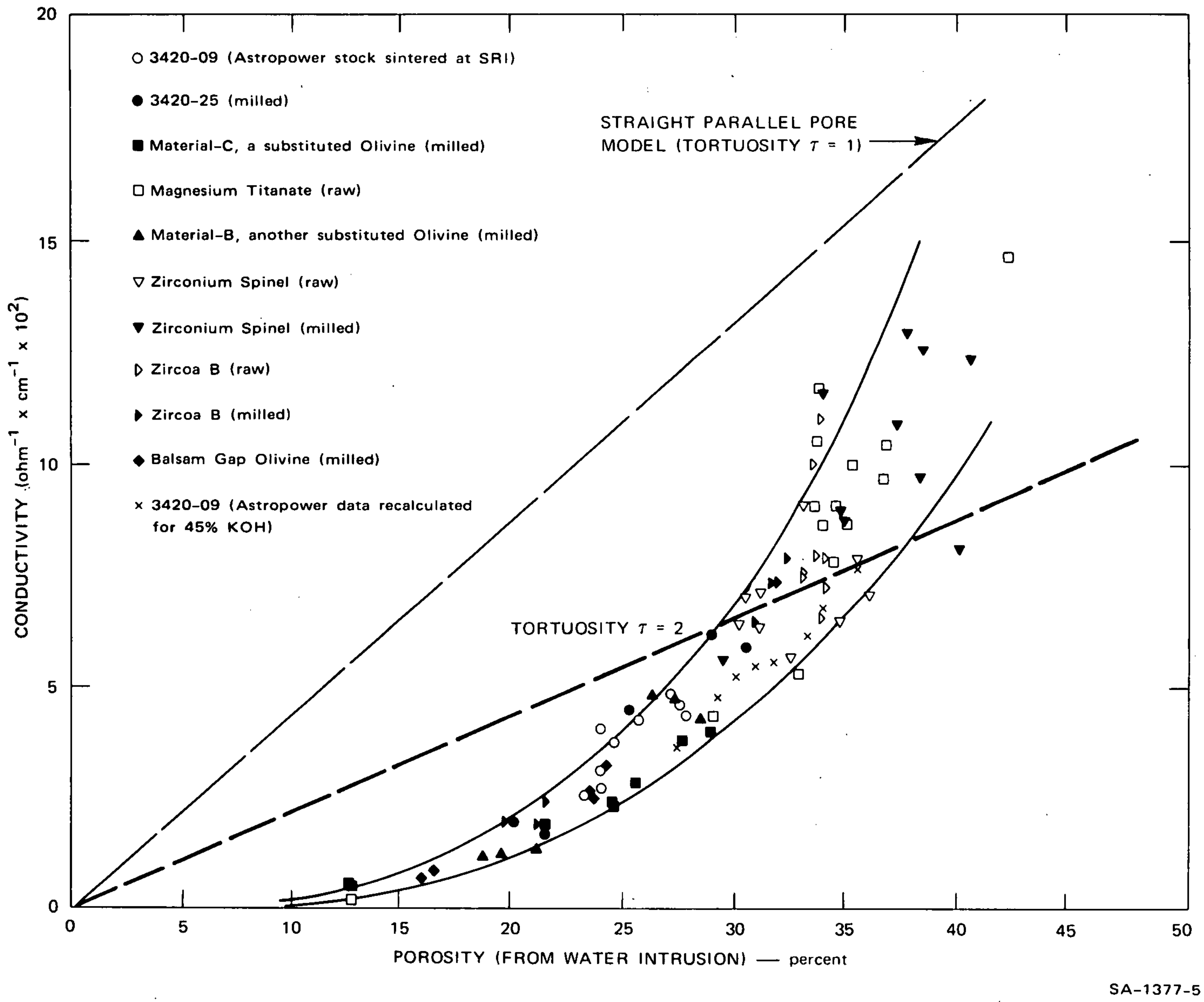

FIGURE 15 SPECIFIC CONDUCTIVITY VERSUS OPEN POROSITY FOR RIGID SEPARATORS

Table 29

RESISTANCE VARIATIONS AS OBSERVED FOR SUCCESSIVE DISK MEASUREMENTS WITH TWO ELECTROLYTES, WITH CLEANING AND DRYING BETWEEN MEASUREMENTS

	Normalized Specific Resistivity* $\bar{\rho}_r$								Average and Range			
Treatment Sequence	1	2	3	4	5	6	7	8	KOH		KCl	
Electrolyte Used	KCl	KCl	KOH	KCl	KOH	KCl	KOH	KCl				
Disk Identification by Porosity--P_w									Avg. $\bar{\rho}_r$	Range %	Avg. $\bar{\rho}_r$	Range %
9.9	2080	628	669	754	1370	787	344	1060	794	+72 -57	1060	+96 -41
10.5	1030	782	591	544	472	603	632	619	565	+11 -16	716	+44 -24
22.2	52.2	68.0	57.6	62.7	69.5	60.2	64.4	55.2	63.8	+9 -10	59.7	+14 -13
23.2	44.5		36.4	45.1	42.0	42.7	39.5	49.6	39.3	+7 -7	45.5	+9 -6
26.8	30.0		26.5	31.2	27.1	29.9	27.2	30.5	26.9	+1 -1	30.5	+2 -2
26.2	30.7		28.2	31.9	28.6	34.3	27.8	33.3	28.2	+1 -1	32.6	+5 -6

*All resistivity results are normalized to the equivalent of 45 wt % KOH at 291°K (18°C).

45 wt% KOH and 0.1N KCl measured for the free electrolytes) separator resistivities depended on the nature of the electrolyte and varied unsystematically with the stage of the test. Unexpectedly, these effects were far greater for the 10% porous disks than for the 24% porous disks, although the precision of resistance data should increase with increasing resistance, that is, decreasing porosity. Thus, the data do indeed suggest chemical factors as influencing resistance measurements: such factors should be more noticeable in a more completely sintered (lower porosity) material with fewer and finer pores more susceptible to being opened by chemical attack or closed by debris generated in this attack.

The ratio of the KOH results to those in KCl for the 24% disks was 0.92; this result is justification for using the more convenient and stable KCl as the electrolyte rather than KOH for resistance measurements for the disks in later batches (which had comparable porosities).

Resistivity: Semiflexible Wafers

The results of resistance measurements on semiflexible wafers are given in Table 28; these measurements were made with KOH only because it was found that semiflexible wafers could not be adequately wetted and infused with KCl solutions. Both specific volume resistivity (ρ_r) and specific area resistivity (κ_r) are presented for three experimental conditions: after initial contact with 45 wt% KOH, after one week's soaking, and after 48 hours' degradation at 80°C. The results of resistivity measurements vary with time, and this variation was systematic and substantial with semiflexible samples. As shown in Figure 16, a rapid decrease in resistance to about 75% of the initial value was observed over 1 to 2 days. Seven weeks later, the resistance had decreased to 1/2 to 2/3 of the original value and a tendency to level out was apparent. Although the data do not permit an accurate extrapolation as to what value is ultimately approached, the resistance data after the seven-day room-temperature soak in 45 wt% KOH are considered to be an adequate basis for choosing resistance values that are representative of semiflexible separator samples in actual cells.

A second question of considerable importance for adequately characterizing semiflexible separators in terms of their resistance concerns the location of the major part of that resistance. Both the asbestos and the coating can be expected to contribute to resistance, and a knowledge of the relative contribution is required not only for correlating resistance with other separator properties but for any future attempts to optimize separator functions. Accordingly, resistance contributions were studied, using semiflexible separators made from material Q. The thickness of the coatings was varied by using different numbers of dips into the coating slurry (see Task II). The results are

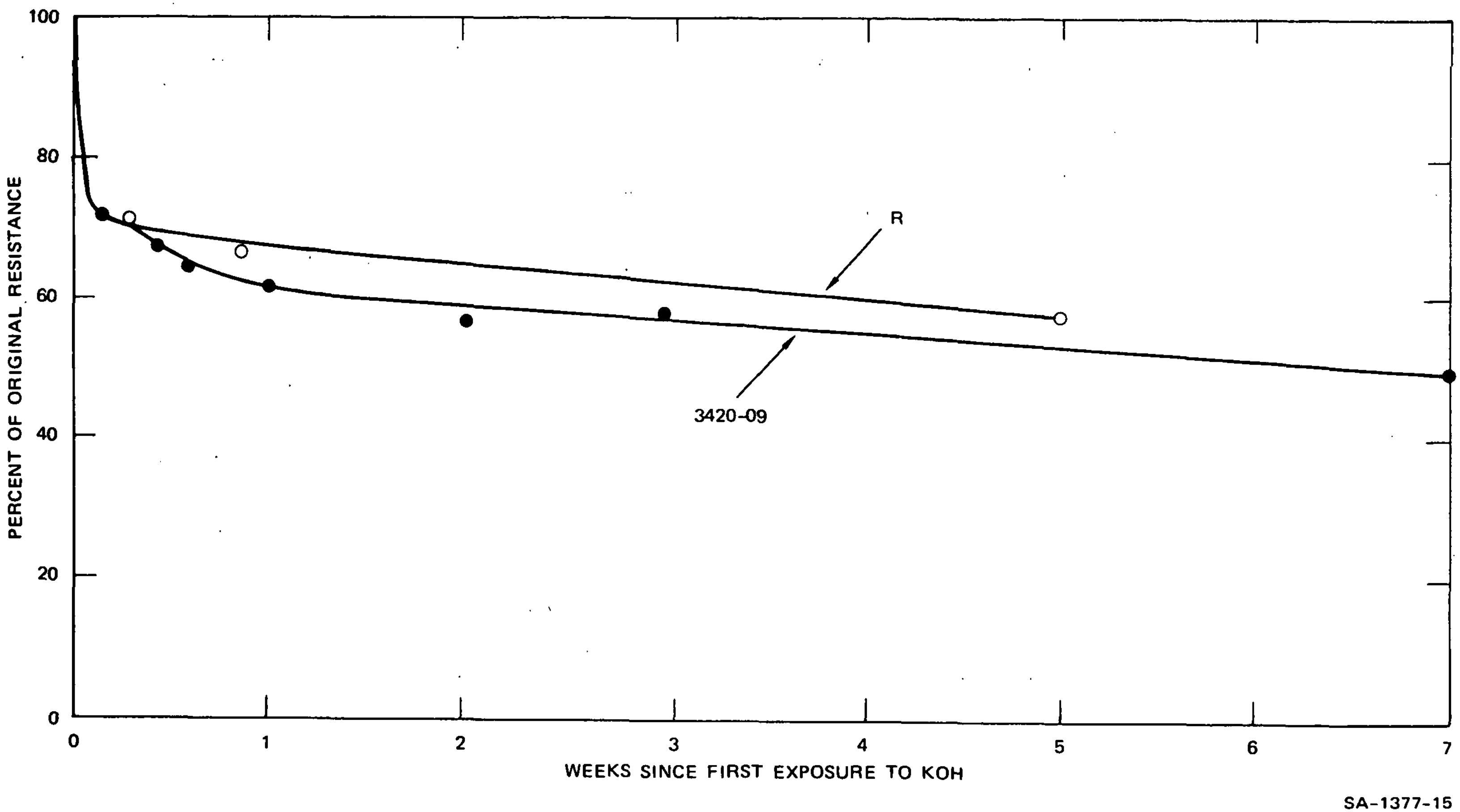

FIGURE 16 CHANGE IN RESISTIVITY WITH TIME AT ROOM TEMPERATURE

given in Figure 17, in which the specific area resistivity is plotted against total bag thickness for two conditions of measurement: after initial exposure of samples to 45 wt% KOH, and after seven days of soaking. The range of results is indicated for each average plotted.

Three tendencies are evident from the curves presented:

(1) Both curves tend to pass through the origin, suggesting that the contribution to total resistance of the separator is approximately the same (per unit thickness) for the coating and the asbestos paper. This finding was surprising as it had been believed that the coating was the major factor in controlling separator resistance.

(2) The reduction in resistance resulting from soaking presented in Figure 17 is again clear. In this case, the resistances were reduced to 75, 70, and 65% of the original values for the various thicknesses of 0.03, 0.045 and 0.055 cm (12, 18, and 22 mils, respectively). It also appears that neither the asbestos nor the coating is unchanged by the KOH; however, the resistance change occurs to a greater extent in the coating.

(3) The scatter in results decreases both as a result of soaking and as the value of resistance increases.

These observations suggest that (1) better cell performance should be observed about a week after initial activation of the cell, and (2) the asbestos paper of the separator contributes significantly to cell resistance and, hence, influences the power capability of the cell.

Porous Structure: Rigid Disks

The porosities of rigid disks, as determined by water intrusion, are summarized in Table 25 and presented in Tables 26 and 27. As discussed in the section on screening tests, these porosities agreed within 10% with results obtained by mercury intrusion to pressures as high as 41,300 N/cm^2 (60,000 psi). This agreement supports our general observation that the rigid disks were easily wetted and completely flooded by water or electrolyte.

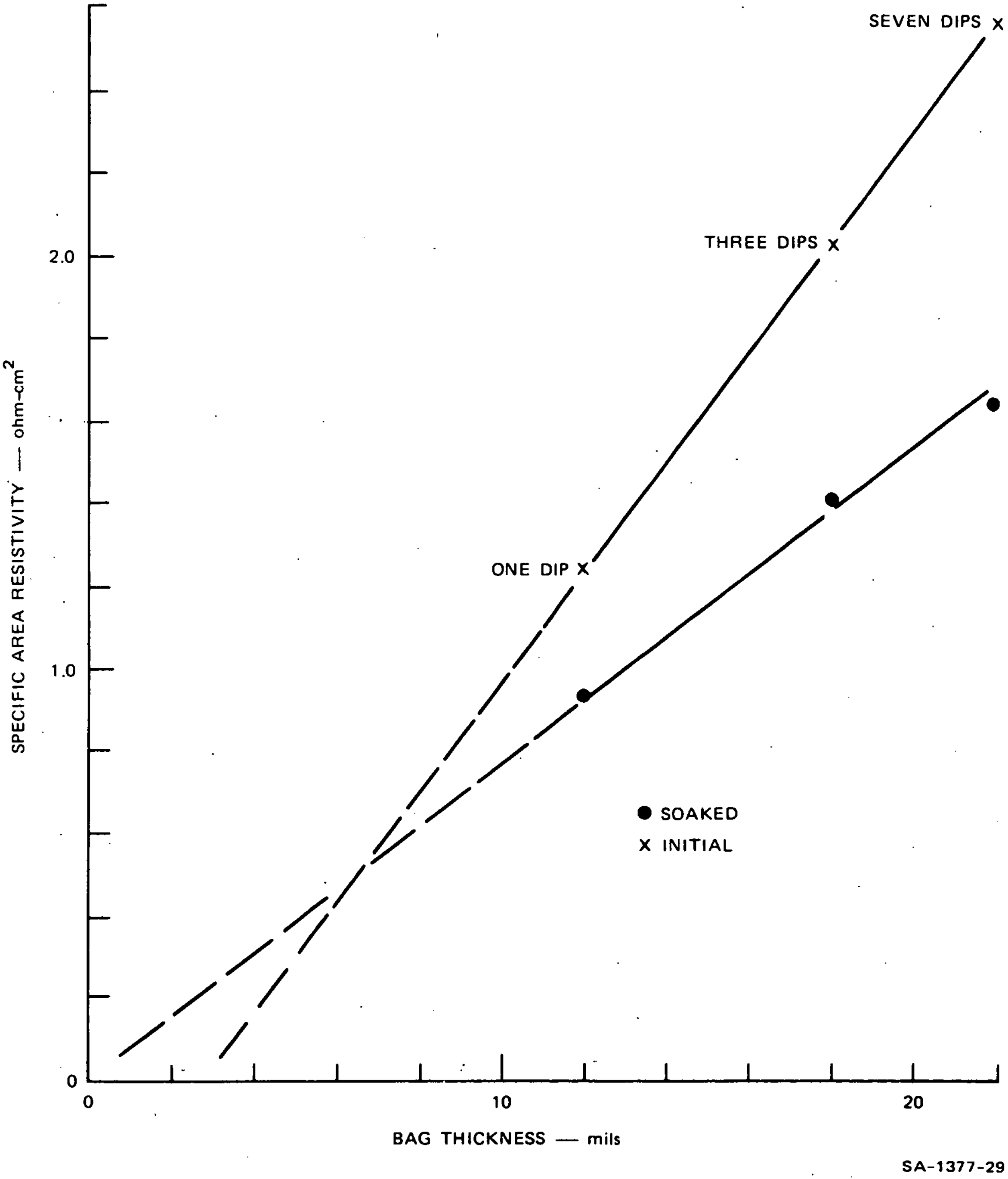

FIGURE 17 AVERAGE VALUES OF $\bar{K}_r$ PLOTTED AGAINST SEPARATOR THICKNESS

Mercury intrusion provides both total void volume and pore size information. It was found that all rigid formulations had very similar mercury intrusion behavior. This behavior is displayed in Figure 18, which is a plot of mercury intrusion against pressure for a disk of material N'. The average pore size indicated for this disk is 0.25 μm, and the pore population falls in the very narrow range between 0.1 and 0.3 μm. As explained in Appendix A, the volume intruded at maximum pressure is a good measure of total void volume if the volume of pores with diameters below approximately 1 μm is neglected.

From measured values for water (or mercury) intrusion volume, the resistivity of a porous separator sample, and the free electrolyte resistivity, a pore tortuosity factor τ_a can be calculated according to

$$\tau_a = \sqrt{P_W \bar{\rho}_r / \rho_N}$$

Calculated values* for this first type of porosity are included in Tables 26 and 27.

Pore size information may also be independently determined by water permeation studies; such studies were performed and evaluated for the rigid disks using the methods and equations given in Appendices A and C, respectively. The results are presented in Tables 26 and 27, expressed as average pore diameters calculated from permeation rates. The data show that the pore size determined by mercury porosimetry is in fair agreement with the pore size as determined by water permeation. However, the pore size determined by mercury porosimetry is always larger than that determined by water permeation, as predicted by tortuosity considerations. Applying the Poiseuille law to a separator

---

*Basis for the calculated values of τ_a is Eq. (17a), Appendix C, which already contains the standard free electrolyte resistivity.

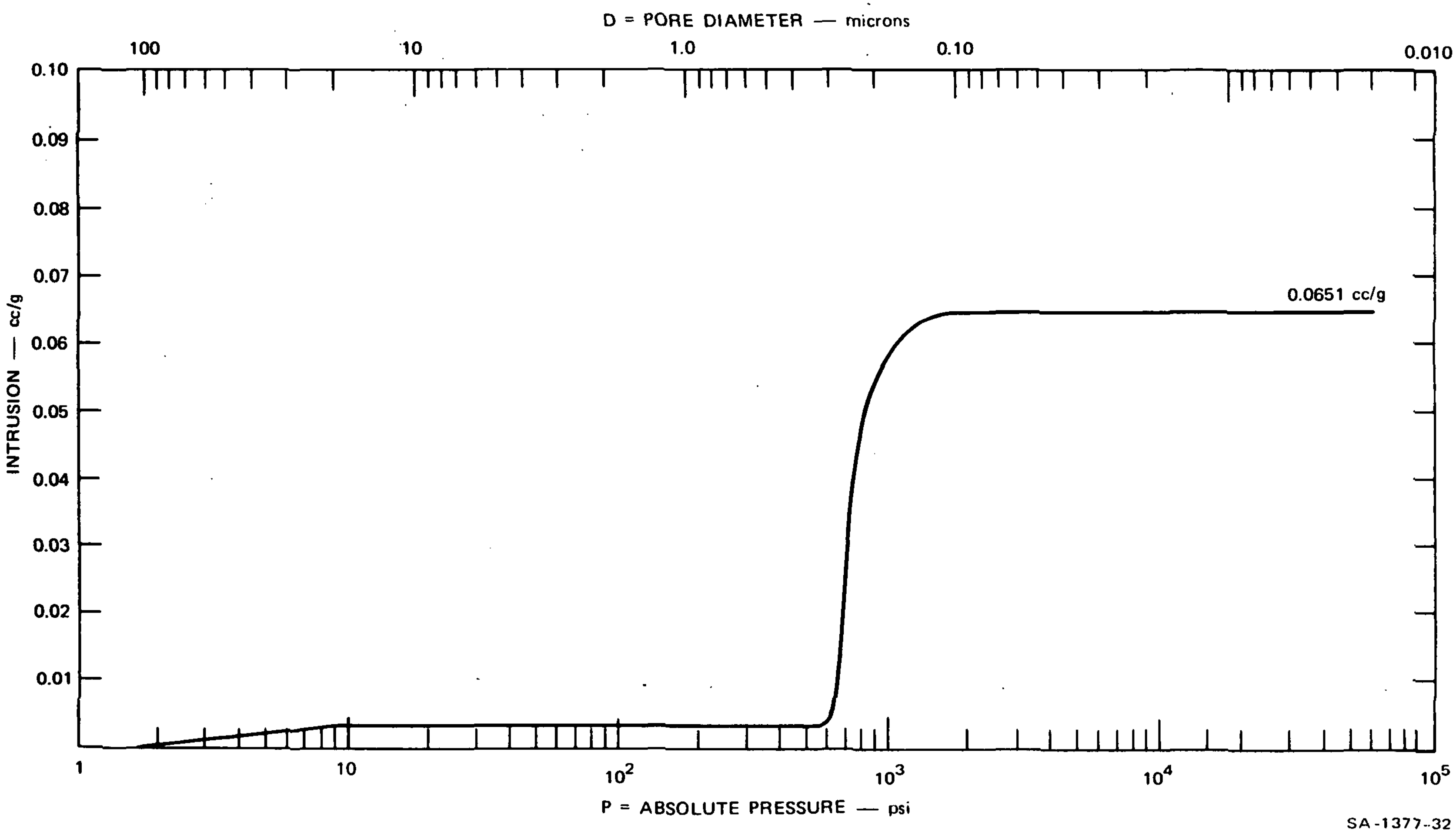

FIGURE 18 TYPICAL POROSIMETRY CURVE FOR A RIGID CERAMIC SEPARATOR

(thickness h) having tortuous pores (tortuosity τ_b) of true (average) radius r_o shows that the expected water flux is

$$f = \frac{P\Delta P r_h^2}{8\eta h} = \frac{P\Delta P r_o^2}{8\eta h \tau_b^2}$$

Measurements of water permeability will yield the hydraulic pore radius r_h. Mercury porosimetry, on the other hand, yields the true pore radius r_o; from the equation above it follows that $r_h = \frac{r_o}{\tau_b} \leqslant r_o$ since by definition $\tau_b \geqslant 1$. Values of this second, independently determined tortuosity factor calculated* from measured hydraulic and porosimetry-derived average pore sizes (diameters or radii) are also included in Tables 26 and 27.

The data of Tables 26 and 27 show that the tortuosities τ_a for the rigid disks generally fall in the range from 1.3 to 2. Similarly, the range for τ_b is 1 to 2. Excluding a few very large, presumably incorrect tortuosities, the τ_a value is larger than the τ_b value in 14 of the 18 cases in which both values are available.

The fact that τ_a tends to be larger than τ_b may be due to the nature of the water permeation test: because this test is very sensitive to larger pores or pinholes, the presence of even relatively few of these imperfections in the disks will tend to result in permeation rates (and, hence, pore sizes) exceeding those expected from the average geometric pore size. This, in turn, would result in unrepresentatively small values of τ_b.* Other possible explanations for the observation that $\tau_a > \tau_b$ include small systematic errors in the determination of resistivities and(or) pore sizes (by porosimetry).

To the extent of agreement between the two indices of tortuosity, and within the precision of the results from which the tortuosity data

---

*See (17b), Appendix C.

are calculated, it may be concluded from Tables 26 and 27 that no single material or class is distinguished from others on the basis of tortuosity. This finding is not unexpected, since all disk samples were sintered from powders of the same range of particle size. The generally similar resistivity and tortuosity results for virgin disks of different chemical composition also suggest that chemical attack by the test electrolytes was small at most.

Porous Structure: Semiflexible Wafers

The porous structure of the semiflexible formulations was investigated using the same tests as for rigids; the results are summarized in Table 28. One result of the mercury porosimetry test was that the porosities of all semiflexible formulations lie within a narrow range. Furthermore the pore size distribution curves were also quite similar for these materials. However, because mercury porosimetry yields information on pore size distribution averaged over a whole sample only, this technique is necessarily less instruction in characterizing the inhomogeneous structures of semiflexible wafers.

The effects on pore size distribution of impregnating and then coating the asbestos backing are displayed in Figure 19; the curve for material R is representative of those obtained for all semiflexible materials. As expected, the total porosity is decreased by progressive fabrication steps, and the number of large pores (for example, those with diameters greater than 1 μm) is reduced. Interpreted the same way as for the rigid samples, the mercury porosimetry data for semiflexible separators show that the major population of pores is in the size range between 0.1 and 1 μm.*

*As shown in Figure 19 (Material R), the mercury intrusion curves were almost flat for pore sizes below 0.1 μm; the curves appear to be completely flat for pore sizes below 0.01 μm according to mercury porosimetry up to 41,300 N/cm^2 (60,000 psi) (performed on some samples by the American Instrument Company, Silver Spring, Maryland).

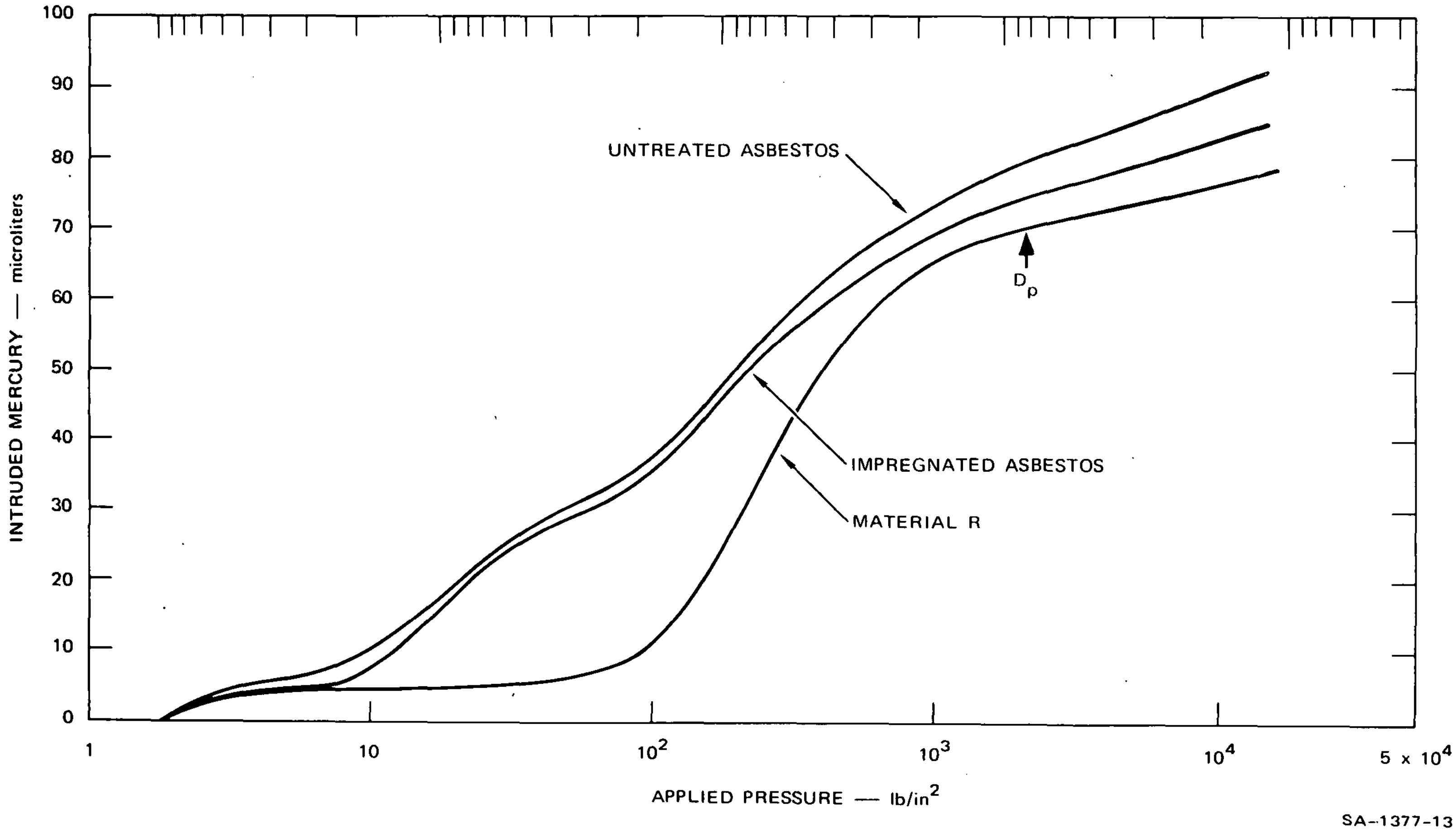

FIGURE 19 EFFECTS OF VARIOUS COATINGS ON OPEN POROSITY

For some impregnated, coated structures (that is, the finished separators), a small step was noted near the 0.3-μm point on the curve. Although suggestive of a second pore size population at this level, this finding was too random in occurrence to reach a firm conclusion regarding its origin.

For rigid separator disks, the independent determination of average pore size by means of the water permeation test had yielded repeatable results that essentially agreed with the mercury porosimetry data. In contrast, water permeation measurements for semiflexible separators were less repeatable* and yielded pore size data that appeared to be inconsistent with the mercury porosimetry results for the same materials. As shown by the data for D_p versus D_m in Table 28, the pore diameters calculated from the permeation data fall in the decade between 0.1 and 0.01 μm, one decade smaller than the range indicated by mercury porosimetry.

Because incomplete wetting of the largely hydrophobic, virgin semiflexible wafers was considered to be one possible explanation for this inconsistency and other anomalous behavior,† a series of supplementary permeation tests was performed. Various wetting agents and different techniques of impregnating test samples with "wet water" were tried; finally, a few permeation tests were run with nitrogen to completely eliminate poor wetting as a cause of the observed nonrepeatabilities

---

*Before collecting routine screening test data, preliminary water permeation tests had been made with wafers of Material R. The results indicated repeatable performance and permeation times, as previously observed for the rigid formulations. However, during the actual screening tests of all 16 materials, water permeation was found to be unexpectedly long in half of the samples studied.

†By the standards of the repeatable and generally similar water permeation rates measured for rigid disks, the test behavior of semiflexibles is considered anomalous in terms of poor repeatability (usually no better than ±40%) and a wide range (up to 100-fold) for different formulations.

and inconsistencies. Representative results obtained in these tests are shown below.

Material	L'	M	P'
Pore size by water, μm	0.015	0.013	0.095
Pore size by N_2, μm	0.085	0.085	0.25

The use of nitrogen tended to reduce the scatter of the permeation data and greatly increased the calculated average pore size for each of these three materials, suggesting that incomplete wetting was at least partly responsible for the difficulties encountered in applying the water permeation test to semiflexible separators. However, the average pore size obtained from the gas permeation rate was still below that indicated by mercury porosimetry.

In further search for an explanation of these pore size data, the tortuosities, τ_a, derived from the porosities (by mercury intrusion) and resistivities of semiflexible separators may be examined. A representative average value (calculated from the data in Table 28) is $\tau_a = 2.1$ (after the standard one-week soak of samples in 45% KOH), compared to an average of $\tau_a = 1.5$ for rigid disks (see Table 27). If we accept the latter value (supported by similar τ_b values) as representative of all separator types (whether sintered or polymer-bonded) based on the inorganic powders of a given particle size range, the two values of τ_a can be reconciled by assuming (basis: Eq. (17a), Appendix C) that the pore volume (as expressed by the porosity P) actually contributing to electrolytic conduction in semiflexible separators is only $(1.5/2.1)^2 = 0.5$ of the total pore volume. The pore size distribution curves then suggest (see, for example, Figure 19, Material R) that only pores with diameters below 0.4 μm are continuous.

On the other hand, the nitrogen permeability data indicate that D_p is in the range of 0.085 to 0.25 μm. Using an average "true" tortuosity

Of 1.5, these data suggest that $D_m = \tau D_p \approx 0.13$ to $0.38\ \mu m$, in approximate agreement with the tentative conclusion stated above.

The fact that pore size distribution curves sometimes show emergence (after the last coating step) of a second pore size population in the range of 0.3 to 0.4 µm can be taken as an additional indication that the pore diameter controlling separator resistance and gas permeability may be in this general size range. By performing mercury porosimetry on one sample from which the asbestos backing had been removed, we found that* the coating itself had a relatively sharp pore size distribution, with an average pore diameter of 0.3 µm.

Thus, although the question regarding true average pore tortuosities in semiflexible separators cannot yet be considered resolved, the data for these materials may be interpreted tentatively to indicate that

- The average pore diameter in semiflexible separators is approximately 0.3 µm, but only about 50% of the total pore volume is in continuous pores contributing to conductivity and permeability; an upper limit for the diameter of these pores is approximately 0.4 µm.
- The asbestos backing and the coating have comparatively similar porosities, resistivities, and diameters of continuous pores; this explains why a separate pore size population (associated with the coating only) is not generally observable in mercury porosimetry. However, the coating is responsible for the observed zinc dendrite penetration resistance, whereas the asbestos contributes a negligible effect. This suggests that the above tests alone are insufficient to fully characterize the composite semiflexible separator.
- Water permeability is not suitable for characterizing pore size in hydrophobic separators but gas permeability appears to give meaningful information.

---

*The resultant specimen was 0.165 mm thick. The coating thickness for this sample, recorded during its fabrication, was 0.14 mm; thus, penetration of the slurry into the asbestos appears to have occurred to a depth of 25 µm or less. The mercury porosimetry results showed the porosity to be 35 vol%, and an average pore size of 0.3 µm; pore volume on either side of the range between 0.6 and 0.1 µm was negligible.

Zinc Dendrite Penetration: Rigid Disks

With the exception of material A, the results range between 90 and 300 minutes for the time required to observe shorting due to zinc dendrite growth. The apparently highly favorable result for material A is not an artifact: an extended test lasting 25 hours was performed and the run was terminated at that time with no evidence of zinc shorting. However, as was known from previous studies, the effectiveness of this material in preventing zinc dendrite shorting is due to its catalytic activity for the reaction of zinc and water. Inasmuch as this catalytic activity is necessarily accompanied by hydrogen evolution, the material cannot be used in sealed cells.

After certain improvements of the test cell (see Appendix A), a rather uniform zinc dendrite growth over the area of the disk was accomplished. A photograph of a representative zinc-dendrite growth is shown in Figure 20. The surface shown is that facing the zinc cathode. The uniform penetration is shown as well as the fan-like structure of dendrites that grew radially outward from the circumference of the fixture. The dendritic pattern displayed is very similar to the patterns of the dendrites that were found on the surface of many separator bags in failed cells (see Task I). Note that, for both the cells and the test device, this pattern is typical for dendrites that have grown perpendicular to the main current path.

Because initial results had shown considerable scatter, a study of the repeatability of the zinc dendrite test was made. Five rigid disks of the same thickness and porosity were chosen of material Q'x. Zinc dendrite shorting times were found to range within 10 minutes of the average of 150 minutes. From these results it was concluded that the zinc dendrite test was adequately repeatable for use with rigid formulations. The thickness of the disk was made a parameter in additional

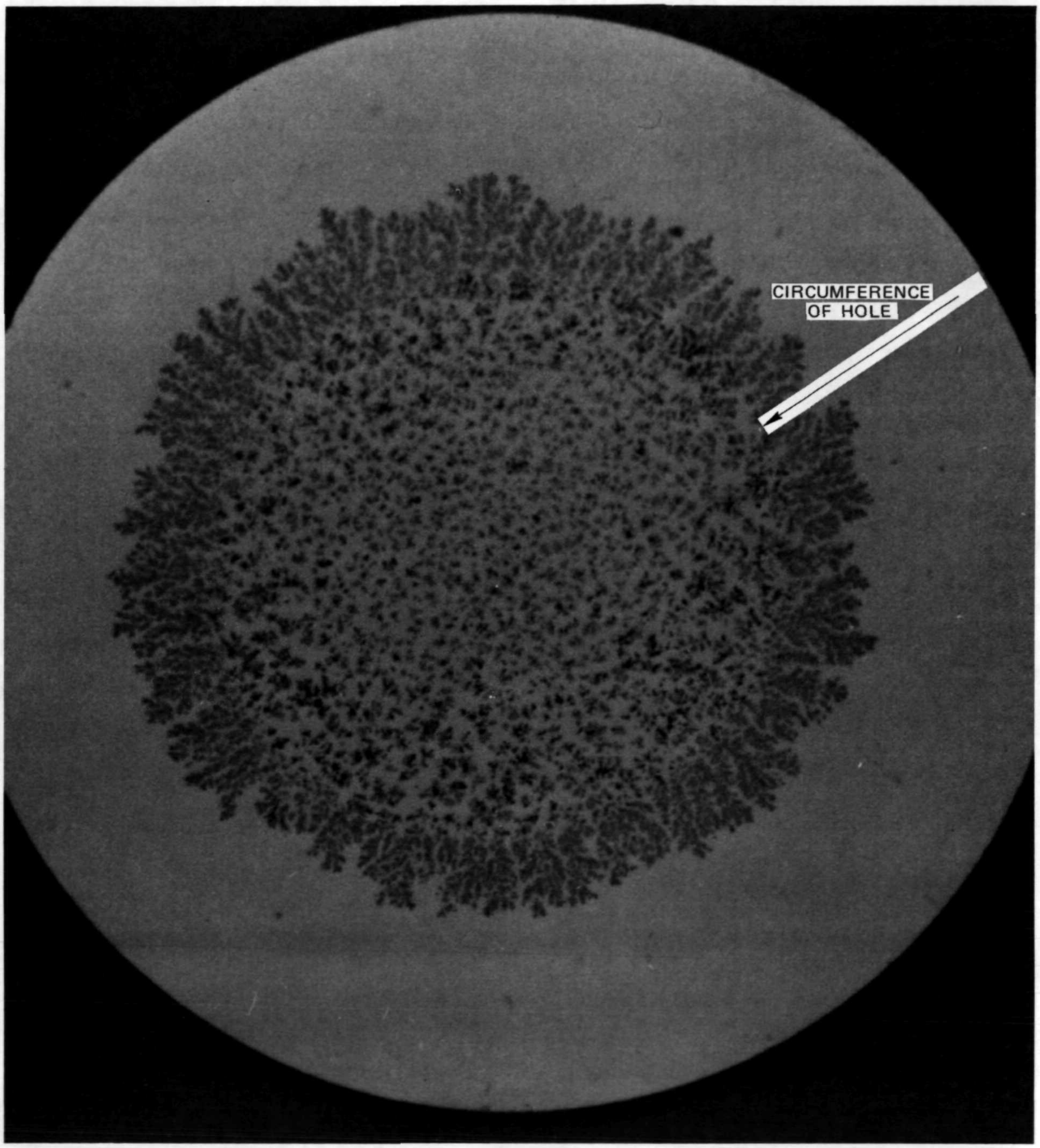

SA-1377-31

FIGURE 20 PHOTOGRAPH OF TYPICAL ZINC-DENDRITE GROWTH PATTERN supplementary zinc dendrite studies. For these disks, whose thicknesses ranged from 0.5 to 2.3 mm, the shorting time was found to vary with thickness in a nonlinear manner; for example, a three-fold increase in thickness over the standard value produced a five-fold increase in shorting time. For this reason, zinc dendrite results are preferably presented as actual shorting times observed, rather than in the less informative form of an inverse penetration rate.

The sensitivity of the zinc dendrite test to changes in surface chemistry or catalysis is demonstrated by another set of supplementary studies. In this study, four disks were subjected to the zinc dendrite test and the shorting times were observed. The zinc in the disks was removed with I_2-KI complex, and the disks were then cleaned, first with KI solution and then by Soxhlet extraction. The zinc dendrite test was repeated. After this sequence, four new disks were selected and the sequence of tests and procedures repeated. It was found that the zinc shorting times observed for the second zinc dendrite test (performed after cleaning) varied from one-half to eight times the shorting time for the virgin disks. Since changes in porosity, pore size, or tortuosity could not have occurred as a result of these mild treatments, the non-repeatability of results suggests that surface chemistry does influence zinc dendrite results.

Zinc Dendrite Penetration: Semiflexible Wafers

The results of zinc dendrite studies of the semiflexible formulations are included in Table 28. Although the semiflexible wafers were one-half as thick as the rigid formulations, the range in average shorting times is similar, ranging from 90 to 390 min. It is interesting to note that of the nine materials that had zinc shorting times longer than average in the rigid formulation, only three are found among the eight materials similarly above the average for the semiflexibles. In fact, of the 15 materials common to both rigid and semiflexible formulations, the relative

Table 30

ZINC DENDRITE SHORTING TIMES
(Minutes)

Sample thickness (cm)	0.03	0.045	0.045	0.055
Number of dips	1	3	3	7
Wafer No. 1	75	270	252	357
Wafer No. 2	115	378	269	479
Wafer No. 3	91	471	92	205
Wafer No. 4	85	285	247	485
Wafer No. 5	107	109	277	--
Average	95	303	227	384

positions (i.e., above or below average) changed in eight cases. Apparently, the results of the zinc dendrite test are not--or, at least, are not only-- dependent on basic composition of the inorganic constituent in semiflexible separators.

Supplementary tests were made to explore the level of repeatability of the zinc dendrite test when applied to semiflexible formulations. Samples of materal Q in different coating thicknesses were studied using wafers cut from the stock prepared for the supplementary resistivity studies previously discussed; the results are presented in Table 30. The two three-dip groups are fairly representative* of the separator formulations studied in the routine screening tests; these groups differ only in that resistance measurements had previously been made on the wafer of the group that averaged 303 minutes.

From the above data it is clear that zinc dendrite time is related to the thickness of the separator. A plot of the data is presented in Figure 21. The averages of the three sets of data fall on a straight line, and extrapolation of the curve passes through the abscissa at a point roughly equivalent to the thickness of the asbestos backing, suggesting that the asbestos had little effect in retarding growth of zinc dendrites.

The zinc dendrite data obtained from the supplementary studies were statistically evaluated, and no essential difference was found between the two groups of three-dip results. Because the screening test results

---

*The value found for the five samples of material Q in routine screening tests is 200 minutes (see Table 28).

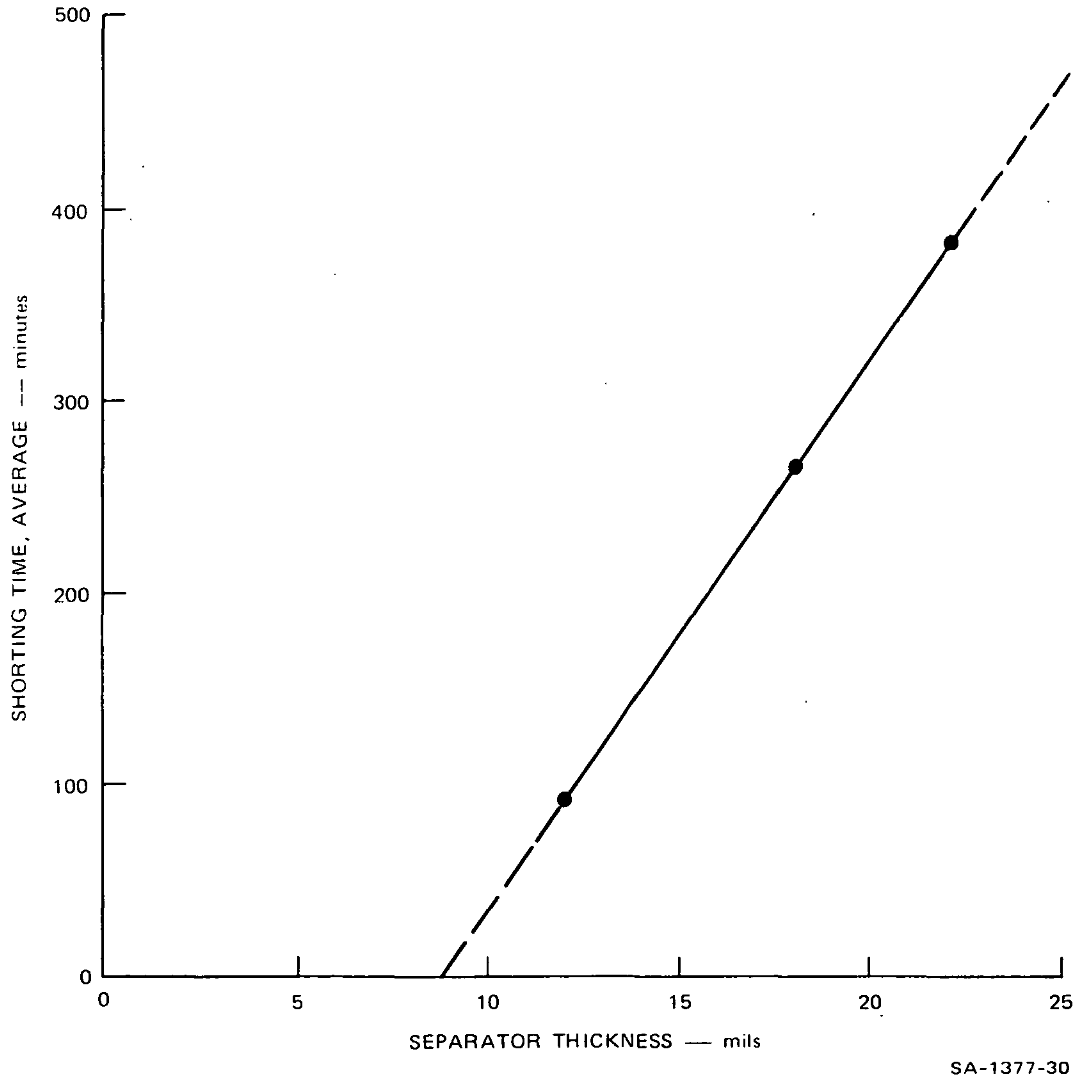

FIGURE 21 RELATIONSHIP BETWEEN AVERAGE ZINC DENDRITE SHORTING TIME AND TOTAL SEPARATOR THICKNESS

showed somewhat improved repeatability of zinc penetration times compared to those from supplementary tests, statistical evaluation* was made for them. The conclusion was that our currently available zinc penetration data are not sufficient to determine with confidence whether particular formulations (or inorganic stock materials) confer improved zinc dendrite penetration resistance to Astropower-type semiflexible separators. For any given semiflexible formulation, the larger scatter of test data (compared to that for rigid disks) suggests that the variations from sample to sample may correspond to real variations in zinc dendrite penetration resistance. If confirmed, this finding would indicate that the dendrite test is sensitive to a separator property to which the resistivity (which does not show corresponding variations) is not sensitive--for example, to the presence of a few larger pores, pinholes, or microscopic cracks in the separator coating. More data on test repeatability, and an increased number of test samples for a given formulation will be required to establish whether test results depend on the materials parameters.

Considering the potential usefulness of the zinc penetration test in characterizing a key separator function, and the established importance of zinc shorting as a failure mode in cells using semiflexible separators (see Task I), a more extensive study and broader application of the zinc dendrite penetration test in further separator development efforts are called for.

---

*Statistical statements made here are based on a 95% confidence level. Data were evaluated by three methods: the Students t test, analysis of variance (parametric), and Kruskal and Wallis' test (nonparametric).

KOH Degradation: Rigid Disks

As shown in Table 26, degradation was found to affect porosity, weight, resistance, and tortuosity. A study of these results indicates that degradation at 393°K (120°C) in a 2:1 volume ratio (which approximates the conditions in cells) is the least degrading of the three conditions studied. Apparently degradation with excess of electrolyte as used in most screening programs is a considerably accelerated test. From the resistance of the disk with the spent electrolyte (see Table 26), it is clear that the KOH electrolyte also changes composition (toward increased specific resistivity) as a result of degradation. This finding has important implications for the use of such separators in batteries.

The degradation process is presumably one of chemical attack, and, therefore, weight loss should correlate with a loss of material and should necessarily result in an increase in porosity according to

$$\Delta P = (1 - P_o)L$$

where:

ΔP is the absolute change in open porosity

P_o is the open porosity before degradation

L is the relative weight loss.

Experimental data for porosity change versus weight loss are shown in Figure 22, based on the data of Batch 2. The agreement between the observed data and the predicted relationship is not particularly good. In some cases, a highly improbable* 50% error in either measurement would have to be assumed to explain the observed deviation from the expected relationship (shown as lines in the figure); point 4 for the E material at maximum degradation is an example.

*Our usual repeatability for either porosity or water intrusion ranges within ±5%. On the other hand, of the 33 data points at least eight would require corrections greater than 25%.

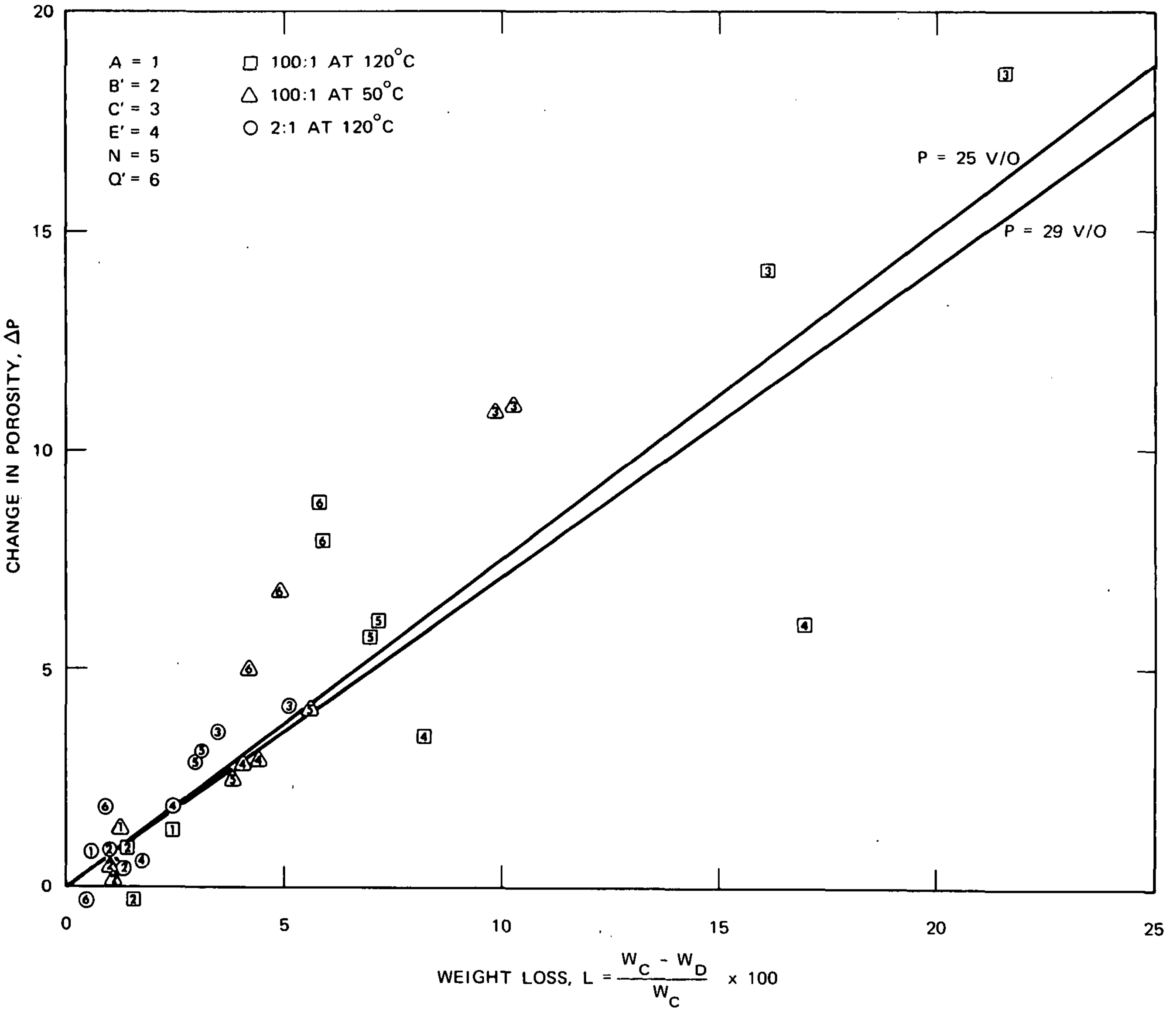

SA-1377-11

FIGURE 22 CHANGE IN POROSITY VERSUS WEIGHT LOSS IN KOH DEGRADATION TESTS

Although reasonable repeatability of the water intrusion and weight loss tests is established, the repeatability of the degradation test is in question. An example of the uncertainties encountered is noted by comparing the ratios of the weight losses for five pairs of disks, made of five different materials and degraded under identical conditions, which were 393°K (120°C) and a 100:1 ratio of electrolyte-to-disk volume. The weight loss ratios were:

Material	B'	C'	E'	N	Q
Ratio of L	0.88	0.75	0.48	0.99	0.98

Most of the departures from the ideal relationship correspond to points above the theoretical lines; that is, changes in porosity were observed to be greater than those expected from the weight loss by our simple model. This could be the result of opening--via the degradation process--void volumes that had previously been closed. Points below theoretical lines, correspondingly, could represent materials whose pores were closed by the degrading process. This might have been caused by gel formation of a hydrated magnesium hydroxide or a silicate, or by mechanical blockage of some pores by loose material formed inside the sample.

The following generalized statements may be made about degradation:

- Weight loss is greater at 393°K (120°C) than at 353°K (80°C).
- Weight loss is dependent on material.
- Porosities increase as a result of degradation.
- Resistivities decrease as a result of degradation.
- Tortuosity is unaffected by degradation.
- The effects of degradation on pore size were not significant.

KOH Degradation: Semiflexible Separators

Degradation was also studied with the semiflexible formulations, and the results are presented in Table 28. The mechanical properties of the semiflexible separators are altered by wetting; for example, the average tensile strength is reduced to 24% of its dry strength by a one-week soak in KOH at room temperature. After a one-week room temperature soak in water, the average burst strength is reduced to 38% of its initial value, which is essentially the reduction observed immediately after wetting. On the other hand, separator flexibility is increased: the dry separator tends to crack if bent around a diameter less than 2 cm, but a wetted separator may be bent around a 0.4-cm diameter without cracking after being wet with KOH for one week. Degradation of the semiflexible formulations also reduced the average specific resistivity to 65% of the value taken as representative--the value obtained after one-week soak. Degradation of the semiflexible formulations also reduced the average specific resistivity to 65% of the value taken as representative--the value obtained after one-week soak.

Based on an average resistance value for degraded wafers, and assuming the porosity still to be 35%, the tortuosity calculated from these average values is 1.8; on the other hand, if it is assumed that the true tortuosity of continuous pores is more nearly 1.5 (see the section on Porous Structure), it follows that the continuous pore volume increased from 50% to $100 \times (1.5/1.8)^2 = 69\%$ of the total volume as a result of degradation--presumably via opening of closed or blind pores.

Zinc Gassing

The zinc gassing test as developed at Astropower and simplified (see Appendix A) at SRI is used to obtain a comparative measure of the catalytic activity of inorganic separator materials in promoting the reaction between zinc metal and electrolyte. To minimize this reaction and the attendant dissolution of zinc and generation of hydrogen, materials with very low or zero activity are required for separators in sealed silver-zinc cells. Accordingly, this screening test was applied in the current program as soon as possible--essentially in parallel with the materials and separator development efforts under Task II. From the results (see Table 25), it is apparent that the gassing rate is significant for several materials, including the olivine component A of the 3420-09 separator, which was known to gas strongly. However, more than half of the inorganic stock materials had gassing rates below 4 cm^3 per 24 hours;* ten of these had lower gassing rates than the material Q'-x, the inorganic component of the successful 3420-25 separator.

Accordingly, nearly all of the inorganic stock materials prepared in this program were considered to qualify, with respect to the criterion of negligible activity for promoting zinc gassing, for further study in rigid and semiflexible separator formulations. It should be emphasized, however, that the catalytic nature of the zinc-electrolyte reaction and its corresponding sensitivity to even minor amounts of catalytic impurities will require care in the handling and processing of inorganic materials to be used in separators: in supplementary studies of a commercial material, we found good repeatability (within ±10%) for a given lot but a more than 100-fold increase in gassing rate when testing another lot of the same CP material. Processing separator materials in steel dies also tended to increase gassing rates, presumably because of the small iron impurity picked up in the process.

---

*Gassing rates of less than about 4 cm^3 per 24 hours were considered to represent essentially zero activity for promoting gassing inasmuch as zinc powder blanks gave rates from zero to 4 cm^3/24 hr, probably because of uncontrolled variations in trace impurity levels.

Ranking and Selection of Separator Materials

As shown in the previous sections, the application of screening tests permitted characterization of candidate separator materials in terms of properties that are expected to be important for their function and compatibility in the cell environment. To accomplish the final objective of Task III--identification and selection of the most promising materials for further evaluation in cells--judgment was required regarding the relevance of specific tests and test results for the projected behavior of separators in batteries. The procedure used in this judgment step and in the subsequent ranking of separator materials was as follows.

(1) For each screening test considered relevant to separator behavior, a weighting factor* was chosen from an arbitrary scale of zero to ten, with increasing factors corresponding to increasingly important tests. These tests included zinc dendrite penetration, zinc gassing, resistivity, weight loss in degradation, tensile strength (semiflexibles), flexibility (semiflexibles), and void volume (by mercury intrusion).

(2) For each separator, test results were normalized using as reference values either a somewhat arbitrary set of separator properties representing acceptable performance standards or, alternatively, the test results for the base line material Q.

---

*Normalization was done using the form

$$T_{i,T} = \pm W_t \left(\frac{R_{i,t} - R_{o,t}}{R_{o,t}} \right)$$

where:

$T_{i,t}$ = normalized, weighted result of test t applied to material i

W_t = weighting factor for test t

$R_{i,t}$ = result of test t applied to material i

$R_{o,t}$ = reference value for test t

A plus sign is used whenever larger values of $R_{i,t}$ represent the more desirable property, a negative sign if the reverse is true.

(3) A figure-of-merit was obtained for each material by summing its normalized, weighted test results according to

$$M_i = \sum_t T_{i,t} .$$

(4) Separator materials were then ranked according to their figures-of-merit.

The values chosen for the weighting factors and, to a lesser extent, those used for the reference properties, will have an influence on the figures-of-merit, and hence on the ranking of the materials. Inasmuch as no accepted, quantitative criteria exist for ranking battery separators, it was considered important to examine how sensitive the ranking of prospective separator materials was to the values chosen. The weighting factors and reference results used in developing five independent separator rankins are listed in Table 31; the resulting rankings are shown in Table 32.

The first ranking was derived by considering only those materials that had more favorable properties than the reference material Q in at least five test categories; this was done largely for expediency inasmuch as this ranking was performed during the last part of the Third Quarterly Review held at SRI in Oct. 1972. Rankings 2 through 5, on the other hand, included all materials, with the exception of A and M which were eliminated from comparison because of excessive gassing and degradation, respectively. On the basis of these rankings, material S' is clearly the best choice, independent of the specific weighting factors and reference results assumed. Material JC is not far behind in all but one of the rankings and appears to be superior to the remaining materials. Accordingly, materials S' and JC are recommended without further qualifications for future evaluations in cells.

Regarding the third choice for continued evaluation,materials B', E', L', and N' are comparatively close together; considering the limitations of screening tests and their quantitative evaluation, it is doubtful whether the differences in the ranking of these materials reflect real,

Table 31

TESTS, WEIGHTING FACTORS, AND REFERENCE VALUES FOR RANKING SEPARATOR MATERIALS

Test \ Ranking Study No.	1 and 2		3		4		5	
	W_t	$R_{i,t}$	W_t	$R_{i,t}$	W_t	$R_{i,t}$	W_t	$R_{i,t}$
Zinc dendrite penetration	10	250 min	10	250 min	10	200 min	8	150 min*
Zinc gassing rate	9	4 cm^3/d	9	4 cm^3/d	9	4 cm^3/d	10	4 cm^3/d
Resistivity (area basis)	8	0.8 Ω cm^2	8	0.8 Ω cm^2	8	1.07 Ω cm^2	6	1.07 Ω cm^2
Resistivity ratio (degraded: soaked)	-	-	-	-	-	-	4	0.519
Weight loss in degradation*	7	2.5 wt%	3	2.5 wt%	-	-	-	-
Pore diameter	7	0.04 μm	3	0.04 μm	-	-	-	-
Tensile strength								
wet separator	1	2070 N/cm^2	1	2070 N/cm^2	1	1650 N/cm^2	-	-
degraded separator	6	483 N/cm^2	6	483 N/cm^2	6	433 N/cm^2	-	-
Flexibility (cracking diameter)								
dry separator	2	2 cm	2	2 cm	2	2 cm	-	-
wet separator	5	0.23 cm	5	0.23 cm	5	0.152 cm	-	-
Void volume (2.54 cm dia. wafer)	3	0.073 cm^3	3	0.073 cm^3	3	0.073 cm^3	-	-

*Data taken for rigid formulations.

Table 32

RANKING OF SEPARATOR MATERIALS

Material \ Test	1	2	3	4	5
B'	3*	4*	4*	6	4*
C'	-	9	10	10	10
D'	4*	5*	5*	7	8
E'	-	7	6*	2*	2*
JC	2*	2*	2*	3*	7*
K	-	5*	8	9	9
L'	-	3*	4*	5	5*
N'	-	4*	3*	3*	3*
P	-	5*	7	8	6*
Q	5	6	7	4	8
R	-	10	11	12	12
R'	-	8	9	11	11
S'	1*	1*	1*	1*	1*

*Materials ranking above Q.

reproducible differences in their behavior as separators. Therefore, we have introduced additional considerations in choosing B' as the third material for a subsequent evaluation study. First, we note (see Table 22) that material E' is a doped modification of the pure compound B' and thus will be somewhat more difficult to produce; accordingly, B' is our choice in this comparison. In choosing between B', L', and N', we note that L' and N' are from the titania- and zirconia-derived separator classes, respectively. With the materials JC and S' selected above, these classes will be represented at least once in the evaluation study. By choosing the olivine B' instead of L' or N', one representative from each of the three major chemical classes of inorganic separator materials examined in this program will undergo further evaluation. This choice is preferred at a stage of inorganic separator development where the question regarding possible chemical effects occurring in, and contributing to the functions of, inorganic separators must still be considered.

CONCLUSIONS AND RECOMMENDATIONS

Task I

The results of this cell testing program, continued from Contract NAS 3-10928, showed that Astropower Laboratory heat-sterilized silver-zinc cells using a proprietary semiflexible separator were able to survive a 21- to 25-month wet stand and then deliver several hundred shallow charge-discharge cycles. Thus, the major objective of the silver-zinc cell development program under Contract NAS 3-10928 has been accomplished.

The survival rate of cells in the reconditioning cycles after stand and their subsequent cycle life were both particularly high if cells were standing in the discharged condition. Half of the few failures in this cell group actually had been subjected to lengthy charged stand at elevated temperature before their routine discharged-stand period--a procedure that might have contributed to their eventual failure. Experimental evidence suggests that even those few discharged-stand cells that failed (in reconditioning because of nominally low capacity) would have been able to cycle. Charged-stand and float charged-stand clearly are detrimental to cell survival rate and cycle life expectancy after standing, but a high survival rate appears achievable by storing cells at a lower temperature [for example, 283°K (10°C)].

Although the limitations of small sample statistics apply to most of the results relating to the secondary testing objectives, the following conclusions appear reasonably well established.

1. Additional layers of separators between bags increase cell cycle life for shallow and deep cycles.
2. Plate-locking electrodes in cells with epoxy cement somewhat reduces cell wet and cycle life; this effect is reduced if the epoxy cement is more thoroughly cured. Environmental testing does not seem to affect cycle and wet life of plate-locked cells.

3. Operating cells as groups in "batteries" has a detrimental effect on cell wet and cycle life, presumably because individual cells can experience overcharge conditions as cell imbalances develop with age.

4. At least over the range of $283^{\circ}K$ to $315^{\circ}K$ (10 to $32^{\circ}C$), cell temperature during cycling does not appear to affect wet and cycle life significantly.

Cell failure analysis shows shorting by zinc nodules to be the single major cause for the early cell failures. However, this failure mode was observed only in cells that had spent an extended period in the charged state and had undergone at least a few deep discharges or, very probably, significant overcharge. It appears that zinc nodule shorts can form under these conditions because semiflexible separators were extensively attacked by dissolved silver oxide and unable to withstand zinc penetration.

Cell shorting by filament-type zinc dendrites appears to have been the almost exclusive cause of all other cell failures, especially those encountered after large numbers of cycles; shorting by silver found deposited in semiflexible separators was not observed. Although many cells had developed a number of faults (mostly leaks and split separator bags, but also a few cases of zinc electrode erosion and slumping), none of these faults correlated significantly with a particular failure mode or the observation of appreciably reduced cell wet and cycle life. The low incidence of zinc electrode slumping (with only the cells of one subgroup showing a modest degree) is noteworthy and points to the potential of Astropower-type electrode-separator composites for achieving extended cycle life in deep cycling of alkaline cells with zinc negatives.

The finding and conclusions of the SRI cell testing program lead us to the following recommendations:

1. If Astropower-type silver-zinc cells using the present designs and semiflexible separators are to be standing for extended periods, discharged stand should be used. If charged stand is an operational requirement, the standing temperature should be 283°K (10°C) or possibly lower.

2. Deep cycling (such as applied in reconditioning or in 100% DOD regimes) should be avoided for cells that have experienced extended periods on charged stand.

3. The possibility of achieving extended cycle and wet life with present cells by maintaining cells in a lower average state of charge should be investigated. Possible approaches (if compatible with aniticpated applications) include cell operation in an "upside-down" cycle, or simply a more rapid charge just prior to discharge.

4. The major cause(s) of cell capacity loss in standing and cycling should be investigated; as part of this effort (or for its own merit) the possibility of developing a "nondestructive" silver electrode capacity test based on the rate of voltage rise should be explored.

5. Operation of cells in batteries is to be avoided unless circuitry is provided that allows cells to be removed individually from charge and discharge.

6. The upper voltage limit for cell charging should be reliably controlled and kept at or slightly below 2.00 V per cell. Charging circuitry should be used that "recognizes" the voltage spike of the silver (I) oxide-silver (II) oxide phase transition and disallows its effect on the electronic mechanism for terminating charging.

7. The separator constituent mainly responsible for forming silver deposits should be identified, and the effect of its elimination on cell behavior and life should be investigated.

8. Improved techniques (and their automation) for enclosing electrodes in bags should be devised. This effort should include the development of better bag seals and the investigation of electrodes with rounded edges that would result in better current distribution and permit improved conformity of bags, thus eliminating void spaces within bags.

9. Improved seals for terminal posts should be designed.

10. Absence of stresses in the ultrasonic weld of cell tops to cases should be ensured through appropriate modifications of the current welding procedure. Also, improved adhesion of the epoxy overcoat should be sought by appropriate surface preparation techniques such as wet vapor blasting.

11. Unless needed for specific applications, plate locks should not be used. If needed, plate locks should be made from fully cured epoxy cements or from chemically neutral, powdered resins, fusible at temperatures compatible with cell structure, thereby acting as immobilizing cements.

Task II

The experience of preparation of inorganic separator materials disclosed that relatively easy techniques of synthesis were possible. The use of oxides or easily decomposable compounts provided the starting point for synthesis of those materials not available commercially. Simple procedures of mixing, compacting, firing, milling, and size fractionation were followed. All syntheses were accomplished at temperatures of about $1623^{o}K$ ($1350^{o}C$) or below at reasonable times (8 hr or less at temperature). Purchased materials were available in acceptable quality.

Rigid, fired ceramic disks of 24-29% porosity, of acceptable quality for screening tests were readily prepared from the powdered stocks of inorganic materials at firing temperatures of $1368-1623^{o}K$ ($1095-1350^{o}C$) in times of 45 minutes or less.

Semiflexible wafers (derived from mechanically dipped separator bags) of high surface quality, suitable for screening tests, were readily made following the procedures disclosed in U.S. Patent 3,625,770 (licensed by SRI). The ratio by volume of the polymer binder to the inorganic filler was kept constant in all formulations.

These conclusions may be reached:

1. The synthesized inorganic stock materials for both rigid and semiflexible separators can be readily made by firing easily available starting compounds, at temperatures at or below $1623^{\circ}K$ ($1350^{\circ}C$) in times less than 8 hours at temperature.

2. Fired ceramic separator disks can be made from all powdered formulations at temperatures of 1368 - $1623^{\circ}K$ (1095 - $1350^{\circ}C$), and firing times of 45 minutes or less.

3. Semiflexible separators can be easily fabricated from all stock formulations following the procedures of U.S. Patent 3,625,770.

4. The preparation of semiflexible separators by controlled mechanical dipping yields much higher surface quality than preparation by hand dipping.

Task III

The work performed on evaluation and application of screening tests shows that the tests commonly used to screen and characterize conventional organic separators for alkaline batteries give meaningful results also when applied--if necessary, with appropriate modifications--to the rigid and semiflexible separator formulations developed in this program. Although there is still some question regarding the significance of a few tests (especially water permeation and zinc dendrite penetration), results could be used to construct a table of weighted separator characteristics which, in turn, permitted selection of the most promising separator formulations for further study.

Specific conclusions from our evaluation of the tests themselves and of the test results are given below. Where specific reference to rigid or semiflexible separators is not made, the conclusions apply to both types.

1. Changes made in the resistance cell and measurement technique give adequate separator resistance data with increased speed and convenience.

2. Porosity measurements made by the water intrusion and mercury porosimetry give equivalent results. Mercury porosimetry also yields readily interpreted pore size distributions for rigid separator samples. Although more difficult to interpret because of sample inhomogeneity and compressibility, pore size distribution data for semiflexible separators are nevertheless indicative of their structural features.

3. For rigid separator samples, pore-size determinations made by water permeation yield smaller diameters than those resulting from mercury porosimetry. From the difference, a measure of pore tortuosity is obtained; this measure of tortuosity was similar to another measure obtained from sample porosities and resistivities. Applied to semiflexible separator samples, the water permeation test is poorly reproducible and yields pore size and tortuosity data that are inconsistent with those calculated from other test results. Measurement of nitrogen gas permeability, on the other hand, appears to yield meaningful values of pore size and tortuosity.

4. The zinc dendrite test appears to yield reproducible zinc penetration data when applied to rigid separators. On this basis, the large scatter in the data from application of the identical test to semiflexible separator samples suggests that the scatter represents real variations in zinc dendrite penetration resistance.

5. Degradation tests are useful in characterizing the chemical resistance and estimating physical changes of separator materials in the cell environment. Because of the greater physical and chemical sensitivity of the asbestos backing compared to that of most inorganic stock materials used in this program, accelerated tests have to be somewhat milder for semiflexible wafers than those applied to rigid disks. The value of degradation tests is considerably increased by using degradation-induced changes of resistance, porosity (rigids) and strength (semiflexibles) in addition to (for semiflexibles: instead of) weight loss as indicator of degradation.

6. The burst test is a suitable and convenient technique for measurement of the relative strength of semiflexible formulations; results are consistent with tensile strength measurements.

7. Screening test data obtained for the rigid and semiflexible separators developed in this program could be used to eliminate two materials (A and M) from further study due to excessive zinc gassing and degradation, respectively.

8. For the twenty rigid formulations examined in detail, the combination of test results for zinc dendrite penetration, zinc gassing and accelerated degradation with the data obtained for resistivity, pore volume and size distribution, water permeability, and mechanical strength permitted a rather complete and consistent characterization in terms of key electrochemical, chemical, and physical characteristics. Sixteen semiflexible separator formulations were characterized in a similar way although their description was somewhat less complete, due, primarily, to their inherently inhomogeneous structure.

9. Ranking the inorganic separator materials by applying various sets of weighting factors and reference values to the results of the screening tests suggested that materials S' and JC were the most promising candidates for further evaluation. Material B is the preferred third choice on the basis of supplementary considerations; materials E', L' and N' also have substantially better properties than the baseline material Q.

These conclusions and the other findings of Task III work lead us to the following major recommendations.

1. The screening test equipment and procedures as developed or modified in this program should form the starting point in future screening tests of inorganic rigid and semiflexible separators.

2. Future screening tests should employ a larger number of separator samples per material and test to increase the statistical significance of the data.

3. Because of the potential implications of the observed data scatter for separator performance in cells, the significance of zinc dendrite test results for semiflexible separator samples should be investigated in detail.

4. The three semiflexible separator materials, S', JC, and B', are recommended for further evaluation in simplified test cells; some consideration should also be given to possible evaluation of materials E', L' and N'.

REFERENCES

1. C. Berger, F. C. Arrance, A. D. Taylor, "Inorganic Separator for High Temperature Silver-Zinc Battery," Final Report, Contract NAS 3-6007, Douglas Aircraft Co., Newport Beach, Calif. (Sept. 1965).

2. H. Frank and M. P. Strier, "Elimination of Pressure Caused by Gassing in High Energy Density Batteries," Interim Report, Contract NAS 5-9594, Douglas Aircraft Co., Newport Beach, Calif.

3. F. C. Arrance, "Program to Develop an Inorganic Separator for a High Temperature Silver-Zinc Battery," Final Report, Contract NAS 3-7639, Douglas Aircraft Co., Newport Beach, Calif. (June 1967).

4. A. Himy, "Heat Sterilizable Battery," Final Report, Contract NAS 2-3819, NASA CR-73110, Douglas Aircraft Co., Newport Beach, Calif. (July 1967).

5. H. Frank, M. P. Strier, "Sealing of Silver Oxide-Zinc Storage Cells", Final Report, Contract NAS 5-10409, McDonnell-Douglas Corp., Newport Beach, Calif. (August 1968).

6. A. Himy, "Development of a Heat-Sterilizable 40 Ahr Sealed Silver-Zinc Cell," Final Report, Contract NAS 3-10928, NASA CR-1812, McDonnell-Douglas Corp., Newport Beach, Calif. (November 1970).

7. J. E. Cooper and Arthur Fleischer, Eds., "Characteristics of Separators for Alkaline Silver Oxide-Zinc Secondary Batteries: Screening Methods," Air Force Aero Propulsion Laboratory, Dayton, Ohio, (1964).

8. W. V. Hartmann, "Quality Control for a Heat-Sterilizable Silver-Zinc Separator Material," p. 303 in Proceedings on Battery Separators, The Electrochemical Society, February 1970.

9. G. Moe and F. C. Arrance, "Inorganic Separators," p. 295 in Zinc-Silver Oxide Batteries, edited by A. Fleischer and J. J. Lander, J. Wiley, New York, 1971.

10. A. Himy, "Development and Testing of a Five Ahr Silver-Zinc Cell," Final Report, Contract NAS 3-10924, NASA CR-72551, McDonnell-Douglas Astronautics Co., Newport Beach, Calif. (May 1969).

APPENDIX A

SCREENING TEST EXPERIENCE AND PROCEDURES

The following is a summary of the procedures used in testing the separator materials developed in this program. General familiarity with screening tests--especially those described in the standard reference[*]--is assumed, and the discussion is largely restricted to those parameters or procedures which are unique to this study. Test experience and procedures are given for sample preparation and the determination of dimensions and volume, water intrusion, resistivity, chemical degradation, water permeation, modulus of rupture, zinc gassing, zinc dendrite penetration, porosity and pore size distribution by mercury porosimetry, burst strength, tensile strength, and flexibility.

Preparation and Weighing

Rigid separator disks were cleaned by Soxhlet extraction prior to the test sequence (see Appendix B), and again between certain sequential tests. The Soxhlet extraction is done with water[†], preferably overnight (16 hours). In the procedure, disks are separated from each other during extraction by use of stainless-steel screen separators (made of 1/4-inch stainless steel screen); three disks are placed on a circular screen in the Soxhlet extractor, another screen is placed above the disks, and the procedure is continued until a group of as many as 40 disks are assembled for cleaning. After Soxhlet extraction, the disks are oven-dried for no less than one hour at 100°C; drying time and temperature were not critical to achieving reproducible sample weights.

---

[*] The Air Force Screening Test Manual for silver-zinc batteries, edited by Cooper and Fleischer, reference 7.

[†] Water is used in all cleaning steps with the exception of the cleaning step between the MOR and mercury porosimetry tests in which wax (used to mount disks for cutting) is removed by Soxhlet extraction with toluene.

Semiflexible wafers cannot be cleaned using this procedure because it produces irreversible changes of the asbestos support. Wafers are tested "as is" after the final drying step in their preparation. Inasmuch as the wafers are not sufficiently hygroscopic to cause measurable weight changes upon exposure to the atmosphere, no further treatment before weighing was required. Rigid and semiflexible separator test samples were weighed on an analytical balance with a maximum uncertainty of ±0.5 mg. Typically, sample weights were around 800 mg for rigid disks, and about 200 mg for semiflexible wafers.

Measurement of Dimensions and Volume

As expected, the rigid porous separator disks prepared in this program did not swell in contact with electrolyte. Accordingly, the dimensions of the virgin disks may be used to calculate geometric volume, apparent density, and other derived separator characteristics. Although some relaxation of the fibrous backing of semiflexible separators was observed upon immersion in electrolyte, this effect involved only a small fraction of the separator dimensions. Accordingly, the thickness measured for dry semiflexible wafers was assumed to hold also after impregnation of the samples with water or electrolyte.

In the procedure, micrometers are used for thickness and diameter measurements for rigid disks. Flat-faced anvils are suitable for diameter measurements; spherical anvils are best for thickness measurements. To allow for slight deviations from the perfect cylindrical shape, thickness and diameter were measured in four to five places and the measurements averaged. The diameter of semiflexible wafers is constant for all samples and equal to that of the close-tolerance punch and die used to cut wafers from sheets. Thickness measurements of wafers are done with wafers under a constant compression force, using a dial indicator equipped with a 2.25 cm-diameter circular anvil and operating against a surface plate. Disk and wafer volumes are then calculated* using Equation (1) of Appendix C.

Water Intrusion

Determination of the volume of open pores in the separators was done routinely by determining the weight increase caused by "absorption" of water. Because rigid and semiflexible separator samples were evacuated before submersion in water, the technique is more nearly one of intrusion than of true absorption as described by Shair and Seiger in the standard reference.

For rigid samples, complete water intrusion was aided by the ready wettability exhibited by the ceramic surfaces. However, pore volumes and porosities calculated from water intrusion were invariably 5 to 10 relative percent lower than those determined by mercury porosimetry. In part, this may be due to removal of some intruded water in the wiping step; on the other hand, mercury porosimetry tends to give high values, as discussed below.

Semiflexible separators were not wetted by pure water. Use of various wetting agents† was tried, but poorly reproducible water intrusion volumes indicated that satisfactory wetting was not achieved with virgin samples. Inasmuch as the technique was inherently less precise for semiflexibles because of their larger surface-to-volume ratio, water intrusion was abandoned in favor of mercury porosimetry. In the procedure,

---

*Careful measurement of sample volumes with a small mercury pycnometer gave excellent agreement with calculated volumes. As a consequence, independent volume measurement could be dropped in favor of calculating sample volumes from measured dimensions.

†For example, an aqueous solution of 0.005 wt% sodium lauryl sulfate.

particulate-free and bacteria-free water obtained by filtering deionized water through a Millipore 0.22-micrometer absolute filter is used. The disks are placed in a wire basket supported from the top of a vacuum desiccator, and electrolyte or water contained in a beaker is placed in the bottom of the desiccator. The pressure in the desiccator is reduced to the vapor pressure of the liquid in the beaker for five minutes, after which time the disks are lowered into the liquid. The pressure is then restored to one atmosphere for five minutes with the disks still immersed. The disks are removed individually from the liquid as they are needed for subsequent steps in the test sequence (such as weighing for water intrusion).

Resistivity

Test apparatus and procedure were based on those given by Salkind and Kelley in reference 7. Initially, two major problems were encountered in operating the conductivity cell acquired from Astropower Laboratory. First, the pressure required to seal the test specimen between the two resistance half cells tended to crack rigid separator disks, and second, variation in the extent of compression of sealing gaskets caused non-reproducible variations in the measured resistance values. The latter effect, and variations in electrolyte temperature and composition (through water and/or carbon dioxide absorption from the atmosphere) tended to cause significant measurement errors that were amplified by the fact that the results are obtained as a difference of two measurements.

A series of corrections and improved procedures were introduced in the early phase of Task III, with the goal to improve precision and convenience in determining separator resistivities. These included (1) cell modification from a variable to a fixed spacing of potential-sensing electrodes, (2) gasket modification to limit the current to a well-defined area of the separator, (3) improved temperature control, and (4) frequent standardization of electrolyte conductivities. A further contribution toward more convenient acquisition of better conductivity data was the decision to routinely use standard 0.1 N KCl as the test electrolyte. This became possible after it was established (for rigid separators) that data obtained under carefully controlled conditions with KCl and KOH electrolytes were related by the expected ratio of their free electrolyte resistivities.

These combined modifications improved the separator resistivity data from an unsatisfactory uncertainty of ±25% to an acceptable ±5%.

In carrying out the measurement procedure, the cell may be operated as a variable-spacing cell as described in Sections 6a and 6b of Reference 7; Equations (7) and (8) of Appendix C are then used to calculate resistivity. More precise results are obtained with a fixed-spacing arrangement of the cell, in which case Equation (10) of Appendix C is employed. Changes in specific resistance of the electrolyte--due to temperature changes and absorption of carbon dioxide and(or) water absorption from the air--will cause erroneous results unless these changes are detected and corrections made;* the appropriate correction is provided for in Equation (10) of Appendix C. Because it is a more stable electrolyte than concentrated potassium hydroxide, one-tenth normal potassium chloride is used for resistance measurements whenever it can be ascertained that resistivity data are not influenced by specific interactions between separator materials and the caustic electrolyte. Equation (10) contains a term normalizing resistance data obtained with 0.1 N KCl to the "standard electrolyte" (45 w/o KOH at 18°C).

---

*This requires measurement of the specific resistivity which is done with a conventional resistivity cell.

Degradation (Chemical Compatibility)

Following the recommendations developed in our initial analysis of screening tests, separator degradation tests were performed at several temperatures. For rigid formulations, the temperatures usually employed were 353 and 393°K (80 and 120°C). Two volume ratios were studied, at the 2:1 and 100:1 levels, wherein the ratio refers to the volume of electrolyte to the volume of the disk; the 2:1 ratio is more representative of actual battery environment while the 100:1 ratio is typical of the ratio commonly employed with screening tests. These conditions were employed for Batch 2 results, and used to guide the design of procedures for Batches 3 and 4.

Degradation studies of semiflexible formulations were performed using resistance as the monitoring index. Experience of preliminary testing showed that 48 hours' exposure to 45 wt% KOH at 353°K (80°C) was equivalent in effect to seven or more weeks exposure to electrolyte at room temperature. Therefore, these conditions were employed in the testing. Degradation tests at higher temperatures (393°K) [120°C] resulted in severe loss of mechanical integrity (to an extent far greater than observed in cells), so higher temperature degradation was not performed for the semiflexible formulations.

In the procedure, the sample was vacuum infused with electrolyte as was done and described above for water intrusion. The sample was then placed in the desired volume of electrolyte contained in an inert (TPX) plastic beaker. The beaker was then enclosed in a glass, screw-cap bottle and placed in an oven at the desired temperature for the desired duration of time. After such treatment, the resistance of the sample was measured. Rigid samples were cleaned by Soxhlet extraction to allow subsequent tests of any changed physical properties.

For small volumes of electrolyte (the 2:1 volume ratio studies) the sample and electrolyte were contained in a small Teflon cup which was supported above a large volume of electrolyte contained in the TPX beaker. This was done to assure constancy of electrolyte concentration.

Water Permeation

Measurement of the permeation rate of water or electrolyte through a porous separator can be used to derive an average value for the diameter of continuous pores. Because laminar hydraulic flux through pores increases with the square of pore diameters, the permeation technique is sensitive to the presence even of very small populations of larger-than-average pores.

For porous materials with a relatively steep pore size distribution such as our rigid separator samples, the hydraulic average determined by the permeation technique should be close to the average pore diameter derived from mercury porosimetry. This, and generally good repeatability (within ±3% or less), was in fact observed for rigid separator disks.

Semiflexible separator samples, on the other hand, generally exhibited erratic permeation behavior, with flow rates increasing or decreasing unsystematically. Approximate values of the hydraulic pore diameters were typically about one order of magnitude below the averages from mercury porosimetry. Possible explanations for this discrepancy, which include incomplete wetting of samples, are discussed in more detail in the main body of the report.

The procedure followed that described by Cooke and Lander in the standard reference. The permeation apparatus constructed in this program comprises a brass housing and a system of vacuum and water lines and valves attached to it. Rigid disks and semflexible wafers are mounted in the housing using silicone rubber O-ring seals, and exposing a circular area of 19 mm (0.75 inch) diameter to the permeating water column. A supporting screen, as used by Cooke and Lander, is not needed for the rigid disks but is required for semiflexible wafers. The screen is 2.54 cm (one inch) diameter and is made of 80-mesh stainless steel screen. (A correction for partial blocking by the screen of the effective permeation area is unnecessary in these studies.)

The vacuum system is used to evacuate the permeation assembly (including the mounted sample) and backfill it with water. Constant gas pressure is then applied to the water column on the sample inlet side, and the sample outlet side is opened to the atmosphere. A pressure of 11 N/cm^2 (16 psig) resulted in conveniently measured water permeation rates for most samples. Permeation rates are measured by noting the passage of the meniscus of water past graduated intervals so that two identical volumes of 0.167 ml are contained between the three graduations. Equation (13) of Appendix C is then used to calculate average pore sizes from permeation data.

<u>Modulus of Rupture</u>--The mechanical strength of rigid formulations can be characterized by their modulus of rupture (MOR). The basic procedures and equipment employed to measure MOR are described in an older Astropower Laboratory Report;* they are based on an ASTM Standard Method (C-328-56). The Astropower equipment was modified to accept a 0.64 cm (1/4-inch) wide strip cut from the one-inch disks. The modulus of rupture data obtained with it had a scatter consistent with experience for this type of test; i.e., the uncertainty in measurement was about ±25%. Equation (12) of Appendix C is used to calculate the MOR from the experimental data; it applies for the 0.64 cm samples placed on the 15.9 mm (5/8-inch) span used in our work and contains a correction for the moment arms of the apparatus.

---

*Reference 10.

Zinc Gassing

This test was developed and routinely used at Astropower Laboratories to characterize inorganic separator materials in terms of their tendency to promote hydrogen evolution when in contact with zinc and electrolyte. This test was used as soon as possible under Task II to screen separator stock materials. Early in that work, we found that gassing rates were essentially identical for pellets pressed from zinc powder and separator stock materials and for an intimate mixture of the powders. Accordingly, the simpler powder technique was adopted for this program.

In the procedure, two grams of reagent grade zinc powder (particle size below 5 micrometers) is used as reactant. The powder is mixed (under noncontaminating conditions) with a weight of material to be tested given by $W = 0.28 \times \rho$ where W = weight in grams of test material, ρ = true density of the test material and the constant 0.28 is the true volume in cc of the two grams of zinc; the weight W will then have 0.28 cc of true volume of test material. The test material must also be ground to a particle size $\sim$ 1-5 micrometers.

The mixed powders* are placed in a small reaction bottle together with 15 cc of 45% KOH. Evolved gas is collected in a graduated cylinder. Gas volumes are measured at times of 5, 10, 15 min and 1, 2, 6, 24 hrs after capping the reaction bottle. The gas volumes collected in 24 hrs served as the basis of comparing the zinc gassing property of the various separator stock materials.

---

*Earlier tests used wafers (2.54 cm diam) of the mixed powders compressed to $\sim 1.4 \times 10^4 N/cm^2$ (20,000 psi). It was found that even the very small amounts of iron abraded from the die contributed to increased gas evolution. The procedure using powders avoided this error and gave reproducible results.

Zinc Dendrite Penetration

The zinc penetration test plays a special role among separator screening tests as the only test that attempts to simulate an important specific separator failure mode. It was therefore an important part of the screening program applied to the separators developed under Task II of this work. In following the general approach described in Reference 7, we solved initial problems with cracking of rigid disks, inconvenient use of the cells, and zinc shorting around separator edges. Even after these improvements, some question remained regarding the repeatability of the zinc penetration test. In a series of specifically designed tests, adequate repeatability was demonstrated* for rigid separator samples, but zinc penetration rates (in thickness per unit time) were found to decrease with increasing sample thickness.

Zinc penetration times (and rates) invariably showed extensive scatter for semiflexible separators. To obtain reasonably meaningful and characteristic data, the test was performed routinely on five samples for each given semiflexible separator formulation. Even so, there is some question whether the differences observed for different materials have statistical significance; this is discussed more fully in the main body of this report.

The test procedure used in our work closely follows the technique and procedure described by Dalin and Solomon in Reference 7. One minor modification in our cell is the use of soft silicone rubber gaskets on both sides of the separator sample to be tested; this prevents electrolyte and current leakage and minimizes the danger of breaking rigid samples. Circular holes in these gaskets are aligned precisely with the zinc button cathode and define the effective area of the test

---

*For example, five disks taken from the same firing all gave zinc penetration times within ±7% of the average.

sample. Equation (14) of Appendix C can be used to normalize the results for a unit thickness of separators but expressing penetration resistance as minutes (for a given sample thickness) is preferred because of the nonlinear relationship between penetration time and separator thickness observed in our work.

Mercury Porosimetry

Intrusion of the pore volume in separators with mercury at increasing pressures provides information on the size distribution and (if the maximum pressure available with a given instrument is sufficient to fill even the smallest pores) the total volume of open pores.

Applied to the rigid and semiflexible separator samples developed in this program, pore size data determined with the SRI mercury porosimeter* were generally consistent with the results of other tests, with the exception of the initial (that is, the low pressure part) of the pore size spectrum up to about 35 to 70 N/cm^2 (50 to 100 psia). Porosimetry data suggested presence of a significant pore volume in the corresponding size range, while other tests indicated that no such volume existed or, at least, contributed to important separator properties.

For rigid separator samples, this initial volume increment probably is due to mercury intrusion between sample segments and into surface roughness and blind pores of the disk segments used as samples in

---

*To check on the calibration of the SRI instrument and explore the presence of micropores, a number of rigid samples were sent to an outside laboratory for mercury porosimetry up to 41,300 N/cm^2 (60,000 psi) corresponding to a pore diameter of about 0.003 micrometers. Good agreement with SRI results and absence of significant micropore volumes was noted for all of the materials investigated.

mercury porosimetry. A similar but somewhat more reproducible effect with semiflexible samples can be explained on the basis of the compressibility of these materials. Inasmuch as this apparent pore volume does not seem to contribute to charge and mass transport phenomena, this volume was disregarded in the analysis of rigid and semiflexible separator pore size distributions. For example, for semiflexible separators this was accomplished formally by normalizing intrusion volumes to zero at about 48 N/cm^2 (70 psia); this procedure tended to result in good agreement between pore size distributions obtained with different samples of a given material. For rigid samples, the "foot" of the distribution curve (see, for example, Fig. 18 in the main body of this report) was disregarded; this improved the agreement with porosity data obtained by water intrusion (the standard method for porosity determination of rigids).

In carrying out mercury porosimetry, the standard procedure recommended by the manufacturer of the SRI instrument [American Instrument Co., Silver Spring, Md., Model 5-7121; maximum pressure 1×10^4 N/cm^2 (15,000 psi)] is followed and a 6.1 ml penetrometer for solid samples is used. The instrument has a digital readout of the intruded mercury volume which is entered in special graph paper supplied by the instrument manufacturer. Pore size distribution and average pore size are derived from these plots using the fixed relationship between intrusion pressure and pore size given on the graph paper. This relationship is based on a mercury-sample contact angle of 130^o which is a representative value for surfaces (such as our samples) that are not readily wetted by mercury.

Burst Strength (Semiflexible Wafers)

A rapid and repeatable test for the strength of semiflexible separators was developed during this program; the test was particularly useful to characterize the strength of KOH-wetted wafers which were difficult to employ in the tensile test (see below).

In carrying out the burst test, the water permeation apparatus described earlier is used but with the supporting screen removed. Gas pressure, increasing at a steady rate of 20.7 N/cm^2 (30 psig) per minute, is applied to the water column until the pressure is sufficient to burst the sample; the instant of burst is detected by a sudden increase in water flow rate; results are reported directly as observed burst pressures. Samples may be used dry, wet with water, or wet with electrolyte. A circular rubber membrane (dental dam) is used to protect the dry wafer from water on the high-pressure side. The dam creates a negligible back pressure for the purposes of this test.

Tensile Strength (Semiflexible Wafers)

A specimen of the semiflexible separator 12.7 mm (1/2 inch) wide and approximately 5 cm (2 inch long) is attached to the jaws of a tensile-testing machine, for example, an Instron tensile tester. The stress required to part the sample is measured and reported. Equation (18) of Appendix C is used to calculate the results which are normalized with respect to sample width but not with respect to sample thickness.

Flexibility (Semiflexible Wafers)

A simple test to characterize the degree of flexibility of semiflexible separators was developed in this program. Separator samples were bent around the decreasing radii of a stepped, plastic mandrel until cracking of the separator coating was observed. This quick test gave repeatable results, both for dry and KOH-wetted samples.

In carrying out the test, a 5 cm x 1.25 cm sample is cut and bent around the following radii (in cm): 10, 7.5, 5, 3.8, 2.5, 2.2, 1.9, 1.25, 0.64, and 0.3. The smallest diameter for which cracking did not yet occur is given as a measure of flexibility. A special designation (d) is used for separators which were sufficiently flexible to be folded over and pressed gently on the fold without cracking.

APPENDIX B

SEQUENCE OF SCREENING TESTS

Batch 1

Batch 1 consisted of 118 rigid disks made from eight different materials. Batch 1 was the first group of separator samples to which screening tests were applied. The purpose was primarily evaluation and refinement of the tests themselves and development of an efficient test sequence rather than generation of test data; routine test data for all rigid separator samples were then obtained in Batches 2 through 4. Disk samples were subjected to a sequence consisting of physical measurements followed by cleaning, resistance tests, a second cleaning, weighing, and porosimetry.

Batch 2

The test sequence used to obtain Batch 2 results is shown in Figure B-1 which is a copy of the data sheet assigned to a small number of disks (usually five to ten) from one firing of a particular material. As indicated in Figure B-1 by the "Porosity Screening" columns, all disks were screened with respect to correct porosity at the outset of screening tests. Disks from a given firing that were found to have porosities in the desired range of about 24% to 29%, were accepted for property screening in the remaining test sequence. As indicated by the four columns, four disks of each material were required, as a minimum, for property screening.

In explanation of the test sequence, consider for example, the history of a disk from Column 3. This disk was subjected to the

SCREENING TEST DATA

MATERIAL: ____________

SAMPLE:
BATCH:

FIRING: NO: ______ TEMP: ______
DATE: ______ TIME: ______

PROGRAM FOR DISK								
T[illegible]	POROSITY SCREENING			PROPERTY SCREENING				
				1	2	3	4	
1. Sox				X	X	X	X	X
2. Wt_s	X	X	X	X	X	X	X	X
3. H_2O Int.	X	X	X	X	X	X	X	X
4. Dim.				X	X	X	X	
5 KOH $\frac{100}{1}$				X 120°	X 80°			
6. KOH $\frac{2}{1}$						X 120°		
7. R.KOH				X	X	X		
8. Sox				X	X	X		
9. Wt_s				X	X	X		
10. H_2O Int.				X	X	X		
11. R. KCl					X		X	
12. Perm				X			X	
13. Dif. Zn							X	
14. Zn Den							X	
15. Dif. Ag								X
16. MOR							X	
17. Hg Por				X			X	
18. Dis.	X	X	X	Σ	X	X	Σ	X

Weight as received, gms ______

Diameter, inches ______

Thickness, inches ______

Pycnometer, weight mercury displaced, gms ______

Weight after Soxhlet, gms ______ ______
Step 1 Step 8

Water Intrusion
Weight sample, wet, gms ______ ______
Step 3 Step 10

Resistance [KOH]= ______ [KCL]= ______
Temperature, °C ______ ______
Cell Blank, mv ______ ______
Membrane, mv ______ ______
Current, ma ______ ______
Frequency Hz ______ ______
Step 6 Step 11

Permeability
Temp °C ______
1 Run 2
Volume Transpired, ml ______ ______
Time sec ______ ______
Pressure lb/in^2 ______ ______

Modulus of Rupture
Rupture Weight, gms ______

KOH Degradation
Volume Ratio ______
Weight after Soxhlet, gms ______
Test period hrs ______
Temperature °C ______

Zn Dendrite
Current ma ______
Time to short min ______

Diffusion
Zinc Silver
[S], moles/ml ______ as Zn^o ______ as Ag^o
I_{SS} (μa) = ______ ______

FIGURE B-1

sequence of tests* indicated by "x" under the "Test" column--in the example, test numbers 1 through 4 and 6 through 10.

The abbreviations in Figure B-1, column 1, denote the following: (1) Sox = soxhlet extraction as an initial normalizing step, (2) Wt_S = weight of the dry disk, (3) H_2O Int = water intrusion test, (4) Dim = dimensions, (5) KOH $\frac{100}{1}$ = KOH degradation in 100 to 1 volume ratio (as indicated, this was performed at either of two temperatures, 120^o or 80^oC, depending on whether the disk was a column 1 or a column 2 disk), (6) KOH $\frac{2}{1}$ = KOH degradation in a volume of electrolyte to disk volume ratio of 2 to 1 at 120^oC, (7) R,KOH = resistance measurement in KOH electrolyte (using the spent KOH contained in the degraded disk), (8) Sox = soxhlet extraction to remove KOH, (9) Wt_S = weight of the dry disk, (10) H_2O Int = water intrusion to determine the void volume of the degraded disk (this step was followed by soxhlet extraction which is not indicated in the flow sheet), (11) R, KCl = resistance measurement made with 0.1 normal KCl, (12) Perm = pore size determination by water permeation, (13) Dif. Zn = zinc diffusion rate determination, (14) Zn Den = zinc dendrite studies, (15) Dif. Ag = determination of silver diffusion, (16) MOR = determination of modulus of rupture, (17) Hg Por = determination of pore size by mercury intrusion porosimetry, (18) Dis = disposition of disk, where X indicates the disk might remain intact to serve for further studies, and Σ indicates that the disk had passed through destructive tests and no longer existed as an integral entity. Disks tested in the sequence given in Figure B-1 were referred to as "Batch 2 disks." Because this sequence was applied to disks at two different times, two groupings, referred to as Batch 2-A

*Test steps 13 and 15 call for zinc and silver diffusion tests. These tests were deleted from the required study.

or Batch 2-B, are distinguished. Disks were given a code containing the batch and column numbers. For example, a disk with the code 2-A-3 was tested in Batch 2-A and subjected to the test sequence of Column 3.

Batches 3 and 4

The sequence used for Batch 2 disks was modified and the changed sequence was used for Batches 3 and 4. This sequence is presented in Figure B-2. The interpretation of test sequence and coding logic follows that presented above for Batch 2.

Semiflexible Series A, B, and C

The semiflexible specimens required preliminary study to optimize tests for this type of sample. Accordingly, a series of preliminary tests (A, B, and C) were run to ascertain appropriate test conditions. In this series the following tests were studied: mercury porosimetry, water intrusion, KOH degradation, H_2O permeability, Zn dendrite, burst strength, and tensile strength. Materials Q and R were used in most of these tests. The modifications in test procedures for semiflexible formulations indicated in Appendix A resulted from these preliminary studies.

Semiflexible Series D: Screening Tests of All 16 Materials

Using the information gained in the preliminary series of tests, a scheme for testing samples of all sixteen semiflexible formulations was devised. This scheme is described below in the listing of tests performed; as noted previously, most tests were applied to fresh samples rather than sequentially to samples previously used in other tests.

SCREENING TEST DATA

SAMPLE: ______

BATCH: ______

MATERIAL: ______

FIRING DATA: no: ______ Temp.: ______ Date: ______ Time: ______

STEP	PROGRAM FOR DISK TEST	COLUMN 1	2	3	4
1	SOX	X	X	X	X
2	Dry Weight	X	X	X	X
3	H_2O INTRUSION	X	X	X	X
4	DIMENSIONS	X	X	X	X
5	KCl RESISTANCE	X	X	X	
6	KOH DEG 100:1, 120°C	X	–		
7	KOH DEG 100:1, 90°C	–	X		
8	SOX	X	X	X	
9	Dry Weight	X	X		
10	H_2O INTRUSION	X	X		
11	KCl RESISTANCE	X	X		
12	SOX	X	X		
13	PERM.	X	X	X	
14	Zn DENDRITE	–	–	X	
15	MOR	X	(1.)		X
16	Hg POR	X	(1.)		X

(1.) If column 1 disk breaks, use column 2 disk.

(2.) The expected results are: R of 1N KCl = 750 Ω, ρ_E = 9.44 Ω cm at 22°C. $\rho_E = \frac{R}{k}$ where k = 79.58 cm⁻¹

DATA

Dry Weight, grams ______ as rec'd ______ step 2 ______ step 5.5 ______ step 9

Diameter, inches ______ ______ ______ ______ ______

Thickness, inches ______ ______ ______ ______ ______

Wet Weight, grams ______ step 3 ______ step 10

Resistance, 1.0N KCl

Conductivity Cell, 100 Hz (2.)

{5.5 DRY WEIGHT}

Temperature, °C ______ ______

Resistance Standard, 1.0N, ohms ______ ______

Resistance Stock 1.0N ohms ______ ______

ρ_E, CALC, Ω cm ______ ______

Resistance Cell, 60 Hz

Temperature, °C ______ ______

Cell Blank, volts ______ ______

Disk volts ______ ______

Current, ma ______ ______

V_E volts ______ ______

step 5 step 11

Permeability

Temperature °C ______

Transportation time, sec

	Run 1	2	3
For 0.166 ml	______	______	______
For 0.168 ml	______	______	______
Pressure, lbs/in²	______	______	______

Zinc Dendrite: 10 ma, Shorting time ______ step 14

Modulus of Rupture

	Run 1	2
Breaking load, grams	______	______

FIGURE B-2

- Physical Measurements
  Weight, thickness, width--done after cutting.

- Mercury Porosimetry
  Done on wafers directly.

- Tensile Tests
  Used SRI instrument. Run on 1/4-inch wide strips under two conditions: (1) dry and (2) after one-week soak at room temperature in 45 wt% KOH.

- Flex Tests
  Done around mandrel of following diameters, in inches: 4, 3, 2, 1-1/2, 1, 7/8, 3/4, 1/2, 1/4, 1/8. Done, as for tensile, under two conditions: (1) dry and (2) after one-week soak at room temperature in 45 wt% KOH.

- Specific Resistivity
  Three wafers of each material studied under three successive conditions: (1) immediately after impregnation with 45 wt% KOH, (2) after one-week soak at room temperature in 45 wt% KOH, and (3) after 48 hours degradation at 80°C in 45 wt% KOH.

- Burst Tests
  Eight wafers of each material studied in groups of two, under four conditions: (1) dry burst using rubber dam, (2) wet burst with water, run after permeation, (3) wet burst with water, run after permeation and one-week soak in water, and (4) wet burst with KOH, run after specific resistivity on degraded wafer.

- Zinc Dendrite
  Run on five wafers of each material. One-week prior soak in 45 wt% KOH was performed before test.

- Permeability
  Four wafers of each material studied in groups of two under two conditions: (1) permeation with filtered, deionized water, immediately after exposure of the wafer to water and (2) after one-week's soak at room temperature in water, with vacuum impregnation at the start and in the middle of the week before permeation run.

The above list of tests and numbers of samples used in each test indicates that a large number of semiflexible samples were required. For the sixteen formulations studies, the tests required a total of 256 wafers and 128 strips. The tally is as follows:

- Strips
  - Tensile and flex
    Two per test x 2 conditions x 2 tests x 16 formulations = 128 strips
- Wafers
  - Permeability
    Two per test x 2 conditions x 16 formulations = 64 wafers
  - Mercury porosimetry
    Two per test x 16 formulations = 32 wafers
  - Undergraded burst
    Two per test x 16 formulations = 32 wafers
  - Specific resistivity and KOH degradation
    Three per test x 16 formulations = 48 wafers
  - Zinc dendrite
    Five per test x 16 formulations = 80 wafers

Appendix C

EQUATIONS AND SYMBOLS FOR EVALUATION OF SCREENING TEST DATA

The symbols used for terms representing data, and the dimensions of those terms, are listed below. Following this is a list of equations employed in data reduction. Equations 7 and 8 apply to Batch 1 data only; they are supplanted by Equations 10 and 11 for subsequent data.

Symbols		Value or Dimension
A =	separator sample area. In the Batch 1 resistance cell, A equals	1.072 cm^2
	in the Batch 2 resistance cell, A equals	0.90 cm^2
	and in the permeation apparatus, A equals	2.85 cm^2
D_A =	area density = weight per unit area	gms cm^{-2}
D_t =	apparent density	g cm^{-3}
D_d =	diameter of disk	inches
D_m =	diameter of pore determined by mercury intrusion	micrometers
D_h =	diameter of permeation cell	inches
D_p =	diameter of pore, determined by water permeation	micrometers
D_t =	true density	g cm^{-3}
D_w =	density of water, taken as 1.000	g cm^{-3}
ΔP =	pressure differential	lbs in^{-2}
F =	index of flexibility	inches of diameter
g =	weight	grams
h =	thickness of separator	inches
h_c' =	thickness of coating of semiflexible separator	inches
h_m =	equivalent thickness of disk calculated from water permeation plus mercury intrusion results	inches

			Value or Dimension
η	=	viscosity of water, at $295^{o}K$ ($22^{o}C$); $\eta = 9.58 \times 10^{-3}$ poise	dyne-sec cm^{-2}
I	=	current	amperes or milliamperes
I_D	=	current used in zinc dendrite test	milliamperes
I_w	=	percent water intrusion	wt%
K	=	cell constant. For the laboratory conductivity cell, K equals	79.6 cm^{-1}
$\bar{\kappa}_r$	=	specific area resistivity h $\bar{\rho}_r$	ohm-cm^2
L	=	percent weight degradation by KOH	wt%
M	=	modulus of rupture	lbs in^{-2}
p	=	breaking load used in modulus of rupture apparatus	g
P_B	=	burst pressure	inches (Hg)
P_m	=	open porosity, by mercury intrusion	vol %
P_r	=	open porosity calculated from $\bar{\rho}_r$	vol %
P_W	=	open porosity, by water intrusion	vol %
ρ	=	specific volume resistivity	ohm-cm
ρ_E	=	specific resistance of electrolyte used in test	ohm-cm
ρ_N	=	specific resistivity of 45 wt% KOH at $291^{o}K$ ($18^{o}C$); taken as	2.56 ohm cm
$\bar{\rho}_r$	=	normalized specific volume resistivity	ohm-cm
ρ_r	=	specific volume resistivity	ohm-cm
$\bar{R}_D$	=	normalized zinc dendrite rate	min mil^{-1}
r_p	=	radius of pore	micrometers
S	=	index of breaking strength, normalized for $\frac{1}{4}$ inch wide sample. Note: S is reported directly as the breaking load for a $\frac{1}{4}$-in. wide sample	grams
T	=	temperature	^{o}C
t	=	time	sec, min

		Value or Dimension
t_D =	zinc dendrite shorting time	min
τ =	tortuosity	dimensionless
τ_a =	tortuosity from resistivity and porosity	dimensionless
τ_b =	tortuosity from water permeation and mercury intrusion	dimensionless
τ_r =	ratio τ_a/τ_b	dimensionless
vol =	volume	cm^3
V =	voltage	mv, or v
V_i =	volume of mercury intruded in mercury porosimetry	cm^3
V_B =	voltage from laboratory resistivity cell without the separator, measurements taken during resistance measurements.	v, mv
V_S =	voltage from laboratory resistivity cell with separator sample	v, mv
V_E =	voltage from laboratory resistivity cell without separator sample and when first filled with electrolyte.	v
W =	weight of dry disk or wafer	grams
W_c =	weight of disk, dry, after soxhlet extraction	grams
W_w =	wet weight of disk after H_2O intrusion	grams
W_d =	dry weight of KOH degraded sample	grams

Equations		Dimensions of Result
1.	Volume $Vol = 12.90\ D^2h$; D and h are in inches	cm^3
2.	Percent water intrusion $I_w = 100(W_w - W_c)/W_c$	wt%
3.	Apparent density $D_a = W_c(Vol)^{-1}$	$g\ cm^{-3}$
4.	Apparent true density $D_t = W_c[Vol(1 - 10^{-2}P_w)]^{-1}$ This equation includes any closed void volume and, therefore, does not necessarily yield true density.	$g\ cm^{-3}$
5.	Open porosity, by water $P_w = 100(W_w - W_c)/(Vol)$ Volume from A-1 above	vol %
6.	Porosity, by mercury intrusion $P_m = \frac{V_i}{VOL} \times 10^{-1}$	vol %
7.	Specific volume resistivity $\rho_r = 1.072\ (V_S - V_B)/(2.54\ Ih)$ I is a parameter and equals 10 ma.	ohm-cm
8.	Normalized specific volume resistivity $\bar{\rho}_r = (2.56\ \rho_r)/2.34 = 1.095\ \rho_r$ This equation presents our specific resistivities on the basis of 45 wt% KOH at 291^oK, whose ρ is defined as 2.56 ohm-cm. The value, 2.34 is the value determined in our laboratory for 45 wt % KOH at room temperature.	ohm-cm
9.	KOH degradation $L = 100\ (W_c - W_d)/W_c$	wt%

Dimensions of Result

10. Specific volume resistivity, normalized

$$\bar{\rho}_r = \frac{2.56}{\rho_E}\left[\left(\frac{V_B}{V_E}\right)\rho_E + \left(\frac{V_S - V_B}{I}\right)\left(\frac{0.902}{2.54h}\right)\right] \qquad \text{ohm-cm}$$

Equation as used for batches subsequent to Batch 1. The current, I, was maintained at 5 ma, rms, at 60 Hz.

11. Specific area resistivity

$$\bar{K}_r = h\,\bar{\rho}_r \qquad \text{ohm-cm}^2$$

where h must be the same h as used in Eq. 10 above.

12. Modulus of rupture

$$M = 2.94 \times 10^{-3}\, P\, h^{-2} \qquad \text{lbs in}^{-2}$$

valid for 0.250-inch wide sample between 5/8-inch span.

13. Water permeation

(a) $$D_p = 29.18\; h\, D_d \left[\Delta P(W_w - W_c)t\right]^{-1/2} \qquad \text{micrometers}$$

(b) $$D_p = 2.258 \times 10^3\, h\, D_d \left[\frac{\text{Vol}}{y\Delta P\, t\, V_i}\right]^{1/2}$$

where y has been shown to be acceptably taken as unity, and where V_i is for a 1.00 -inch diameter wafer

14. Zinc dendrite. Normalized to minutes per mil at 10 ma/cm^2

$$\bar{R}_D = 7.894 \times 10^{-5}\, t_D\, I_D\, h^{-1} \qquad \text{min/mil}$$

15. Open porosity ratio, I_w/v_i dimensionless

For each disk, calculate the ratio of I_w (Eq. 2) to volume of mercury intruded per gram data from mercury porosimetry. The equation is $100(I_w)(\text{Vol Hg/g})^{-1}$ and yields the ratio in vol %.

	Dimensions of Result

16. Pore size ratio. — dimensionless

Determine pore size ratio between water permeation and mercury porosimetry. Define mercury pore size as diameter corresponding to intrusion of one-half of total mercury intrusion volume. Take ratio of pore sizes: permeation to mercury intrusion.

17. Tortuosity. — dimensionless

Tortuosity may be calculated from two comparative sets of data: (a) resistivity and open porosity, (b) permeability diameter and mercury porosimetry diameter.

(a) Tortuosity by resistivity and open porosity.

$$(\tau_a)^2 = \frac{\bar{\rho}_r \text{ (from Eq. 10)}}{2.56\ \Omega\text{cm} \times (P_w/100)^{-1}}$$

P_w from Eq. (5)

$$(\tau_a)^2 = \bar{\rho}_r\ P_w \times \frac{1}{156} = 3.906 \times 10^{-3}\ P_w\ \bar{\rho}_r$$

(b) Tortuosity by mercury intrusion and water permeation.

The effective thickness can be calculated. Let

$$\tau_b = \frac{h_m}{h},$$

where h_m is thickness calculated using both water permeation results and mercury porosimetry results.

Equation 13 (a) is

$$D_p = 29.18\ h\ D_d\ [\Delta P\ (W_w - W_c)t]^{-1/2}$$

Let D_m be the diameter in microns determined by mercury porosimetry, and let h be represented by h_m, then

$$h_m = \frac{D_m[\Delta P(W_w - W_c)T]^{1/2}}{29.18\ D_d}$$

Dimensions of Result

or, since $D_p = 29.18 \ h \ D_d \ [\Delta P(W_w - W_c)]^{-1/2}$

and $D_m = 29.18 \ h_m \ D_d \ [\Delta P(W_w - W_c) t]^{-1/2}$

$h_m/h = D_m/D_p = \tau_b$.

18. Tensile strength, — grams

$$S = P \times \frac{0.25 \text{ inches}}{\text{measured width of sample in inches}}$$

where P is breaking load in grams.

19. Index of flexibility. — inches of diameter

20. Open porosity via resistance.

$$P_r = 400 \frac{\rho_N}{\bar{\rho}_r}, \text{ where } \rho_N = 2.56 \ \Omega\text{cm}$$ — vol%

and a tortuosity of 2.0 is assumed.

Note: The relationship is $\tau_a = \left(\frac{\bar{\rho}_r P_m}{100 \rho_N} \right)^{1/2}$

21. Zinc dendrite shorting time — t_D

expressed as shorting time in minutes.

22. Thickness of semiflexible separators — h

h = measured thickness of separator, (usually 0.015 inches).

h_c = measured thickness of coating (usually 0.005 inches).

23. Wafer area density — g/cm^2

$$D_A = \frac{W}{\text{area}}$$

where area $= \pi[(1.00)^2/4] \times (2.54)^2$.

DISTRIBUTION LIST FOR
FINAL REPORT UNDER
CONTRACT NAS3-15686

National Aeronautics & Space Administration
Lewis Research Center
21000 Brookpark Road
Cleveland, Ohio 44135

Attn: G. M. Ault (MS 3-13)
V. Hlavin (MS 3-10)
L. W. Schopen (MS 500-206)
Technology Utilization Office (MS 3-19)
Dr. L. Rosenblum (MS 302-1)
J. Toma (MS 302-1)
H. J. Schwartz (MS 309-1)
Dr. J. S. Fordyce (MS 309-1)
W. J. Nagle (MS 309-1)
D. G. Soltis (MS 309-1)
J. Bozek (MS 309-1)
W. A. Robertson (MS 309-1)
Library (MS 60-3)
Report Control (MS 5-5)

National Aeronautics & Space Administration
Washington, D. C. 20546
Attn: E. M. Cohn RPP
A. M. Greg Andrus ECC
R. C. Livingston MHE
U/Technology Utilization Office K7

National Aeronautics & Space Administration
Goddard Space Flight Center
Greenbelt, Maryland 20771
Attn: Thomas Hennigan, Code 716.2
Gerald Halpert, Code 764.3
Louis Wilson, Code 430.0

National Aeronautics & Space Administration
Langley Research Center
Instrument Research Division
Hampton, Virginia 23365
Attn: J. Bene

National Aeronautics & Space Administration
George C. Marshall Space Flight Center
Huntsville, Alabama 35812
Attn: C. B. Graff (S&E-ASTR-EP)

National Aeronautics & Space Administration
Manned Spacecraft Center
Houston, Texas 77058
Attn: William R. Dusenbury (EP-5)
J. B. Trout (EP-5)

National Aeronautics & Space Administration
Langley Research Center
Langley Station
Hampton, Virginia 23365
Attn: Harry Ricker (MS 474)

National Aeronautics & Space Administration
Scientific & Technical Information Center: Input
P.O. Box 33
College Park, Maryland 20740
(2 copies plus 1 reproducible)

National Aeronautics & Space Administration
Ames Research Center
Pioneer Project
Moffett Field, California 94035
Attn: Arthur Wilber/A. S. Hertzog

National Aeronautics & Space Administration
Ames Research Field, California 94035
Attn: Jon Rubenzer
Code PBS (MS 244-2)

Jet Propulsion Laboratory
4800 Oak Grove Drive
Pasadena, California 91103
Attn: Dr. R. Lutwack (MS 198-220)
A. A. Uchiyama (MS 198-220)

Department of the Army

U.S. Army Mobility Equipment R&D Center
MERDC
Fort Belvoir, Virginia 22060
Electro Technology Lab
Energy Conversion Research Division

Commanding General
U.S. Army Weapons Command
Attn: AMSWE-RDR, Mr. G. Reinsmith
Rock Island Arsenal
Rock Island, Illinois 61201

U.S. Army Research Office
Box CM, Duke Station
Durham, North Carolina 27706
Attn: Dr. Wilhelm Jorgensen

U.S. Army Research Office
Chief, R&D
Department of the Army
3D442, The Pentagon
Washington, D.C. 20546

U.S. Army Natick Laboratories
Clothing and Organic Materials Division
Natick, Massachusetts 01762
Attn: L. A. Spano

Commanding Officer
U.S. Army Electronics R&D Labs
Fort Monmouth, New Jersey 07703
Attn: Power Sources Division
AMSEL-KL-P

Army Materiel Command
Research Division
AMCRD-RSCM-T-7
Washington, D.C. 20315
Attn: John W. Crellin

Army Materiel Command
Development Division
AMCRD-DE-MO-P
Washington, D.C. 20315
Attn: Marshall D. Aiken

Commanding Officer
Picatinny Arsenal
Dover, N.J. 07801
Attn: M. R. Merriman
SMUPA-FR-S-P

U. S. Army TRECOM
Fort Eustis, Virginia 23604
Attn: Leonard M. Bartone (SMOFE-ASE)

U.S. Army Mobility Command
Research Division
Warren, Michigan 48090
Attn: O. Renius (AMSMO-RR)

Harry Diamond Laboratories
Room 300, Building 92
Connecticut Ave. & Van Ness St., N.W.
Washington, D.C. 20438
Attn: Nathan Kaplan

Department of the Navy

Office of Naval Research
Arlington, Virginia 22217
Attn: Director, Power Program,
Code 473

Office of Naval Research
Department of the Navy
Arlington, Virginia 22217
Attn: H. W. Fox, Code 472

Naval Research Laboratory
4555 Overlook Avenue
Washington, D.C. 20360
Attn: A. C. Simon, code 6160

Naval Ship R&D Center
Annapolis, Maryland 21402
Attn: J. H. Harrison, Code 2724

Naval Air Systems Command
Department of the Navy
Washington, D.C. 20360
Attn: Code AIR-340C

Naval Ship Systems Command
Washington, D.C. 20360
Attn: Bernard B. Rosenbaum, Code 03422

Commanding Officer
U.S. Naval Ammunition Depot
Crane, Indiana 47522
Attn: D. Miley, Code QEWE

U.S. Naval Observatory
4301 Suitland Road
Suitland, Maryland 20390
Attn: R. E. Trumble, STIC, Bldg. 52

Naval Ordnance Laboratory
Silver Spring, Maryland 20910
Attn: Philip D. Cole, Code 232

Naval Ship Engineering Center
Center Building, Prince Georges Center
Hyattsville, Maryland 20782
Attn: F. Himy, Code 6157D

Bureau of Naval Weapons
Department of the Navy
Washington, D.C. 20360
Attn: Bernard B. Rosenbaum, Code 03422

Department of the Air Force

Aero Propulsion Laboratory
Wright-Patterson AFB, Ohio 45433
Attn: James E. Cooper, APIP-1

AF Cambridge Research Lab
Attn: CRFE
L. G. Hanscom Field
Bedford, Massachusetts 01731
Attn: Dr. R. Payne

AF Cambridge Research Lab
L. G. Hanscom Field
Bedford, Massachusetts 01731
Attn: Edward Raskind (Wing F), CREC

Headquarters, U.S. Air Force (AFRDR-AS)
Washington, D.C. 20325
Attn: Major G. Starkey

Headquarters, U.S. Air Force (AFRDR-AS)
Washington, D.C. 20325
Attn: Lt. Col. William G. Alexander

Rome Air Development Center, ESD
Griffis AFB, New York 13440
Attn: Frank J. Mollura (EMRED)

Space Systems Division
Los Angeles Air Force Station
Los Angeles, California 90045
Attn: HQSAMSO
(SMTAE/Lt. R. Ballard)

Other Government Agencies

National Bureau of Standards
Washington, D.C. 20234
Attn: Dr. W. J. Hamer

National Bureau of Standards
Washington, D.C. 20234
Attn: Dr. A. Brenner

Office, Sea Warfare System
The Pentagon
Washington, D.C. 20310
Attn: G. B. Wareham

U.S. Atomic Energy Commission
Auxiliary Power Branch(SNAP)
Division of Reactor Development
Washington, D.C. 20325
Attn: Lt. Col. George H. Ogburn, Jr.

Lt. Col. John H. Anderson
Advanced Space Reactor Branch
Division of Reactor Development
U.S. Atomic Energy Commission
Washington, D.C. 20325

Bureau of Mines
4800 Forbes Avenue
Pittsburgh, Pennsylvania 15213
Attn: Dr. Irving Wender

Mr. Donald A. Hoatson
Army Reactors, DRD
U.S. Atomic Energy Commission
Washington, D.C. 20545

Clearing House for Scientific &
Technical Information
5285 Port Royal Road
Springfield, Virginia 22151

Private Organizations

Aerojet-General Corporation
Chemical Products Division
Azusa, California 91702
Attn: William H. Johnson

Aeronutronic Division of Philco Corp
Technical Information Services
Ford Road
Newport Beach, California 92663

Aerospace Corporation
P.O. Box 95085
Los Angeles, California 90045
Attn: Library Acquisition Group

Aerospace Corporation
Systems Design Division
2350 East El Segundo Boulevard
El Segundo, California 90246
Attn: John G. Krisilas

A.M.F.
Attn: R. J. Mosny/M. S. Mintz
689 Hope Street
Stamford, Connecticut 06907

American University
Mass. & Nebraska Avenue, N.W.
Washington, D.C. 20016
Attn: Dr. R. T. Foley
Chemistry Dept.

Arthur D. Little, Inc.
Acorn Park
Cambridge, Mass. 02140
Attn: Dr. John Parry

Atomics International Division
North American Aviation, Inc.
8900 DeSoto Avenue
Canoga Park, California 91304
Attn: Dr. H. L. Recht

Battelle Memorial Institute
505 King Avenue
Columbus, Ohio 43201
Attn: J. E. Clifford

Bell Laboratories
Murray Hill, N. J. 07974
Attn: U. B. Thomas/D. O. Feder

The Boeing Company
P.O. Box 3999
Seattle, Washington 98124
Attn: Sid Gross (MS 88-06)

Borden Chemical Company
Central Research Laboratory
P.O. Box 9524
Philadelphia, Pennsylvania 19124

Burgess Battery Company
Foot of Exchange Street
Freeport, Illinois 61032
Attn: M. E. Wilke, Chief Eng. 53473

C & D Batteries
Division of Eltra Corporation
3043 Walton Road
Plymouth Meeting, Pennsylvania 19462
Attn: Dr. Eugene Willihnganz

Calvin College
Science Building
3175 Burton Street, S.E.
Grand Rapids, Michigan 49506
Attn: Prof. T. P. Dirkse

Communications Satellite Corporation
Comsat Labs
P.O. Box 115
Clarksburg, Maryland 20734
Attn: Mr. Robert Strauss

ChemCell Inc.
150 Dey Road
Wayne, New Jersey 07470
Attn: Peter D. Richman

Catalyst Research Corporation
6309 Blair Hill Lane
Baltimore, Maryland 21209
Attn: Mr. F. Tepper

Cubic Corporation
9233 Balboa Avenue
San Diego, California 92123
Attn: Librarian

Delco Remy Division
General Motors Corporation
2401 Columbus Avenue
Anderson, Indiana 46011
Attn: J. A. Keralla

Dynatech Corporation
17 Tudor Street
Cambridge, Massachusetts 02139
Attn: R. L. Wentworth

Eagle-Picher Industries, Inc.
P.O. Box 47
Joplin, Missouri 64801
Attn: E. P. Broglio

ESB, Inc.
P.O. Box 11097
Raleigh, N. C. 27604
Attn: Director of Engineering

Energy Research Corporation
15 Durant Avenue
Bethel, Connecticut 06801
Attn: M. Klein

ESB, Inc.
Research Center
19 West College Avenue
P.O. Box 336
Yardley, Pennsylvania 19067
Attn: Librarian

Electrochimica Corporation
2485 Charleston Road
Mountain Voew, California 94040
Attn: Dr. Morris Eisenberg

E.I. DuPont Nemours & Co.
Engineering Materials Laboratory
Wilmington, Delaware 19898
Attn: J M. Williams, Bldg. 304

Energetics Science, Inc.
4461 Bronx Boulevard
New York, N.Y. 10470
Attn: Dr. H. G. Oswin

Elgin National Watch Company
107 National Street
Elgin, Illinois 60120
Attn: T. Boswell

Emhart Corporation
Box 1620
Hartford, Connecticut 06102
Attn: Dr. W. P. Cadogan

Engelhard Industries, Inc.
497 Delancy Street
Newark, N. J. 07105
Attn: Dr. J. G. Cohn

Dr. Arthur Fleischer
466 South Center Street
Orange, New Jersey 07050

General Electric Company
R&D Center
P.O. Box 43
Schenectady, New York 12301
Attn: Dr. R. P. Hamlen

General Electric Company
Space Systems
P.O. Box 8555
Philadelphia, Pa. 19101
Attn: K. L. Hanson, Room M-2700

General Electric Company
Battery Business Section
P.O. Box 114
Gainesville, Florida 32601
Attn: P. R. Voyentzie

General Electric Company
Research & Development
Center
P.O. Box 8
Schenectady, N.Y. 12301
Attn: Whitney Library

General Telephone & Electronics Labs
Bayside, New York 11352
Attn: Dr. Paul Goldberg

Gould Ionics, Inc.
P.O. Box 1377
Canoga Park, California 91304
Attn: Dr. J. E. Oxley

Globe-Union, Inc.
P.O. Box 591
Milwaukee, Wisconsin 53201
Attn: Dr. E. Y. Weissman

General Electric Company
777 - 14th Street, N.W.
Washington, D.C. 20005
Attn: D. F. Schmidt

Gould-National Batteries, Inc.
Engineering & Research Center
2630 University Avenue, S.E.
Minneapolis, Minnesota 55418
Attn: D. L. Douglas

Gulton Industries
Battery & Power Sources Division
212 Durham Avenue
Metuchen, N.J. o8840
Attn: E. Kantner

Grumman Aerospace Corporation
OAO Project
Bethpage, Long Island, N.Y. 11714
Attn: S. J. Gaston (Plant 41)

Heliotek
12500 Gladstone Avenue
Sylmar, California 91342
Attn: Dr. H. N. Seiger

Hughes Aircraft Corporation
Centinda Ave.& Teale Street
Culver City, California 90230
Attn: T. V. Carbey

Dr. P. L. Howard
Centreville, Maryland 21617

Hughes Aircraft Corporation
Building 366, MS 524
El Segundo, California 90245
Attn: M. E. Ellison

Hughes Research Laboratories Corp.
3011 Malibu, California 90265
Attn: T. M. Hahn

ITT Research Institute
10 West 35th Street
Chicago, Illinois 60616
Attn: Dr. H. T. Francis

Institute for Defense Analyses
R&E Support Division
400 Army-Navy Drive
Arlington, Virginia 22202
Attn: Mr. R. Hamilton

Invention Talents Inc.
1149 Chesapeak Avenue
Columbus, Ohio 43212
Attn: Dr. J. McCallum

Institute for Defense Analyses
R&E Support Division
400 Army-Navy Drive
Arlington, Virginia 22202
Attn: Dr. R. Briceland

International Nickel Company
1000 - 16th Street, N.W.
Washington, D.C. 20036
Attn: N. A. Matthews

Idaho State University
Department of Chemistry
Pocatello, Idaho 83201
Attn: Dr. G. Myron Arcand

John Hopkins University
Applied Physics Laboratory
8621 Georgia Avenue
Silver Spring, Maryland 20910
Attention: Richard E. Evans

Johns-Manville R&E Center
P.O. Box 159
Manville, N.J. 08835
Attn: J. S. Parkinson

Leesona Corp.
Warwick, R.I. 02887
Attn: Dr. A. Moos

Honeywell Inc.
Livingston Electronic Laboratory
Route 309
Montgomeryville, Pa. 18936
Attn: Library

Lockheed Missiles & Space Company
P.O. Box 504
Sunnyvale, California 94088
Attn: R. E. Corbett
Dept. 62-25, Bldg. 157

Life Systems, Inc.
23715 Mercantile Road
Cleveland, Ohio 44122
Attn: Dr. R. A. Wynveen

Lockheed Missiles & Space Company
Department 62-30
3251 Hanover Street
Palo Alto, California 94304
Attn: J. E. Chilton

Lockheed Missiles & Space Company
Technical Information Center
3251 Hanover Street
Palo Alto, California 93404

P. R. Mallory & Company, Inc.
Northwest Industrial Park
Burlington, Massachusetts 01803
Attn: Dr. Per Bro

P. R. Mallory & Company, Inc.
Technical Services Laboratory
Indianapolis, Indiana 46206
Attn: A. S. Doty

P. R. Mallory & Company, Inc.
3029 E. Washington Street
Indianapolis, Indiana 46206
Attn: Technical Librarian

Marquardt Corporation
16555 Saticoy Street
Van Nuys, California 91406
Attn: Dr. H. G. Krull

Martin Marietta Corp.
Electronics Research Department
P.O. Box 179
Denver, Colorado 80201
Attn: William B. Collins (MS 1620)
M. S. Imanura (MS F8845)

McDonnell Douglas Astronautics Co.
5301 Bolsa Avenue
Huntington Beach, California 92647
Attn: Library

Melpar
Technical Information Center
7700 Arlington Boulevard
Falls Church, Virginia 22046

Molecular Energy Corp.
82 Naylon Ave.
Livingston, N.J. 07039
Attn: Mary W. Taylor

North American Rockwell
Autonetics Division
P.O. Box 4181
Anaheim, California 92803
Attn: R. F. Fogle, GF18

Metals and Controls Division
Texas Instruments, Inc.
34 Forrest Street
Attleboro, Mass. 02703
Attn: Dr. J. W. Ross

Midwest Research Institute
425 Volker Boulevard
Kansas City, Missouri 64110
Attn: Physical Science Laboratory

G & W. H. Corson, Inc.
Plymouth Meeting, Pennsylvania 19462
Attn: Dr. L. J. Minnick

North American Aviation, Inc.
12214 Lakewood Boulevard
Downey, California 90241
Attn: Burton M. Otzinger

North American Aviation, Inc.
Rocketdyne Division
6633 Canoga Avenue
Canoga Park, California 91304
Attn: Library

North American Aviation Co.
S&ID Division
Downey, California 90241
Attn: Dr. James Nash

Oklahoma State University
Stillwater, Oklahoma 74075
Attn: Prof. William L. Hughes
School of Electrical Eng.

Philco-Ford Corporation
Power & Control Eng. Dept., MS R26
3939 Fabian Way
Palo Alto, California 94303
Attn: Mr. D. C. Briggs

Power Information Center
University City Science Institute
3401 Market Street, Room 2107
Philadelphia, Pa. 19104

Prime Battery Corporation
15600 Cornet Street
Santa Fe Springs, Calif. 90670
Attn: David Roller

Portable Power Sources Corp.
166 Pennsylvania Avenue
Mount Vernon, N.Y. 10552
Attn: L. Schulman

RAI Research Corporation
225 Marcus Boulevard
Hauppauge, L.I., N.Y. 11787

Radio Corporation of America
415 South Fifth Street
Harrison, N.J. 07029
Attn: Dr. G. S. Lozier
Bldg. 18-2

Rensselaer Polytechnic Institute
Dept. of Chemistry
Troy, N. Y., 12180
Attn: Prof. G. J. Janz

Southwest Research Institute
P.O. Drawer 28510
San Antonio, Texas 78228
Attn: Library

Marathon Battery Corp.
8301 Imperial Drive
Elmsford, N.Y. 10523

Stanford Research Institute
Menlo Park, California 94025
Attn: Dr. F. R. Kalhammer

Texas Instruments, Inc.
P.O. Box 5936
Dallas, Texas 75222
Attn: Dr. Isaac Trachtenberg

Teledine Isotopes
110 West Timonium Road
Timonium, Md. 21093
Attn: C. F. Williams

TRW Systems, Inc.
One Space Park
Redondo Beach, California 90278
Attn: Dr. W. R. Scott M-2/2154

TRW, Inc.
23555 Euclid Avenue
Cleveland, Ohio 44117
Attn: Librarian (TIM 3417)

Tyco Laboratories, Inc.
Bear Hill
Hickory Drive
Waltham, Massachusetts 02154
Attn: Library

Union Carbide Corporation
Development Laboratory Library
P.O. Box 6056
Cleveland, Ohio 44101

Union Carbide Corporation
Parma Laboratory
P.O. Box 6116
Parma, Ohio 44130
Attn: Dr. Robert Powers

University of California
Space Science Laboratory
Berkeley, California 94720
Attn: Dr. C. W. Tobias

University of Pennsylvania
Electrochemistry Laboratory
Philadelphia, Pennsylvania 19104
Attn: Prof. John O. M. Bockris

University of Toledo
Toledo, Ohio 43606
Attn: Dr. Albertine Krohn

Westinghouse Electric Corporation
Research and Development Center
Churchill Borough
Pittsburgh, Pennsylvania 15235
Attn: Dr. C. C. Hein/Dr. A. Langer

Whitakker Corporation
3850 Olive Street
Denver, Colorado 80207
Attn: L. K. White

Yardney Electric Corporation
82 Mechanic Street
Pawcatuck, Connecticut 02891
Attn: Director of Engineering